THE EFFECT OF SURFACE-ACTIVE BLOCK COPOLYMERS ON TWO-PHASE FLOW

by

Jeffrey D. Martin

B.E., Youngstown State University, 2003

Submitted to the Graduate Faculty of

the School of Engineering in partial fulfillment

of the requirements for the degree of

Doctor of Philosophy in Chemical Engineering

University of Pittsburgh

2007

UNIVERSITY OF PITTSBURGH

SCHOOL OF ENGINEERING

This dissertation was presented

by

Jeffrey D. Martin

It was defended on

August 28, 2007

and approved by

Robert Enick, Ph.D., Professor, Chemical and Petroleum Engineering Department

Steve Little, Ph.D., Assistant Professor, Chemical and Petroleum Engineering Department

Ian Nettleship, Ph.D., Associate Professor, Department of Mechanical Engineering and Materials Science

Dissertation Director: Sachin Velankar, Ph.D., Assistant Professor, Chemical and Petroleum Engineering Department

THE EFFECT OF SURFACE-ACTIVE BLOCK COPOLYMERS ON TWO-PHASE FLOW

Jeffrey D. Martin, PhD

University of Pittsburgh, 2007

Blending two thermodynamically immiscible polymers to create a material with desirable properties is an attractive alternative to synthesizing polymers from new monomers. The microstructure of the blend often determines its physical properties and thus its uses. It is therefore beneficial to control the microstructure during blending, and it is well known that compatibilizers (macromolecular surfactants) can alter the morphological evolution of polymer blends. This work aims to examine the effect of compatibilizers on flow phenomena in which interfacial tension plays an important role, i.e. two-phase flow during the morphological development of immiscible polymer blends. We study compatibilizer effects on the two-phase flow of polymers at two length scales: single drops and macroscopic blends. A key concern is the effects of compatibilizer on rheological properties.

Experiments on the effect of surfactant on single drop dynamics in a PEO/PPO/Pluronic system showed complex and previously unknown and unusual behavior. We hypothesize that this unusual behavior was caused by the sample preparation protocol.

For multi-drop systems, or blends, of a PIB/PDMS model system near phase inversion, we identify the key role of the compatibilizer as immobilizing the interface, and we also identify the effect of such immobilization on two-phase rheology and coalescence suppression. Also, the compatibilizer affected the morphological development by decreasing the drop size through a combination of a decreased interfacial tension and coalescence suppression.

We attempted to exploit this coalescence suppression phenomenon as a mechanism of kinetically trapping the morphology in desired states. By varying the sequence of mixing, a double emulsion morphology was created. These double emulsion blends show complex relaxation behavior and an increase in viscosity due to the increased effective droplet volume fraction. We also attempted to exploit coalescence suppression to create a blend with a dispersed phase volume fraction exceeding 50%, but were unsuccessful, even with reactive compatibilization in a PA/PS system. New experimental work suggests it might be possible to use reactive compatibilizers that crosslink at the interface to effect large changes in two-phase morphology not possible with traditional compatibilizers.

TABLE OF CONTENTS

LIST OF TABLES

LIST OF FIGURES

LIST OF SYMBOLS

Symbol	Description	Units
α	interfacial tension	[N/m]
α_{eq}	equilibrium interfacial tension	[N/m]
α_{CC}	interfacial tension found by the CC method	[N/m]
α_{TOS}	interfacial tension found by the TOS method	[N/m]
$\Delta\alpha$	characteristic change in α induced by viscous stress	[N/m]
β	interfacial dilation modulus	[N/m]
δ	phase angle	[degrees]
ε	capillary disturbance amplitude	[m]
ε_0	initial capillary disturbance amplitude	[m]
ϕ	volume fraction	[-]
ϕ_{eff}	effective dispersed phase volume fraction	[-]
γ	strain	[-]
γ_0	amplitude of oscillatory strain	[-]
$\dot{\gamma}$	shear rate	[s^{-1}]
η	viscosity	[Pa.s]
η^*	complex viscosity	[Pa.s]
η_0^*	terminal complex viscosity	[Pa.s]
η_e	effective viscosity used in the CC model	[Pa.s]
Λ	capillary disturbance wavelength	[m]
Λ_{max}	dominant capillary disturbance wavelength	[m]

$\lambda_{1/2}$	time for half recovery	[s]
γ_∞	ultimate recovery	[-]
ν_k	natural log of the high-frequency modulus	ln[s^{-1}]
ρ	density	[kg/m^3]
$\Delta\rho$	density difference between dispersed and matrix phase	[kg/m^3]
σ	stress	[Pa]
τ_k	natural log of the droplet relaxation time	ln[s]
ω	angular frequency	[radians/s]
Ω	rotational rate	[rev/min]
a	droplet radius	[m]
A	interfacial area	[m^2]
Ca	Capillary number	[-]
Ca_{crit}	critical Capillary number	[-]
Ca_{ss}	steady-state Capillary number	[-]
D	droplet diameter	[m]
G	capillary disturbance growth rate	[s^{-1}]
G'	storage modulus	[Pa]
G''	loss modulus	[Pa]
G^*	complex modulus	[Pa]
k_{max}	dimensionless maximum capillary disturbance wavenumber	[-]
L	length of extended drop	[m]
M_w	weight-average molecular weight	[g/mol]
Ma	Marangoni number	[-]
p	viscosity ratio	[-]
R	droplet radius	[m]

ACKNOWLEDGEMENTS

I would foremost like to thank my advisor Dr. Sachin Velankar for his support, his constant enthusiasm, his patience, and most importantly, the knowledge that I have gained. It has been very enjoyable working in a group with such a good attitude and learning so many new things during the course of my work. I also thank all of my committee members: Dr. Enick, Dr. Little, and Dr. Nettleship for providing me with guidance and helpful insight into my work.

I would also like to thank the members of my group: Jun Wang, Todd Crosby, Prachi Thareja, Hsin-Ling Cheng, and Candice DeLeo for their helpful discussions and for generally making the lab an enjoyable place to work. Also, I thank the members of the Complex Fluids and Polymer Engineering group and all at NCL India, especially Dr. Ashish Lele, Shailesh Nagarkar, and Anurag Pandey, for making my stay in India extremely enjoyable and productive.

Furthermore, I gratefully aknowledge Purv Purohit and Mrs. Anuya Nisal for experimental assistance on TEM experiments; Mr. Anil Gaikwad, Melissa Angeles, and Hsin-Ling Chen for assistance on SEM experiments, Mr. Harshawardhan Pol and the PPC at NCL for assistance on microcompounding experiments, and the Center for Biological Imaging at the University of Pittsburgh for the use of their confocal microscope. I gratefully acknowledge BASF, Rhodia, Soltex, DuPont, Dow, and for raw materials used in experiments, and especially the Laboratory of Applied Rheology at the Katholieke Universiteit Leuven for supplying the PIB-PDMS diblock.

Finally, I would like to thank my family, my friends, and Katie for helping me along the way and helping to make me who I am today.

1.0 INTRODUCTION

Blending two thermodynamically immiscible polymers to create a material with desirable properties is an attractive alternative to synthesizing new polymers. A common example is rubber toughening. A small amount of rubbery polymer is dispersed into a glassy polymer in the melt state, and the resulting material is often much tougher and has a higher impact strength when compared to the bulk glassy polymer.[1] The microstructure of the blend often determines its physical properties. For example, a droplet-matrix morphology is desired for rubber toughening; a lamellar morphology is often used to improve the physical properties of a polymer, e.g. diffusion resistance; and a co-continuous morphology where a conductive material is co-continuous with an insulating polymer has interesting possible uses.

A compatibilizer is often used to control the morphology of polymer blends.[2-4] In the most general sense, a compatibilizer is an additive, not necessarily comprised of the two homopolymers, that modifies the interface of a polymer blend, stabilizes the blend, and improves the dispersion of one polymer into another. In the simplest case, compatibilizers are diblock copolymers (bcps) or graft copolymers of the two homopolymers in the blend. They are either synthesized in situ by an interfacial chemical reaction during blending, or pre-made and added to the blend.[2]

Compatibilizers generally serve two purposes: they improve dispersion by stabilizing the morphology during blending, and they improve interfacial adhesion in the final solid state of the blend. Due to their interfacial activity, compatibilizers affect the two-phase microstructural processes occurring during blending. Specifically, interfacial tension is important due to the two-phase nature of the flow, and compatibilizers modify the interfacial forces. Thus the blend morphology is a direct result of a competition between viscous and interfacial forces.

This work aims to examine the effect of compatibilizers on flow phenomena in which interfacial tension plays an important role, e.g. in microstructural detail (by studying the interfacially-driven shape evolution of a single, non-spherical drop), and in a bulk sense, e.g. by studying the morphology and rheology of a droplet-matrix blend. A key concern is the effects of compatibilizer on rheological properties.

2.0 BACKGROUND

2.1 DROP DYNAMICS UNDER QUIESCENT CONDITIONS

Perhaps the simplest example of flow in which interfacial tension is important is the shape evolution of a single, non-uniform drop under quiescent conditions. In this case, flow is entirely driven by interfacial tension. In our work, a spinning drop tensiometer (SDT) is used to study the effect of surface-active block copolymers on the dynamics of a single polymeric drop dispersed into another immiscible polymer. A schematic of a typical SDT is shown in Figure 2.1.

In this instrument, the higher density fluid is loaded into a glass tube and a drop of the lower density fluid is suspended in it. The tube is spun rapidly to cause the drop to centrifuge to the center and achieve an elongated, nearly spherocylindrical, shape.[5] This shape represents an equilibrium between interfacial and centrifugal forces, and the interfacial tension, α, can be calculated from[6]

$$\alpha = \frac{\Delta\rho\Omega^2 a_0^3}{4} \text{ provided } \frac{L_0}{a_0} > 4 \tag{1.1}$$

where $\Delta\rho$ is the density difference between the droplet and the matrix, Ω the rotational speed, and a_0 and L_0 the radius and half-length, respectively, of the spherocylindrical drop. In the equilibrium method of determining interfacial tension, a surfactant generally only decreases the interfacial tension between the two fluids. If all of the surfactant is not at the interface, the drop shape may change with time at a constant rotational speed as surfactant from the bulk diffuses onto the interface.

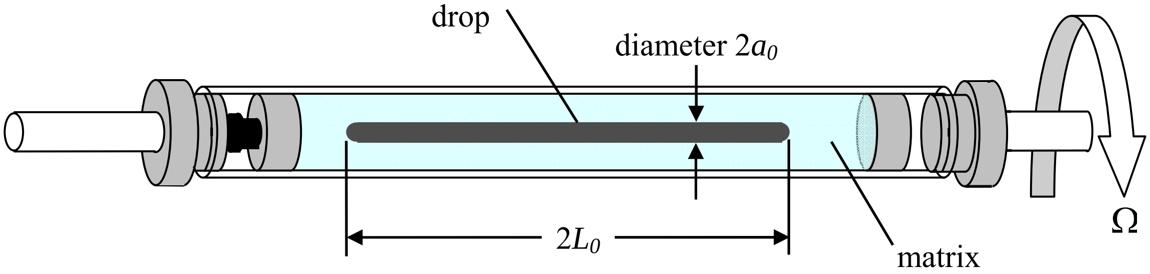

Figure 2.1: Schematic of a spinning drop tensiometer.

Apart from measuring interfacial tension, the SDT offers a simple means to deform a drop into a cylindrical shape in a controlled fashion and then study its interfacially-driven evolution under quiescent conditions. In the following two sections, we will review the behavior of surfactant-free, elongated drops and briefly discuss the possible effects of surfactant on the interfacially-driven flow of these drops. While the fundamentals of shape evolution are drawn from previous literature, we will also discuss how the SDT provides a convenient method to study such shape evolution.

2.1.1 Short Drops

The deformation of viscous drops was first studied by Taylor,[7] who studied small deformations. Rallison[8] provided a comprehensive review of the work on drop deformation, and Luciani *et al.*[9] extended this work to drop retraction after cessation of flow. They showed that, for short drops, retraction to an equilibrium shape is an exponential process and that the interfacial tension can be calculated from the shape evolution of the drop (the "deformed drop retraction method", DDRM).[9]

Longer drops are spherocylinders and the drop forms a dumbbell shape during retraction (see Figure 2.2). This occurs because for longer drops, retraction occurs mainly from the ends since there are no capillary pressure gradients near the drop center. Methods have been devised to calculate interfacial tension from the shape evolution of longer, retracting drops. Two such methods are the Cohen and Carriere method,[10] an approximate model, and the Tjahjadi, Ottino, and Stone method,[11] which is more rigorous model that takes into account the exact shape evolution of the drop.

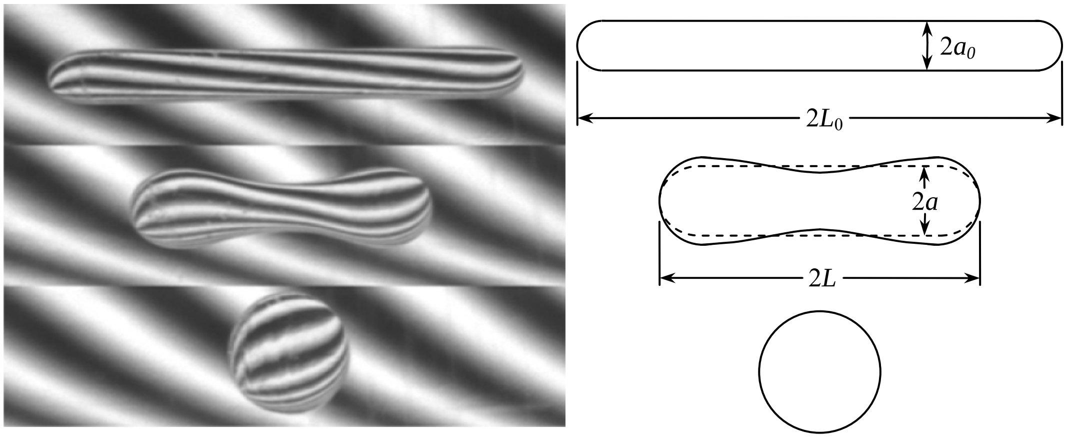

Figure 2.2: Images and schematic of a retracting drop. Drop depicted in dotted lines is a spherocylinder with volume equal to the actual drop.

No experiments or simulations have been done for retraction under quiescent conditions for a uniform surfactant coverage. There are however experiments and simulations that study retraction under quiescent conditions with flow-induced non-uniformities in interfacial surfactant concentration. These experiments and simulations will be discussed in Section 2.2.1. For an initially uniform surfactant coverage, we hypothesize that as retraction progresses the surfactant concentration at the tips will increase because initially retraction occurs mainly from the drop tips. As a result, there will be Marangoni stresses acting from the drop tips to the drop waist (high to low interfacial surfactant concentration). We hypothesize that these Marangoni stresses will retard the flow and slow retraction.

2.1.2 Long Drops

For very long drops having an aspect ratio (L_0/a_0) of about 10-15, the extended drop will break up during retraction thorough end-pinching (developing bulbous ends which pinch off) and capillary instabilities.[12] If the aspect ratio is moderate, the drop will develop bulbous ends which will break (end-pinching). An important advantage of the SDT for studying surfactant-related phenomena is that, before studying interfacial flow, the drop can be extended and held until the equilibrium between surfactant adsorption and desorption on the interface is achieved.

Capillary instabilities first studied by Lord Rayleigh,[13] who disregarded the fluid viscosities and studied an interially-dominated case of a liquid jet in air. Tomotika[14] later extended the theory to the viscous-dominated case of breakup of a Newtonian thread in a Newtonian matrix where no external flow fields are present. Tomotika showed that when random, infinitesimally small sinusoidal disturbances of varying wavelength (such as random temperature fluctuations) occur on the edge of a cylinder with an initial radius of a_0, only disturbances with a wavelength, Λ, larger than the initial thread circumference grow because the surface area is being reduced.[14] The disturbance amplitude, ε, grows exponentially with time according to the equation[14]

$$\varepsilon = \varepsilon_0 \exp(Gt) \tag{2.2}$$

where ε_0 is the initial disturbance amplitude, and t is time. The growth rate G is defined as

$$G \equiv \frac{\alpha}{2\eta_m a_0} f(p) \tag{2.3}$$

where η_m is the viscosity of the matrix, p the viscosity ratio, and $f(p)$ a tabulated function of the viscosity ratio.[14] The time evolution of a typical breaking thread is shown in Figure 2.3a, and a schematic of a breaking thread is shown in Figure 2.3c, with approximate internal and external flows shown as light arrows. Figure 2.3b will be discussed later. For a given viscosity ratio p, there will be one dominant wavelength, Λ_{max}, which grows fastest, and hence the thread will have a dominant wave number, k_{max}, as well.[14]

The spinning drop tensiometer can also be used to study capillary instabilities. In the SDT, a drop of the lower density fluid is centrifuged to form a long cylinder. The rotation is then abruptly stopped or decreased to nearly zero and the thread begins to retract and breakup by capillary instabilities.

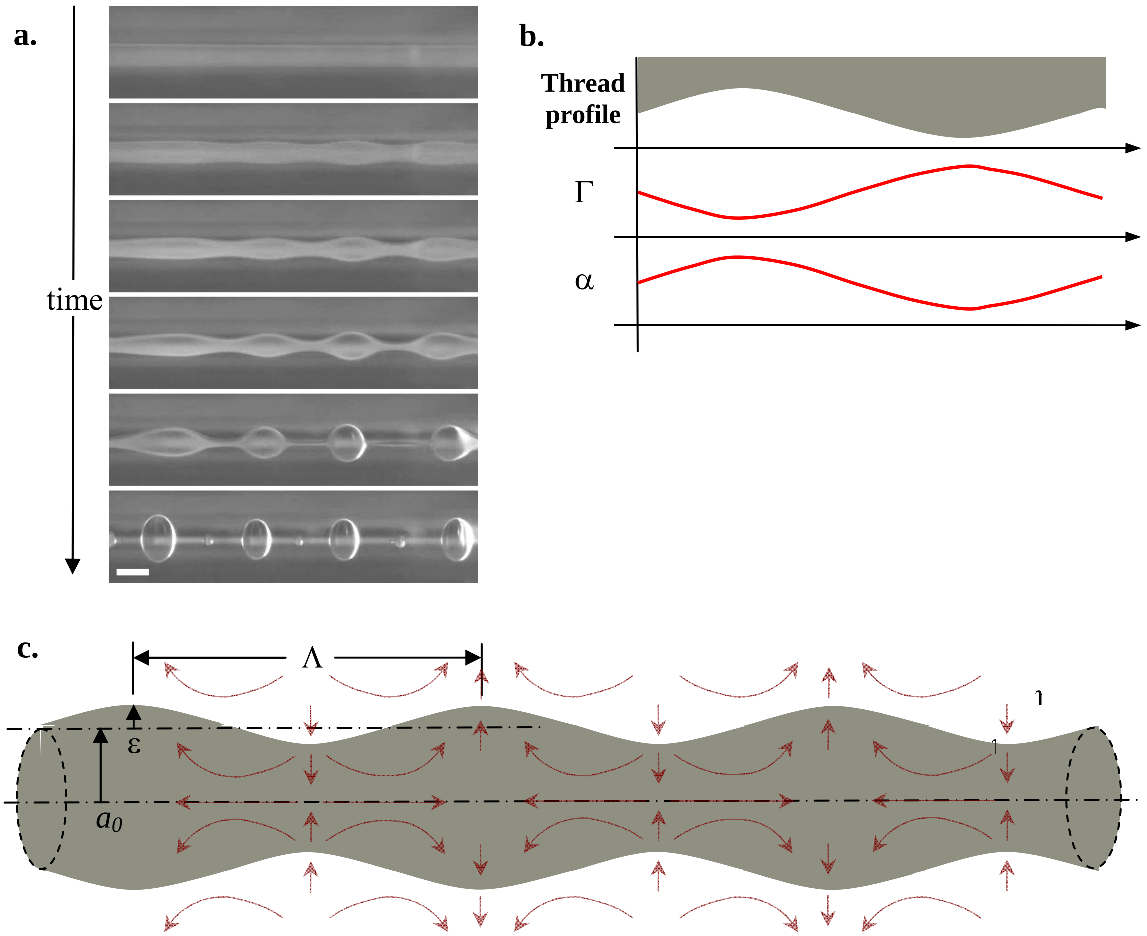

Figure 2.3: Schematic of a breaking thread. a.) image of a breaking thread (scale bar represents 1 mm), b.) approximate interfacial surfactant concentration and interfacial tension along the thread profile, and c.) showing approximate internal and external flows.

A method called the "breaking thread method"[15] has been devised to calculate the interfacial tension from the growth rate of capillary instabilities. In the standard breaking thread method, a thread of solid polymer of high aspect ratio is sandwiched between two sheets of the matrix polymer. The sample is then heated, the polymers melt, and the thread breaks up as shown in Figure 2.3a. By measuring the initial thread diameter and the evolution of the disturbance amplitude with time, the interfacial tension can be found from Equation 2.2.

The effect of surfactant on the dynamics of the capillary instabilities in the breaking thread method are predicted to be quite complex. As the instabilities form and begin to grow, there is a complex coupling between the flow inside the thread, the interfacial deformation, and the interfacial surfactant concentration. Locally, instabilities grow and form necks and waists, as seen in Figure 2.3. The higher capillary pressure caused by the higher curvature at the necks causes flows inside the thread that begin at the necks and flow toward the waists. These flows convect the surfactant along the interface from the necks to the waists, producing concentration gradients of high surfactant (lower interfacial tension) at the waists to low surfactant (higher interfacial tension) at the necks. In Figure 2.3b, a qualitative representation of the interfacial surfactant concentration, Γ, and interfacial tension are shown as a function of the position along the breaking thread. The concentration gradients induce Marangoni stresses that act tangentially along the surface from areas of low to high interfacial tension (waists to necks).[16] The Marangoni stresses retard the internal flow caused by the difference in capillary pressure, and slow the growth of the instability.

Hansen *et al.*[17] used linear stability analysis to determine the effect of a surfactant on the stability of a viscous fluid filament in a viscous fluid. They concluded that, for the case of low surfactant surface and bulk diffusivity, as is most likely the case in polymeric experiments, the growth rate is slowed by the compatibilizer at viscosity ratios far from one. Also, they concluded that the dimensionless wavenumber, defined as

$$k_{\max} = \frac{4\pi a_0}{\Lambda_{\max}} \tag{2.4}$$

increases (wavelength decreases, See Figure 2.3) upon addition of compatibilizer for systems with a viscosity ratio far from one. One of the goals of this work is to experimentally test this qualitative picture of the effect of surfactant.

2.2 DROP DYNAMICS UNDER FLOW

In addition to effects under quiescent conditions, surfactants can also affect drop dynamics under flow conditions. We will focus on the dynamics of an immiscible blend containing many drops. Immiscible blends are ubiquitous in the polymer, cosmetics, and food industries, among others. Apart from the scientific relevance of blends themselves, much knowledge on the dynamics of drops with and without a surfactant can be gained by studying blends.

In immiscible blends, there is a competition between viscous, interfacial, and inertial effects. Because polymers have relatively high viscosities, they offer a means to study systems where inertia is negligible. We will first discuss micro-processes and then the macroscopic rheology of compatibilized and uncompatibilized polymer blends in shear flow.

2.2.1 Single drop deformation and breakup

When a drop is subjected to simple shear flow it will deform, orient in the flow, and possibly break up. We will first discuss drop deformation, and then drop breakup. When a drop is under flow, there is a balance of viscous forces that tend to deform the drop, and interfacial forces that try to keep the interfacial area to a minimum and therefore resist deformation. Therefore, it makes sense to define a ratio of viscous to interfacial stresses, the capillary number, given by

$$Ca = \frac{\text{viscous stress}}{\text{interfacial stress}} = \frac{R\eta_m\dot{\gamma}}{\alpha} \tag{2.5}$$

where R is the drop radius and $\dot{\gamma}$ the shear rate. Under *steady shear* flow conditions, many different steady-state deformed drop shapes are possible depending on the capillary number and viscosity ratio. At low p, drops tend to form ellipsoids at low Ca and sigmoidal shapes at higher Ca.[18] For p of order unity, drops form ellipsoids; and at high p drops form ellipsoids at low Ca and slightly deformed spheres which rotate in flow at high Ca.[18]

Under shear flow, for a given viscosity ratio there exists a critical capillary number, Ca_{crit}, above which the drop will break up and below which the drop will attain an equilibrium, deformed shape oriented at some angle to the flow field. Experiments by Grace[19] indicate that droplet breakup is not possible for $p > 4$ in simple shear flow, the drop does not deform but instead exhibits rotational motion in the shear field. However, extensional flows can be used to break up drops of any viscosity ratio.[18]

For drops in shear flows, the mode of breakup is dependant on viscosity ratio for Ca slightly larger than Ca_{crit}. For $p \approx 1$ the extended drop thins at the waist and pinches off into two large drops, with several smaller satellite drops between; and for $p << 1$, the drop forms a pointed sigmoidal shape and small droplets are released from the end (tip streaming). For $p < 4$ and $Ca >> Ca_{crit}$, the drop stretches into a long fiber and breaks up by capillary instabilities.

We will now turn to surfactant effects on drop deformation and breakup. The most obvious effect of surfactant, the lowering of interfacial tension, acts to rescale Ca (see Equation 2.5). Beyond the simple rescaling of Ca, Stone and Leal[20] studied the effect of surfactant on drop deformation and breakup numerically and found two competing effects at large Ca. The first, convection of surfactant to the drop tips, lowers the interfacial tension and increases deformation (at low viscosity ratios, the increased deformation at the drop tips can cause tip streaming).[20] However, these interfacial tension gradients in turn induce Marangoni stresses that retard surface flow (see Figure 2.4b). Secondly, as the drop is stretched the interfacial area increases, and the surfactant becomes diluted, raising the interfacial tension and decreasing deformation. A significant increase in Ca_{crit} is seen for large values of a parameter β which is a measure of the sensitivity of the interfacial tension to changes in surfactant concentration. Stone and Leal[20] attribute this increase in Ca_{crit} to increased Marangoni stresses, larger steady deformations, and dilution effects. With a larger value of Ca_{crit}, higher capillary numbers (higher shear rates) are needed to deform drops to the point of breakup.

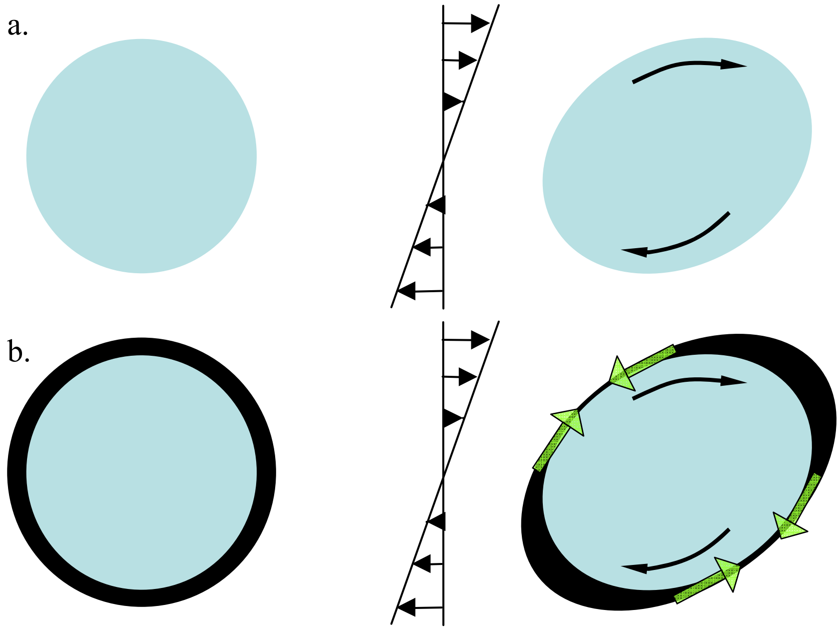

Figure 2.4.: a.) Uncompatibilized droplet at rest and in shear flow for finite *Ca*, b.) compatibilized droplet at rest and for *Ca* → 0. The thickness of the drop boundary is indicative of the local compatibilizer concentration. Thin arrows show streamlines; thick arrows show Marangoni stresses.

In later work, Milliken and Leal[21] studied the same problem (extensional flow, insoluble surfactant), taking into account Marangoni stresses caused by gradients in interfacial tension, which in turn are caused by gradients in surfactant interfacial concentration along the interface which arise from the convection of surfactant by the bulk flow. The most important observation was that Marangoni stresses act to retard the surface flow, thus slowing the droplet dynamics. Pawar and Stebe[22] extended this work to incorporate a nonlinear equation of state for describing the surfactant on the interface, a feature lacking in earlier work. Milliken and Leal[23] later extended their earlier work to incorporate a surfactant that is soluble in the bulk, and found that surfactant diffusion from the bulk to the interface tended to relax somewhat, but not entirely, the interfacial tension gradients and therefore the Marangoni stresses. Stebe *et al.*[24] showed that if a soluble surfactant has fast interfacial sorption kinetics and its bulk concentration is above the critical micelle concentration (CMC), the drop behaves like a surfactant-free drop, save for a uniform, reduced interfacial tension. This occurs because any interfacial surfactant concentration gradients that arise can be quickly relaxed simply by adsorption onto the interface from the excess surfactant molecules (micelles) in the bulk.

Much research has been done on this problem (i.e. effect of the ratio of the droplet to matrix viscosity, ability of the surfactant to decrease the interfacial tension, surfactant-surfactant association on the interface, etc.) and the present consensus is that, for simple flows (shear and extensional), Marangoni effects dominate at low viscosity ratio and low to intermediate surface coverage, and the dilution effect is significant at high surface coverage. At higher viscosity ratios, the dynamics of a surfactant-free drop are much slower, so surfactant effects that tend to slow down the droplet dynamics do not have as large of an effect.[25] Numerical simulations by Gonzalez-Mancera[26] confirm the aforementioned conculsions, where comparable. Furthermore, these simulations show that the internal circulation flow of a surfactant-laden drop in extensional flow is greatly affected by the dynamics at the interface.[26] For example, in the case of intermediate surfactant concentration where surfactant is accumulated at the drop tips and Marangoni stresses are large, the circulation flow inside the drop shifted to the center of the drops, leaving stagnation points at the tips; and for the case of complete surface coverage, the interface was shown to be immobile with no internal flow.[26]

Moreover, if surfactant accumulates at the drop tips, the curvature will increase to accommodate the decrease in interfacial tension. This leads to tip stretching and may cause tip streaming.[27,28] Tip streaming occurs when there is a large curvature at the drop tips causing the tips to thin and eject a stream of small drops.

2.2.2 Coalescence

When an emulsion is sheared, the flow induces collisions, and sometimes coalescence, of the drops. As droplets collide, their interfaces deform and a film of matrix fluid is formed between them. For the droplets to coalesce, the film must drain to a critical value where van der Waals forces between the droplets become important and the film ruptures. If the time it takes for the film to drain and rupture is less than the time in which the droplets are in contact, coalescence will occur. If not, the droplets will not coalesce (see Figure 2.5).

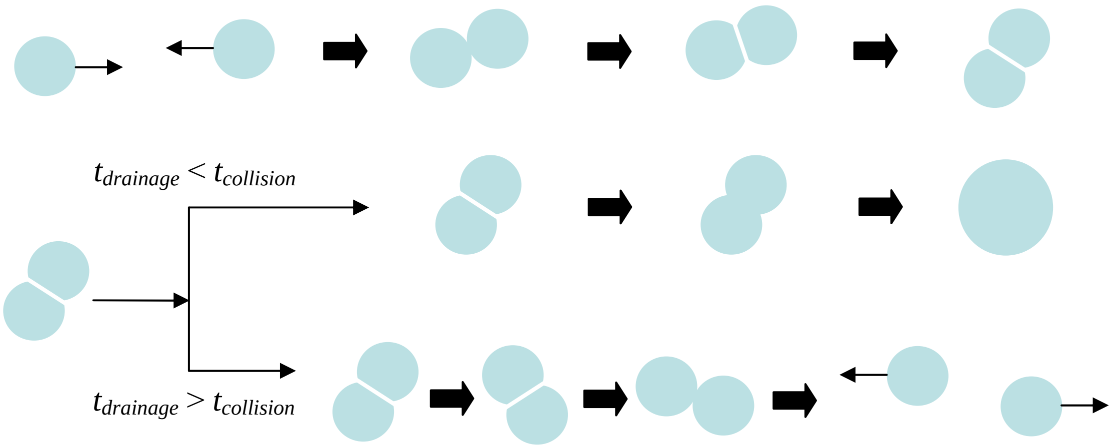

Figure 2.5: Coalescence process in emulsions.

The mobility of the interface during the collision and drainage steps is very important in determining whether or not droplets coalesce. For example, when $p \approx 1$ the interface is said to be partially mobile, and most of the resistance to film drainage comes from the viscous stresses within the droplet. When $p << 1$, the interface is fully mobile and the droplet provides little resistance to film drainage, making coalescence more likely for a given collision time. However, the drops deform more and the area that the film must drain from becomes larger, decreasing the likelihood of coalescence. For a system with $p >> 1$ the interface is said to be immobile and the interfaces do not deform, making coalescence less likely for a given collision time.

Surfactants can sometimes suppress droplet coalescence, and two mechanisms[29] have been proposed as to why: a Marangoni stress mechanism and a steric hindrance mechanism. The Marangoni stress mechanism[30-32] proposes that, as the drops approach each other, the drainage flow between the two drops causes the surfactant to be squeezed out of the region between the two drops. This causes a gradient in the compatibilizer concentration and thus a gradient in interfacial tension. In an attempt to relax the interfacial tension gradients, Marangoni stresses act tangentially along the interface in the direction opposite to the drainage flow, thus retarding the surface flow and drainage flow. The interface can become either partially or fully immobile (depending on the strength of the Marangoni stresses), which severely decreases the rate of coalescence. The Marangoni stress mechanism ignores the nature (macromolecular or not) of the surfactant: the only requirement is that the surfactant is able to decrease the interfacial tension. The steric hindrance mechanism,[3] which applies more to macromolecular surfactants (compatibilizers), postulates that, as two drops approach each other, the surfactant layer on the interfaces must compress and a compressive force and thus repulsive potential arises between the drops, inhibiting coalescence.

2.3 MORPHOLOGICAL DEVELOPMENT OF BLENDS

As mentioned in Section 1.0 , the morphology of a blend often determines its physical properties, which in turn determine suitable end-uses of the blend. Primarily, the morphology of a blend is determined by the volume fractions and viscosities of each component, and the strength and type of flows that the blend encounters. First, the effects of component volume fraction and viscosity ratio on the morphology will be discussed. Then, the effects of flow will be covered. Finally, the effect of a compatibilizer on the morphological development will be discussed.

For droplet volume fractions $\phi_d << 1$, a morphology with discrete drops in a continuous matrix is expected. As the dispersed phase volume fraction increases, eventually the blend will undergo phase inversion and the dispersed phase will become the continuous phase, and vice versa. Near the phase inversion point, the blend may or may not adopt a co-continuous morphology. Two main factors determine where the phase inversion point lies: the component volume fractions and the viscosity ratio. Paul and Barlow[33] stated that the condition for phase inversion can be expressed as

$$\frac{\phi_A}{\phi_B} = \frac{\eta_A}{\eta_B} \tag{2.6}$$

When $p \neq 1$, the low-viscosity fluid tends to become the matrix and the high-viscosity fluid tends to become the dispersed phase, even if the volume fraction of the high-viscosity fluid is significantly higher (see Figure 2.6).[1]

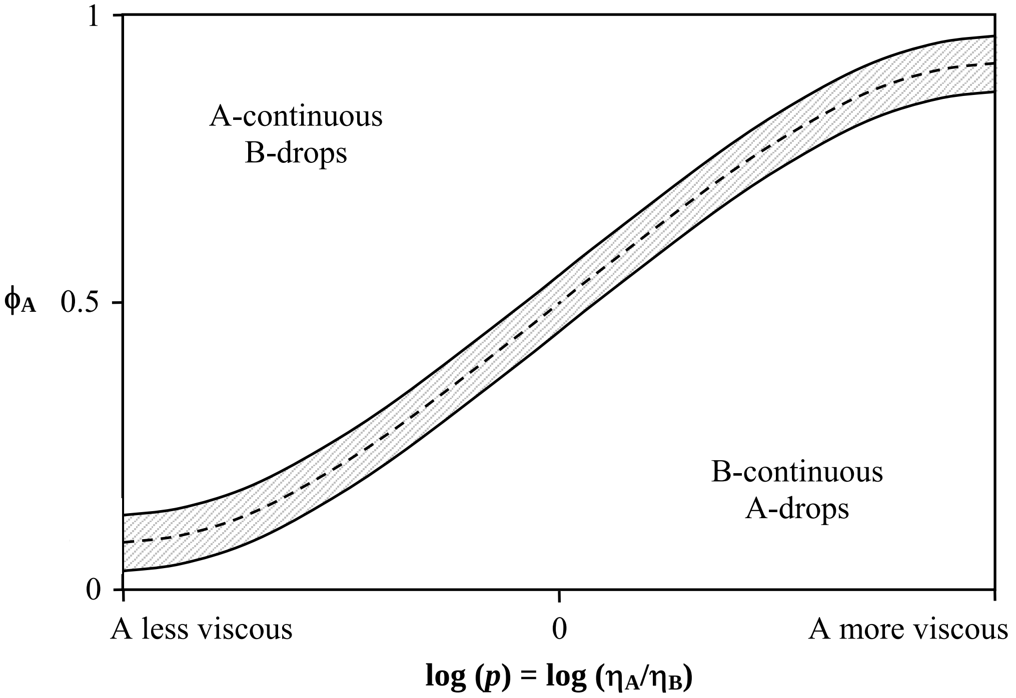

Figure 2.6: Volume fraction of component "A" versus viscosity ratio for an immiscible A/B binary polymer blend (adapted from Utracki[1]). The shaded area denotes a co-continuous morphology. Dotted line is for a blend that does not show co-continuous behavior.

When a blend is processed, the drops can undergo many different types of behavior, all of which affect the blend morphology. These behaviors include deformation, breakup, coalescence, and retraction. Note that, as discussed in Section 2.2.1 for a *single drop*, when the viscosity ratio is larger than about four, a drop cannot be broken by simple shear, only extensional flow. For Ca slightly larger than Ca_{crit} the modes of breakup for shear flow are as follows: for $p \approx 1$, the extended drop thins at the waist and pinches off into two large drops with several smaller satellite drops between, and for $p << 1$, the drop forms a pointed sigmoidal shape and small droplets are released from the end (tip streaming). For $Ca >> Ca_{crit}$, the drop stretches into a long fiber and breaks up by capillary instabilities.

For *blends* at steady state, the drop size (for blends with droplet-matrix morphologies), and hence the morphology, is determined by a balance of breakup and coalescence events. For example, if a drop in a blend has a certain size such that, at an applied stress or shear rate, its capillary number is below the critical capillary number Ca_{crit} (see Equation 2.5 and Section 2.2.1), it will not break up in the applied flow field. Instead, it will become oriented along the flow field and will be deformed to an extended shape that is determined by a balance of viscous and interfacial stresses. As the blend is sheared, this deformed drop will continually collide with other deformed drops and a coalescence event will eventually occur. As this drop grows in size, its capillary number also grows. Once the drop has grown in size to such an extent that its capillary number is at or above Ca_{crit}, the drop will breakup and rupture into two or more smaller droplets, all of which now have $Ca < Ca_{crit}$. These smaller drops then orient and deform, and can coalesce with other deformed droplets. This process repeats indefinitely and a steady-state droplet size is obtained where the steady-state capillary number $Ca_{ss} = Ca_{crit}$. This is a simplified picture, and sometimes reaching steady state can take a very long time. Such cases include dilute droplet volume fractions (less than a few percent), and instances where coalescence is suppressed or retarded, such as in compatibilized blends, blends with higher viscosity ratios, and blends with large drop sizes.

When the capillary number of the droplets is much larger than Ca_{crit}, for instance in startup flows or when a sufficiently large step up in shear rate or stress is performed, the droplets become highly extended and break up into much smaller droplets by capillary instabilities (see Figure 1 in Tucker and Moldenaers[18]). These small drops then orient and deform, and the dynamic equilibrium between coalescence and breakup begins.

Compatibilizers generally tend to reduce the drop size in blends through a combination of a decreased interfacial tension (drops deform easier) and coalescence suppression.[34] Two mechanisms that have been proposed as to why compatibilizers are able to suppress droplet coalescence have been discussed in Section 2.2.2. Regardless of the mechanism by which compatibilizers suppress droplet coalescence, the decrease of the average drop size is generally substantial, and adding compatibilizers often causes a much finer morphology, i.e. a much smaller droplet size compared to the uncompatibilized blends. It should be noted that if coalescence is not suppressed, the morphological development is qualitatively the same as in uncompatibilized blends, but with a decreased drop size due to the lower interfacial tension.

Our own work suggests that compatibilizers (premade and reactive) are not able to affect the phase inversion point (see Section 5.0). Studies on the effect of compatibilizer on the phase inversion point are lacking, but there have been studies on the effect of compatibilizer on co-continuous morphologies. For example, Galloway *et al.*[35] found that premade, symmetric diblock copolymers of varying molecular weights (ranging from 6,000 to 200,000 g/mol) were able to reduce the phase size and coarsening rate of a co-continuous polystyrene/high density polyethylene blend. A block copolymer of 40,000 g/mol was shown to have the most significant effect on the blend morphology and coarsening rate, most likely due to a balance between the ability of the compatibilizer to diffuse to the interface and its ability to lower the interfacial tension.[35] These effects, slower coarsening kinetics and decreased characteristic length scales, are analogous to compatibilizer effects on droplet-matrix blends.

To summarize, the morphological development of polymer blends during processing is a complicated process that depends on the volume fractions of each component, the viscosity ratio, and the type and strength of flow. For dilute blends, a droplet matrix morphology with the minority component dispersed as droplets is expected, and as the concentration of the dilute component is increased, phase inversion will occur. For viscosity ratios larger or smaller than order unity, the more viscous component tends to form the dispersed phase, even if it is the majority component (see Figure 2.6). The steady state drop size is determined by a dynamic equilibrium between breakup and coalescence in shear flow (for $p < 4$ in shear flow). Under start-up flow conditions or a large step-up in shear rate or stress, the drops deform to a large extent and break up by capillary instabilities. The resulting small droplets then undergo the dynamic equilibrium between breakup and coalescence. A compatibilizer decreases the drop size of the blend through a combination of a decreased interfacial tension and, coalescence suppression. Possible mechanisms that explain why coalescence suppression occurs include a steric hindrance mechanism, and a Marangoni stress mechanism.

2.4 RHEOLOGY OF BLENDS

Rheology, the study of material properties during flow and deformation, is often used to gain information about the viscoelastic properties of a material. By applying simple flow fields, the deformation within the sample is kept homogeneous and much information and insight into the properties of a material can be gained. The rheology of blends is particularly interesting in that a blend of two Newtonian fluids shows non-Newtonian, viscoelastic behavior. For example, mechanical energy can be stored by interfacial deformation.

2.4.1 Dynamic oscillatory behavior

Small-amplitude oscillatory shear is often used to probe the dynamics of structured fluids such as polymer blends without significantly affecting the microstructure. This is accomplished by subjecting the blend to a sinusoidal strain (γ) at various frequencies (ω) as per Equation 2.7

$$\gamma = \gamma_0 \sin(\omega t) \tag{2.7}$$

The stress response of the sample, which is out of phase with the strain by a phase angle δ, is given by

$$\begin{aligned} \sigma = \sigma_0 \sin(\omega t + \delta) &= (\sigma_0 \cos\delta)\sin(\omega t) + (\sigma_0 \sin\delta)\cos(\omega t) \\ &= \gamma_0 G' \sin(\omega t) + \gamma_0 G'' \cos(\omega t) \end{aligned} \tag{2.8}$$

where *G'* and *G"* are the storage and loss moduli, respectively. *G'* is indicative of solid-like or elastic behavior and *G"* is indicative of liquid-like or viscous behavior. The complex modulus is defined as

$$G^* \equiv G' + iG'' \tag{2.9}$$

where $i = \sqrt{-1}$, and the magnitude of G^* is given by

$$\left|G^*\right| = \sqrt{G'^2 + G''^2} \tag{2.10}$$

The complex viscosity, η*, is defined as

$$\eta^* \equiv \frac{G^*(\omega)}{i\omega} \tag{2.11}$$

and often the magnitude of the terminal complex viscosity, given by

$$\left|\eta_0^*\right| \equiv \lim_{\omega \to 0} \frac{\left|G^*(\omega)\right|}{\omega} \tag{2.12}$$

is used as an indication of the zero-shear viscosity of a material.

A polymer blend shows an enhanced elastic response, i.e. larger *G'*, at low frequencies that arises due to the droplets, which become deformed from the applied strain and relax because of interfacial tension. The frequency at which the relaxation time of the droplets occurs is proportional to the drop size, and if the frequency at which the relaxation time of the drops occurs is much smaller than those for the bulk phases, the droplet relaxation time will appear as a distinct shoulder in a plot of *G'* versus ω. The relation between the drop size and the relaxation time makes small-amplitude oscillatory shear experiments a very useful microstructural probe.

Reimann *et al.*[36] and Van Hemelrijck *et al.*[37] showed that at low to moderate compatibilizer loadings, a second shoulder appeared in the plot of *G'* versus ω, indicative of a slow relaxation process caused by the compatibilizer. We have also shown this result in our work.[38] This slow relaxation process has been attributed to interfacial viscoelasticity.[39,40] At low to moderate compatibilizer loadings, the applied oscillatory shear causes compatibilizer concentration gradients along the interface, which relax by Marangoni stresses. This interfacial relaxation process is manifested as a second shoulder in *G'* that occurs at low frequencies and is insensitive to the drop size.[37,38] As the compatibilizer content is increased, this second shoulder moves to higher frequencies and eventually the timescale of the interfacial relaxation process becomes comparable to the timescale of the droplet relaxation, causing the two shoulders to merge.[37,38,41] Thus, at high compatibilizer loadings, the *G'* curves look qualitatively similar to uncompatibilized blends. However, just because there appears to be only one shoulder in the *G'* curves does not mean that interfacial viscoelasticity is absent.[41]

2.4.2 Other rheological properties

Blends of Newtonian fluids show a wide range of non-Newtonian behavior. For example, dispersions of deformable drops have viscosities higher than both bulk fluids because of hydrodymanic interactions between drops. When shearing a dispersion of deformable drops, the drops become oriented along the direction of flow. This global orientation of the interface leads to a normal stress difference and shear thinning of the blend. Because of shear thinning, steady shear viscosities are always less than $\left|\eta_0^*\right|$. Upon cessation of flow, interfacial tension causes the deformed drops to retract to spheres. This induces elastic recovery of the blend. Much other non-Newtonian behavior has been documented elsewhere.[18]

There is only a small amount of information on how a compatibilizer affects the steady shear viscosity, normal stress difference, creep recovery, and shear thinning behavior of polymer blends. It has been shown that, in a ten weight percent PIB in PDMS blend, a compatibilizer causes the steady shear viscosity to increase at all p, and reduces the shear-thinning tendency of the blends and the interfacial contribution to the first normal stress difference at low p.[41] Van Helemrijck *et al.*[42] showed that for highly compatibilized poly(isoprene)/PDMS blends of viscosity ratio nearly unity, the compatibilizer causes the steady shear viscosity to increase and the first normal stress difference to decrease. It has also been shown that a compatibilizer tends to increase the ultimate recovery after cessation of shear, but also tends to slow down the recovery kinetics in 10, 20, and 30 weight percent PIB in PDMS blends.[43] One goal of this work is to experimentally investigate the effect of block copolymers on the rheology of polymer blends *with nearly equal amounts of the two phases*.

3.0 DROP DYNAMICS UNDER QUIESCENT CONDITIONS

As discussed in Section 2.1, the dynamics of a single, deformed drop depend on the initial aspect ratio and the shape of the drop. Short drops retract exponentially, moderately extended drops develop bulbous ends (which may or may not pinch off) during retraction, and long drops develop bulbous ends which pinch off while the rest of the drop breaks up by capillary instabilities. Surfactants affect the two-phase flow during breakup primarily through Marangoni stresses, which retard interfacial flows. Variables affecting surfactant effects on two-phase flow are viscosity ratio, bulk solubility and bulk and surface diffusivity of surfactant, and the surfactant's ability to reduce the interfacial tension (therefore interfacial concentration gradients will induce Marangoni stresses).

In this section we present experimental results on single-drop systems. The effect of viscosity ratio on drop retraction is studied in Section 3.1, and the effect of surfactant on capillary instabilities is studied in Section 3.2. It should be noted that while our primary interest is on the effect of surface-active block copolymers, we recognized a deficiency in the literature on drop retraction in the absence of surface-active species. Specifically, a common method for analyzing IFRM data was found to be incorrect. This will be addressed in Section 3.1.

3.1 DROP RETRACTION UNDER QUIESCENT CONDITIONS

Traditional methods of measuring the interfacial tension between low molecular weight fluids e.g. the pendant or sessile drop method, the Wilhelmy balance, and the spinning drop method do not work well for molten polymers because their high viscosity requires unacceptably long times for equilibration. Therefore "dynamic" methods that use the kinetics of interfacial tension-driven motion to obtain the interfacial tension have been devised for polymers.[9,10,15,44-46] One such method, the Imbedded Fiber Retraction method (IFRM), is the subject of this section. The purpose is to demonstrate that the Cohen and Carriere (CC) model[10,44] that is commonly used to analyze fiber retraction experiments can cause large errors in interfacial tension, whereas an alternate analysis by Tjahjadi, Ottino and Stone (TOS)[11] gives reliable interfacial tension values. A notable feature of our experimental approach is that the fiber retraction experiments are benchmarked rigorously: we are able to measure the *equilibrium* interfacial tension *in the same experiment* as the fiber retraction.

In a typical IFRM experiment, a drop is extended to a modest aspect ratio (usually less than ten) and the interfacial tension is calculated from the evolution of the drop shape during retraction. The tips of an extended fiber have a higher capillary pressure than the mid-section due to the higher curvature, and this pressure gradient drives the retraction of a surfactant-free fiber.[12] Stone and Leal[12] showed that retraction occurs mainly from the ends, and as a result the drop develops bulbous ends during retraction (see Figure 2.2). From a plot of the drop length L versus the initial drop diameter $2a_0$ or D_0, the interfacial tension can be calculated. Two such methods of calculating interfacial tension, the Cohen and Carriere (CC),[10] and Tjahjadi, Ottino, and Stone (TOS)[11] methods were available, and it was not clear which method was superior. In the preliminary portion of this research, we investigated this experimentally.

Previous publications have attempted to evaluate whether different dynamic methods give reliable interfacial tension values. Unfortunately, most of these publications suffered from poor benchmarking. In some cases, the results of the dynamic method being evaluated were compared against benchmark values of interfacial tension also measured by other dynamic methods. In some publications, comparisons against equilibrium interfacial tensions were indeed made, however the equilibrium values were measured under considerably different conditions (e.g. an equilibrium single pendant drop experiment versus a dynamic experiment on an immiscible blend). Poor benchmarking such as this is most likely the reason why the error in the CC method went unnoticed. In this section we instead compare the results of fiber retraction with the *equilibrium* interfacial tension measured *independently in the same experiment.* Such a rigorous test of the fiber retraction method has not been performed previously.

The effect of a surfactant on drop retraction when the initial surfactant concentration is uniform, as we expect would be the case in our SDT, is not known. Velankar *et al.*[47] studied the retraction of surfactant laden drops through numerical simulations; however, their drops were deformed in the simulations by first shearing the matrix, and then allowed to retract. The shear flow creates a non-uniform distribution of surfactant with a high surfactant concentration at the drop tips and a low surfactant concentration at the waist. Velankar *et al.* showed that this non-uniform surfactant concentration causes errors in the measurement of interfacial tension by the IFRM. Even though we expect the surfactant concentration to be uniform on all drops in the SDT prior to retraction, retraction begins at the drop tips and this non-uniform flow is expected to lead to a non-uniform distribution of surfactant, i.e. a pileup of surfactant in the drop midsection which will lead to surfactant concentration gradients and Marangoni stresses that slow retraction. Thus the retraction of a surfactant-laden drop is expected to be qualitatively different from that of a surfactant-free drop. Investigating this is one of the goals of this work.

3.1.1 Materials and Methodology

Poly(dimethylsiloxane) (PDMS) (Rhodia Silicones) and polyisobutylene (PIB) (Soltex Chemicals) were used as the matrix and drop phases, respectively, for viscosity ratios of 0.368, 0.722, 2.03, and 5.18. For a viscosity ratio of 0.0330, PDMS was used as the matrix phase and polybutadiene (PB) (Aldrich) as the drop phase. The properties of all materials used are listed in Table 3.1. All materials were Newtonian under experimental conditions and their viscosities were measured at room temperature using a TA Instruments AR 2000 rheometer. All polymers were used as received.

Table 3.1: Materials used in single drop retraction experiments.

Fluid	Density (g/ml)	Viscosity (Pa.s)
PDMS 30,000	0.972	33.1
PDMS 100,000	0.972	93.2
PIB 24	0.898	34.3
PIB 32	0.904	67.3
PIB 124	0.904	483
Polybutadiene	0.90	3.08

Experiments were performed at room temperature in a home-built SDT using a precision bore glass tube of inner diameter 12.7 mm. Due to lensing effects of the cylindrical tube, images of drops inside the tube appear distorted and accurate calibration of the drop dimensions along the axial and the radial direction of the tube is crucial. Calibration was done as follows: In all pairs of fluids, the PDMS is the higher density phase and forms the matrix. Accordingly, each

PDMS fluid was loaded into the SDT tube, a solid polyethylene sphere of known diameter was suspended in it, and the tube was spun. Since polyethylene has a lower density than PDMS, the sphere centered itself along the axis of rotation and was subsequently imaged. In the images, the sphere appeared elliptical, with the ratio of its radial dimension to its axial dimension being roughly 1.4. This ratio, which is close to the refractive index of PDMS as expected,[48] was used to correct the images of drops so as to obtain their dimensions accurately.

The desired PDMS was loaded into the SDT tube, and the desired PIB or PB was added as a drop. The tube was spun at constant speed (Ω typically 3000 to 9000 rpm) until a steady drop shape of a convenient aspect ratio was reached, and the drop was imaged. The rotational speed was then abruptly reduced to a low value (about 500 rpm), and the subsequent retraction was imaged. Rotation could not be ceased altogether because the droplet would rise to the top of the tube due to gravity, and therefore wall effects would interfere with the retraction process. This procedure (equilibration at a certain aspect ratio, followed by retraction) was repeated for at least four rotational speeds. In all cases, the diameter of the retracting drop was no more than 20% of the inner diameter of the tube.

The radii, a_0, of the drops during steady spinning gave the equilibrium interfacial tensions, α_{eq}, from Equation 1.1. These are listed in Table 3.2. Consistent values were obtained at all rotational speeds giving confidence that equilibrium was indeed reached.

Furthermore, radii, a_0, and the lengths, L_0, of the drops during steady spinning also gave the drop volumes from Equation A.1. The images of the drops recorded during retraction gave $L(t)$ directly; these combined with the drop volume gave the effective radius, $a(t)$ of the drops during retraction. See Appendix Section 1.01(a)(i)A.1 for details of the implementation of the CC method, and Appendix Section 1.01(a)(i)A.2 for details of the TOS method.

3.1.2 Results

Substituting $\alpha = \alpha_{eq}$ into Equations A.2 and A.5 result in predictions of the retraction kinetics of the CC and the TOS models respectively. Here we will first compare these predictions to the measured retraction kinetics at all values of the viscosity ratio p, but only for drops with initial aspect ratios close to eight. These will qualitatively illustrate whether the two models are able to successfully reproduce the retraction kinetics or not. This is done in Figure 3.1a and b.

Furthermore, Equations A.2 and A.5 can also be fitted to the measured data using α as a fitting parameter to obtain α_{CC} and α_{TOS} as the values of interfacial tension obtained by the CC and TOS methods respectively. A comparison of these values with α_{eq} quantifies the success of either model. Results at all viscosity and aspect ratios are presented in Table 3.2.

Table 3.2: Interfacial tension in mN/m calculated for various viscosity ratios and initial aspect ratios.

System	p	L_0/a_0	α_{eq}[a]	α_{CC}[b]	α_{TOS}[c]
Polybutadiene / PDMS 100,000	0.0330	2.95		3.9	5.0
		5.13	4.9	4.9	5.0
		5.72		4.6	4.8
		6.42		4.3	4.5
		7.92		4.4	4.5
		8.72		4.8	4.6
PIB 24 / PDMS 100,000	0.368	3.47		1.9	2.1
		6.20	1.7	1.8	2.0
		9.43		1.6	1.8
		10.3		1.6	1.7
PIB 32 / PDMS 100,000	0.722	4.05	2.2	3.2	2.8
		4.95		3.1	2.8
		8.28		2.8	2.7
		9.63		2.6	2.6
		14.1		2.6	2.2
PIB 32 / PDMS 30,000	2.03	4.65	2.9	5.3	3.3
		8.61		5.5	2.9
		8.78		7.0	3.4
		9.72		7.3	3.2
PIB 124 / PDMS 100,000	5.18	5.32	3.0	8.3	3.5
		5.85		8.7	3.5
		7.33		9.0	3.3
		7.98		9.4	3.4
		8.48		8.9	3.3

[a] From Equation 1.1; average of spinning drops with $L_0/a_0 > 4$.

[b] Least squares fit of Equation A.2 to $f\left(\frac{a}{R_0}\right) - f\left(\frac{a_0}{R_0}\right)$ versus t data.

[c] Least squares fit of Equation A.5 to L/R_0 versus t data.

Figure 3.1a presents retraction data at $L_0/R_0 \approx 8$ in the format suggested by the CC model. The solid lines represent Equation A.2 with $\alpha = \alpha_{eq}$. It is clear that the lines capture the retraction kinetics very well at low viscosity ratio, but very poorly for p exceeding unity. Fitting Equation A.2 to the data using α as the fitting parameter results in α_{TOS} values that are close to α_{eq} at low p but much larger than α_{eq} at high p (Table 3.2). We note that when performing fits, the "linear" region of these plots must be defined somewhat arbitrarily, and significant error may result from improper fitting. Indeed, Demarquette *et al.*[49] reported an unexpectedly high α_{CC} value even for a sample at $p = 0.06$; this may perhaps be related to fitting in an unsuitable region. The conclusion then is that α_{CC} will necessarily be much larger than α_{eq} at high p, and α_{CC} may approach α_{eq} at low p, provided the appropriate range of data is chosen for fitting.

Figure 3.1b replots the same results in the format suggested by the TOS model. The solid lines are Equation A.5 with $\alpha = \alpha_{eq}$. Clearly, the lines track the data reasonably well at all viscosity ratios. Fitting Equation A.5 to the data with α as a fitting parameter results in α_{TOS} values that are comparable to α_{eq} at all p. The most significant deviations (up to 24%) appear at the smallest aspect ratios; these are at the limit of the expected experimental errors. At lower aspect ratios than those presented here, even larger errors were evident. The conclusion then is that the TOS model yields interfacial tension values close to the equilibrium interfacial tension. Furthermore, while the fits were performed using a linear least squares analysis, nearly identical values were obtained by "eyeballed" fits, suggesting that the procedure is robust and easy to implement.

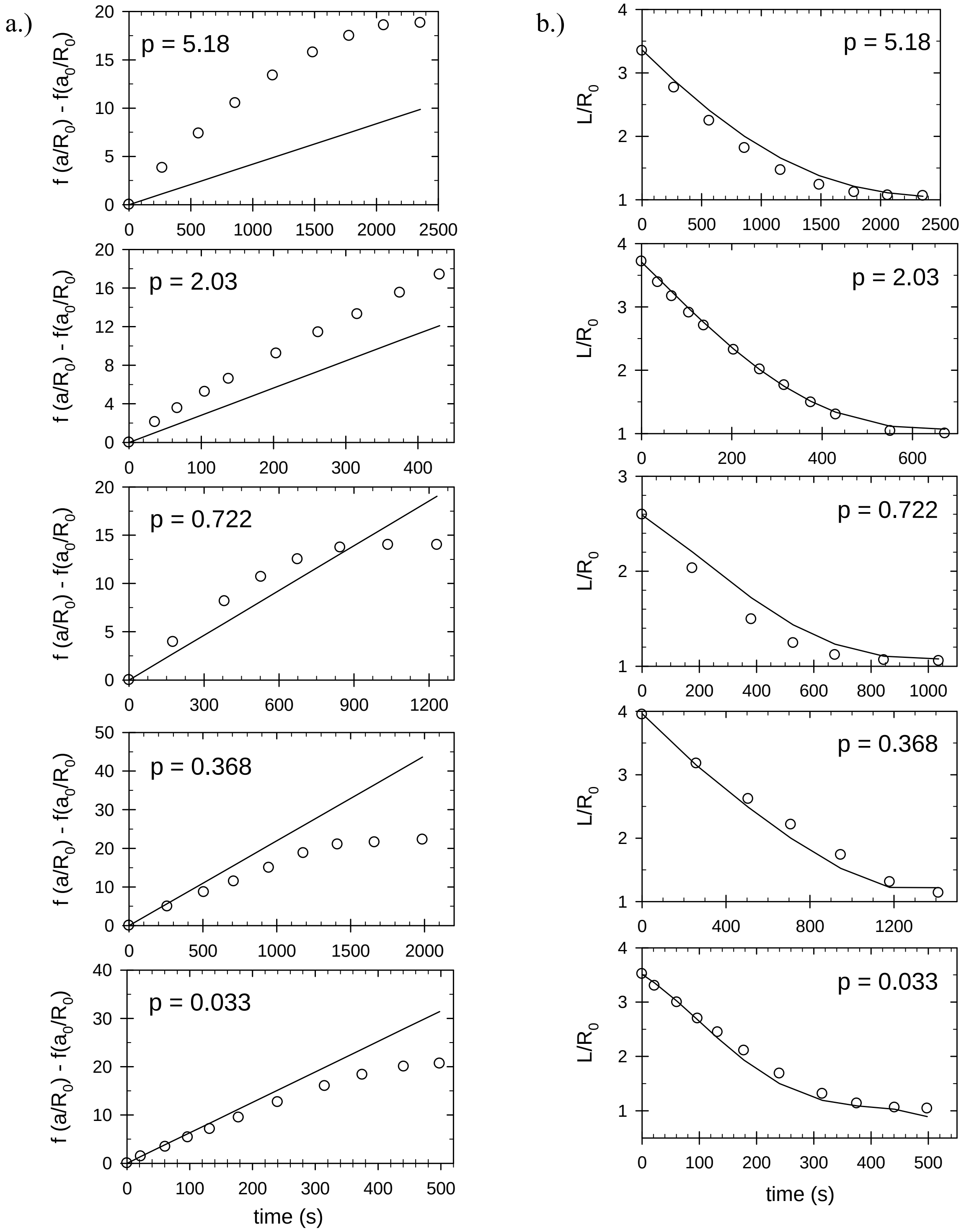

Figure 3.1: Retraction analysis using the a.) CC and b.) TOS methods. Solid lines represent Equation A.2 for a.) and Equation A.5 for b.), both using an equilibrium interfacial tension calculated from Equation 1.1.

In summary, the CC model can give interfacial tension values close to the equilibrium value only at low viscosity ratios, whereas the TOS model gives values close to the equilibrium value at all viscosity ratios. We believe that the CC model fails at high viscosity ratios because the model is only approximate. In particular, Equation A.2 was derived from a heuristic argument ($\mathrm{d}L/\mathrm{d}t$ is proportional to $-\mathrm{d}A/\mathrm{d}L$, where A is the interfacial area of the fiber). Furthermore, the fiber was assumed to be spherocylindrical at all times; certainly a questionable approximation for dumbbell shapes (see Figure 2.2). Finally, and perhaps most importantly, Equation A.4 is a semi-empirical approximation of the effective viscosity that was based on parameter fits of a few data sets.[10,44] It may be possible to propose an alternative dependence for η_e on p so that the CC method works well at all viscosity ratios. However, this would just be an empirical fix to the CC model. Instead, we recommend that the TOS method be used. It is itself reliable, theoretically rigorous, and also easier to apply than the CC method: $a(t)$ does not have to be calculated from Equation A.1, and the fits of Equation A.5 to the L/R_0 versus t data can be done accurately even by visual observation rather than least squares fits. It is interesting to note that while the TOS model was proposed in 1993, most fiber retraction experiments are still analyzed by the CC model. In fact, a review article on interfacial tension measurements of polymers in 2000[45] even cited a section on capillary instabilities in Tjahjadi *et al.*,[11] but nevertheless ignored the section on fiber retraction analysis. These reviewers instead still illustrated the CC model as the only means of analyzing of fiber retraction. A later review[49] and article[50] by Demarquette *et al.* did state that the CC model gave higher interfacial tensions than the TOS model but did not evaluate the effects of viscosity ratio or aspect ratio of the fibers. Finally, Zeigler and Wolf[51] have also commented that interfacial tensions by the CC method seem to be at variance with that from elliospidal drop retraction analyses, but no comparisons with the equilibrium interfacial tension or with the TOS analysis were made in their work.

3.2 CAPILLARY INSTABILITIES UNDER QUIESCENT CONDITIONS

We now turn to the primary topic of interest in this Chapter: the effects of surfactant on drop retraction and capillary breakup. As mentioned in Section 2.1, one of the simplest ways to gain insight into interfacially-driven two-phase flow is to study the dynamics of a single drop of an immiscible fluid dispersed in another fluid under quiescent conditions. If a drop is extended to an aspect ratio of generally larger than 15 and allowed to retract, it will undergo capillary breakup during retraction.[12] The principal concern of this section is to study the effect of surfactant on capillary instabilities. Specifically, we seek to use the SDT to experimentally test the predictions of Hansen *et al.,*[17] who used linear stability analysis to determine the effect of a surfactant on the stability of a viscous fluid filament in a viscous fluid. As discussed in Section 2.1.2, Hansen *et al.* concluded that, for the case of low surfactant surface and bulk diffusivity, as is most likely the case in our polymeric experiments, the growth rate is slowed by the compatibilizer at viscosity ratios far from one. Also, they conclude that the dimensionless wavenumber (see Equation 2.4) increases (wavelength decreases, See Figure 2.3) upon addition of compatibilizer for systems with a viscosity ratio far from one.[17]

In the following sections, results will be presented for a poly(ethylene oxide) / poly(propylene oxide) / surfactant system. This system was intended to be a model polymeric system to test the predictions of Hansen *et al.*[17] and determine the effect of surfactant on capillary instabilities under quiescent conditions. However, surprisingly complex behavior was encountered and, as a result, the system was abandoned. First, the SDT-based experimental method will be developed and validated in the surfactant-free case, and finally, the unusual complex behavior will be discussed in Section 3.2.4.

3.2.1 Materials

The immiscible components chosen need to fulfill several requirements to produce a suitable system. Because the goal of this work is to study surfactant effects, we would like to avoid bulk viscoelasticity. The viscosity ratio should be easily adjustable by varying either temperature or molecular weight. Finally, the bulk components should be completely immiscible and the block copolymer must be surface active and produce a significant decrease in interfacial tension.

Poly(ethylene oxide) (PEO), obtained from BASF, and poly(propylene oxide) (PPO), obtained from Aldrich and BASF, were chosen as the matrix and droplet phases, respectively. Both bulk polymers are available in a fairly wide range of molecular weights, allowing for sufficient variation of the viscosity ratio. Moreover, PPO has a sufficiently lower density than PEO, allowing for proper drop centrifugation in the SDT.

Triblock copolymers of PEO and PPO are commercially available from BASF under the name Pluronic (PEO-PPO-PEO) and Pluronic R (PPO-PEO-PPO). Seven such materials were tested (Table 3.4) but only one, Pluronic P105, was found to significantly lower the interfacial tension of a PEO/PPO system. Furthermore, a “pseudo-diblock” named Pluracol WSB125 was also found to reduce the interfacial tension of a PEO/PPO system. The WSB125 has been termed a “pseudo-diblock” because it consists of a PPO block linked to a butyl alcohol-terminated PEO block. Both Pluronic P105 and Pluracol WSB125 were found to reduce the interfacial tension of a PEO/PPO system by a factor of two at room temperature. The bulk materials and copolymers obtained are listed in Tables 3.3 and 3.4, respectively.

Table 3.3: Bulk materials used in single-drop experiments. The number in each component name denotes its average molecular weight in grams per mole.

Name	**Viscosity in Pa.s**			
	25 °C	**65 °C**	**70 °C**	**80 °C**
PEO-400	0.108	0.0431	-	-
PEO-1000	-	0.0596	-	-
PEO-6000	-	0.633	0.560	0.430
PEO-8000	-	1.65	1.45	1.17
PEO-20000	-	28.5	20.1	15.2
PEO-35000	-	-	111	95.5
PPO-2000	0.333	0.0736	0.0593	0.0526
PPO-3500	0.982	0.153	0.137	0.111
PPO-4000	0.890	-	-	-

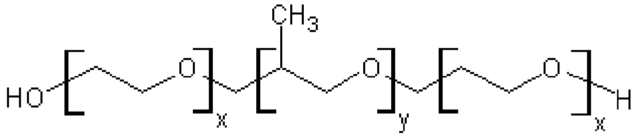

Pluronic

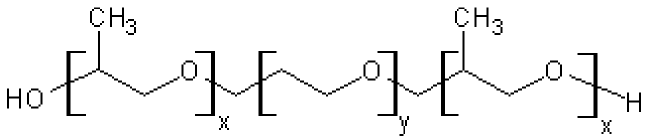

Pluronic R

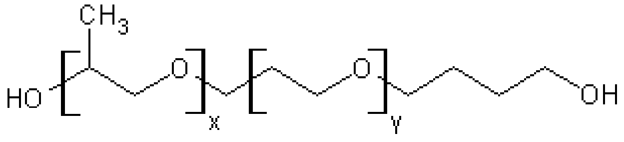

Pluracol WSB125

Figure 3.2: Block copolymers used in single-drop experiments. Values of “x” and “y” block molecular weights are listed in Table 3.4.

Table 3.4: Block copolymers used in single-drop experiments.

Pluronic	**Molecular Weight in g/mol**			**Total**	**Wt.% PEO**
	PEO	**PPO**	**PEO**		
L35	450	900	450	1800	50
L64	600	1800	600	3000	40
P65	900	1800	900	3600	50
F38	1800	900	1800	4500	80
P105	1500	3000	1500	6000	50
Pluronic R	**Molecular Weight in g/mol**			**Total**	**Wt.% PEO**
	PPO	**PEO**	**PPO**		
10R5	500	1000	500	2000	50
25R4	1300	1700	1300	4300	40
Pluracol	**Molecular Weight in g/mol**			**Total**	**Wt.% PEO**
	PEO	**PPO**	**Butyl alcohol**		
WSB-125	1000	1000	73	2100	50

3.2.2 Methodology

For the surfactant-free samples the PEO was loaded into the SDT tube and degassed under vacuum. The PPO drop was then injected into the tube using a syringe and the tube was sealed and placed into the SDT.

For samples containing block copolymer, the desired amount of PPO, typically 0.2 to 1% by weight, and the desired amount of surfactant were first dispersed into the PEO and hand mixed in a petri dish for 5-10 minutes. This was to ensure that there were no diffusion limitations for surfactant adsorption onto the PEO/PPO interface. The blend was poured into the SDT tube, degassed, then allowed to stand upright until the dispersed PPO droplets rose to the top of the tube and coalesced into a few large drops. The tube was then spun in the SDT until the few large drops centrifuged to the center of the tube and coalesced into a single elongated drop.

For all samples, the drop was stretched into an elongated shape by spinning the tube, the equilibrium interfacial tension was measured, and the drop was then allowed to retract and/or break up by reducing the rotational speed to about 500 rpm. It was not possible to reduce the rotational speed to zero because of buoyancy effects. However, if the final rotational speed is chosen to be sufficiently low (i.e. centrifugal forces are much smaller than interfacial forces), such retraction is essentially identical to that under quiescent conditions. Interfacial tension values obtained from the retraction of PIB drops of varying sizes in a PDMS matrix were not significantly affected by rotating at 500 rpm during the retraction process.[52] The retraction and/or capillary instabilities of the drop were then imaged using a CCD camera and laptop computer.

The sample tube spins in an electrically-heated oven allowing for temperature control up to 100 °C. By selecting materials of varying molecular weights and varying the sample temperature, the viscosity ratio was varied from about 5.5×10^{-4} to 0.045.

3.2.3 Results

Typically, the drops studied began as spherocylinders with an aspect ratio of ≥ 30. During retraction, end-pinching occurred at the ends of the drops and images were taken near the center of the drop where the capillary instabilities occurred. To obtain the drop diameter needed for the calculation of the equilibrium interfacial tension in Equation 1.1, the images were digitized and processed with an edge detection algorithm using a commercially available image analysis software package (Scion Image, Scion Corporation). The images of the drops undergoing capillary breakup were also analyzed using Scion Image. The disturbance wavelength and amplitude at various times during breakup were determined by fitting the capillary instabilities to sinusoids using the Gnuplot software. From the time evolution of the disturbance amplitude, a value of the interfacial tension could be calculated from Equation 2.2 and compared to the equililibrium value obtained before breakup. Due to lensing effects of the cylindrical tube, images of drops inside the tube appear distorted and accurate calibration is crucial. Therefore, each matrix fluid (PEO) was loaded into the SDT tube and a solid polyethylene (PE) sphere of known diameter was suspended in it and spun. Since PE has a lower density than PEO, the sphere centered itself along the axis of rotation and was imaged. These images served to calibrate the lengthscale of images parallel and perpendicular to the tube length.

The average wavelength of the disturbances was found from the image analysis of the capillary instabilities, converted into an average dimensionless wavenumber using Equation 2.4, and plotted in Figure 3.3a. Using the equilibrium interfacial tension prior to breakup and the growth rate G obtained from fitting a curve of ε versus t to a single exponential, the dimensionless growth rate was calculated using Equation 2.3 and plotted in Figure 3.3b. The experimental results show the same qualitative behavior as the linear stability analysis of Hansen *et al.*[17] (since this case is the limit of no surfactant, it is actually the Tomotika analysis[14]), but the linear stability analysis seems to underestimate our experimental values for both the wavenumber and growth rate.

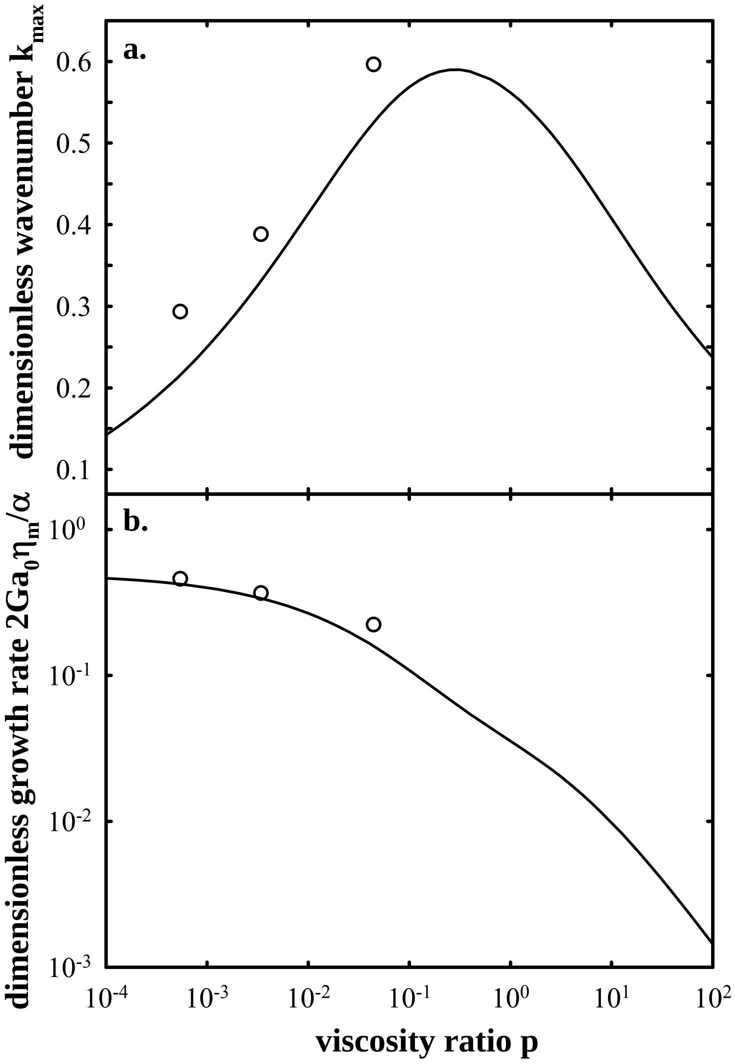

Figure 3.3: Dimensionless wave number and growth rate as a function of viscosity ratio. Solid lines are for the case of low surface and bulk diffusivity: linear stability analysis, adapted from Hansen *et al.*[17]

To summarize, the SDT method seems well-suited to study capillary instabilities. The growth rate and wavelength of the instabilities can be successfully determined in our SDT for surfactant-free drops. Unfortunately, when performing experiments on systems containing surfactant (the main focus and common thread of our work), we noticed some unusual dynamics. Specifically, highly-extended surfactant-free drops broke up by capillary instabilities; however, surfactant-laden drops did not break up by capillary instabilities. Furthermore, they underwent incomplete retraction. This was studied in more detail with drops at more modest aspect ratios ≤ 35, and will be discussed in Section 3.2.4.

3.2.4 Nonretraction and Autoextension upon heating

Figure 3.4a-b shows an example of a *surfactant-free* PPO-3500 drop in PEO-400 spun at 5100 rpm to achieve an aspect ratio of about 13. Upon reducing the rotational speed to 290 rpm, it retracts into a sphere within a few seconds. Figures 3.4c-d shows the first unexpected observation: the same experiment repeated on the same system but with Pluronic L35 surfactant retracts partially from an aspect ratio of 11 within a few seconds, and then stops retracting, retaining its highly non-spherical shape. This non-spherical shape persisted with no change for several hours. In Figures 3.4c-d, we note that there appears to be many small droplets that have not yet coalesced with the main droplet. However, this is not likely to be the cause of the nonretraction behavior. In fact, the surfactant concentration on the drop (which we do believe to be the cause of the nonretraction behavior) would be even higher than if all drops had coalesced.

Figure 3.5a-d shows the final non-spherical shapes of the drop as the initial rotational speed (i.e. the initial aspect ratio) is varied. Figure 3.5e-h shows the dependence of the final shape on the surfactant concentration. It is clear that increasing the initial aspect ratio, or increasing the surfactant concentration induces more severely deformed final shapes. Interestingly, if the samples in Figures 3.4 and 3.5 were heated to 65°C, the non-spherical drops retracted to spherical shapes and the non-retraction behavior disappeared upon cooling.

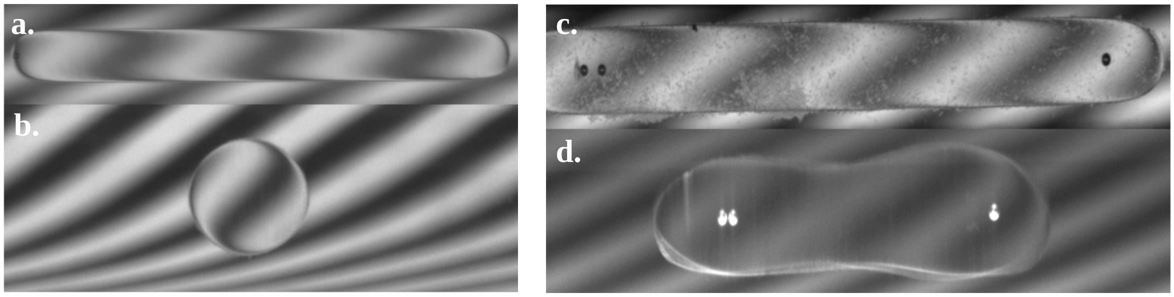

Figure 3.4: Retraction of a PPO-3500 drop suspended in PEO-400 in the SDT. a.) Initial shape at 5100 rpm to b.) 290 rpm with no surfactant; and retraction from c.) 3750 rpm to d.) 540 rpm for a sample with 0.1 percent by weight Pluronic L35.

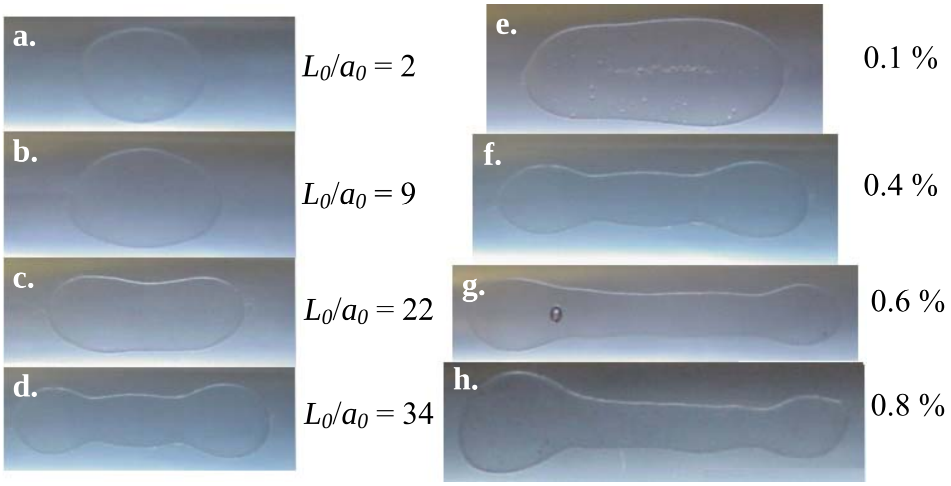

Figure 3.5: Final shapes of PPO-3500 drops in PEO-400 with Pluronic L35. a-d.) Surfactant concentration is fixed at 0.4%; initial aspect ratios are listed alongside each picture. e-h.) Initial aspect ratio is fixed at 34 +/- 2; surfactant concentrations in overall weight percent are listed alongside each picture.

Retraction is expected to stop only when the capillary pressure is the same everywhere; for surfactant-free fibers this implies an equal curvature everywhere, i.e. a spherical shape. There are at least three reasons why the retraction of surfactant-laden drops may not proceed to sphericity. The first is the possibility of the bulk fluid possessing a yield stress: when the capillary pressure becomes comparable to the bulk yield stress, retraction must stop. We discount this possibility since it would cause non-retraction even in the absence of surfactant, which we do not see. The second possibility is an interfacial yield stress. Surface-active species can give interfaces mechanical properties such as a dilational or shear modulus, shear viscosity, and possibly a yield stress. A last possibility is gradients in interfacial tension: since the retraction occurs from the tips, the surfactant concentration at the tips is expected to be higher than that at the mid-section, giving the tips a lower interfacial tension. This raises the possibility that the capillary pressure (product of the local interfacial tension and local curvature) may be equal at the tips and at the mid-section, thus eliminating the capillary pressure gradient driving the retraction. This is unlikely as well: the final shapes in Figures 3.4 and 3.5 are quite complex and it is unlikely that they have the precise surfactant distribution required to produce exactly the same capillary pressure everywhere. Moreover, even in the absence of capillary pressure gradients, Marangoni stresses should be able to drive retraction. Finally, any gradients in surfactant concentrations should relax by diffusion of the surfactant on the interface and into the bulk, and the persistence of the non-spherical shapes for several hours would require an unreasonably low diffusivity for the surfactants.

Thus, the only possibility is the presence of an interfacial yield stress. (Note that while the term “stress” is used here, an interfacial yield stress has units of N/m, same as those of interfacial tension.) What may cause such an interfacial yield stress? While an interfaciallyadsorbed surfactant may itself endow the interface with unusual mechanical properties, the fact that heating erases this behavior *irreversibly* suggests that the surfactant adsorption *per se* is not the cause. Most likely, some impurity in the surfactant or some aggregated structure formed by the surfactant that is responsible for this behavior. Regardless of its cause, the yield stress may confound experiments that use the PEG/PPG/Pluronic as a model system.

In light of the previous observations, it seems judicious to heat all drops to 65°C prior to further experimentation for studying capillary instabilities. To keep the drop away from the walls, we preheat while spinning at a constant, slow speed of about 300 rpm. During such preheating steps, a second surprising observation was made: when heating a drop containing either Pluronic P105 or Pluracol WSB125 surfactant at a low rotational speed, it would first stretch out strongly and then retract gradually over 30-45 minutes into a sphere. Sometimes this stretching would produce a cylinder of such a large aspect ratio that it would break up by capillary instabilities into a series of drops (see Figure 3.6a). Both of these findings suggest that at some time during heating, the interfacial tension undergoes a minimum before increasing again, i.e. the drop first stretches strongly due to its low interfacial tension, and then retracts or breaks up as the interfacial tension rises again (see Figure 3.6b). Such behavior was evident only in drops with the P105 and the WSB 125 surfactants; drops with all other surfactants and drops without surfactant stretched only slightly upon increasing temperature (suggesting a slight decrease in interfacial tension with increasing temperature), but never showed a subsequent increase in interfacial tension. Henceforth, this phenomenon of a large increase in length upon heating (all other variables held constant) is dubbed “autoextension”.

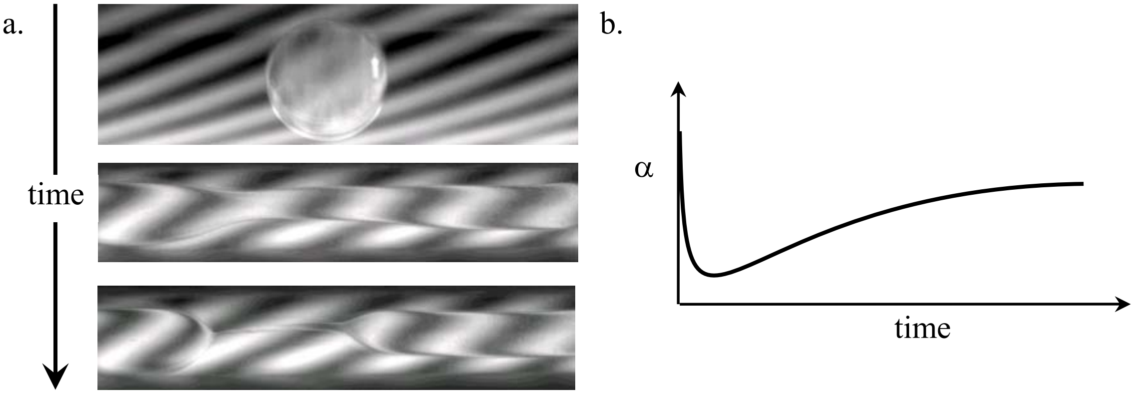

Figure 3.6: a.) a sample containing 0.1% WSB125 being heated while spun at 300 rpm. b.) qualitative schematic of interfacial tension changes with time during autoextension and subsequent breakup.

This autoextension phenomenon was found to depend on the thermal / mechanical history of the drop, and we investigated this in greater detail. Experiments in the SDT are tedious and furthermore, temperature control of the SDT under dynamic conditions is poor, therefore, experiments were conducted using scintillation vials in a water bath. The essence of the autoextension experiments in the SDT is that the initial drop shape is the result of an equilibrium between interfacial and centrifugal forces, and heating decreases the interfacial forces thus causing autoextension. This can be reproduced in a vial: the initial drop shape is simply an equilibrium between interfacial forces and gravity (see Figure 3.7), and heating should alter this balance and induce autoextension as well.

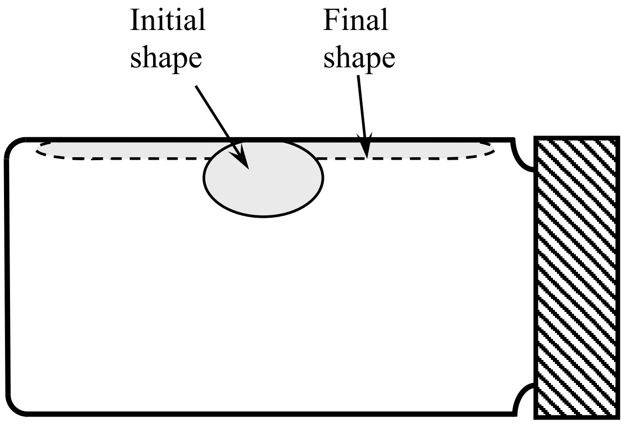

Figure 3.7: Scintillation vial and drop for autoextension experiments. Drop is PPO-3500 and matrix fluid is PEO-400.

For the surfactant Pluracol WSB 125, two blends were prepared in 20 mL glass scintillation vials. These blends contained the same weight fraction of surfactant and PPO as the SDT experiments. The two blends were then subjected to two different thermal / mechanical histories. In the first protocol (Protocol A), the blend was prepared by mixing all components by shaking the vial, and then the vial was placed horizontally in water bath at 60°C while being stirred by a magnetic stir bar for 30 minutes. The blend was then allowed to cool to room temperature, still under stirring. The cooling process took approximately one hour. Next, the stirring was ceased and the blend was allowed to coalesce under quiescent conditions (while still horizontal) at room temperature for 3 days. In the second protocol (Protocol B), the blend was again prepared by mixing all components by shaking the vial. Next, the vial was laid horizontally in a water bath at 60°C and the blend was allowed to coalesce under quiescent conditions at for two days, then cooled to room temperature. All blends were then reheated to about 50°C at a rate of about 1.5 degrees per minute, and the drop behavior was observed. To summarize the two protocols, Protocol A can be succinctly put: blend, stir while hot, cool under stirring, *coalesce while cold*, reheat; Protocol B can be summarized as: blend, *coalesce while hot*, cool to room temperature, reheat. All vials were kept horizontal throughout the conditioning/experimental steps so as not to deform the drop and possibly cause non-uniformities in the interfacial surfactant distribution.

With the differences in these two protocols, we attempted to test whether or not the autoextension behavior was caused by an excess concentration of surfactant on the droplet interface. By coalescing while the blend is cold, we hypothesize that much of the surfactant will become trapped on the interface, creating an excess. The diffusion of the surfactant in the bulk phases and the surfactant's ability to desorb off of the interface should be much smaller when coalescing while cold than coalescing while hot. By going from a blend with many small drops to one large drop, the reduction in surface area is drastic, and therefore we expect much more surfactant to be trapped on the droplet interface in the blend that was coalesced while cold. If a surface excess surfactant concentration is the cause of the autoextension phenomena, we should see a difference in the autoextension behavior between the two protocols, namely, the drop that was coalesced while cold would extend to a greater degree.

Furthermore, the surfactant may form some sort of aggregated structure on the droplet interface, causing the autoextension behavior. For example, if there is a surface excess concentration of surfactant on the interface and the surfactant is in some sort of aggregated structure, as the blend is heated up, the surfactant aggregate phase may "melt", releasing the excess surfactant which in turn becomes mobile on the interface, thus lowering the interfacial tension drastically.

Figures 3.8a-f show the reheating after Protocol A, and Figures 3.8g-l show the reheating after Protocol B for the WSB125 samples. It appears as though the sample prepared by Protocol

A (coalesce while cold) undergoes autoextension, whereas the sample prepared by Protocol B does not. The drop from Protocol A begins to autoextend at 38°C and becomes transparent at 44°C (note that the melting point for the bulk Pluracol WSB125 surfactant is quoted by BASF to be 40°C), and the drop from Protocol B (coalesce while hot) shows a slight extension at higher temperatures, most likely due to the decrease in interfacial tension with increasing temperature. Furthermore, it appears as though the sample prepared by Protocol A is slightly more cloudy than the sample prepared by Protocol B. Because the drop prepared by Protocol A showed autoextension, and the drop prepared by Protocol B did not, it can be concluded that the autoextension behavior is most likely due to a surface excess concentration of surfactant. This surface excess concentration may or may not exist in some kind of aggregated structure at lower temperatures (note that the temperatures at which the Protocol A drop showed autoextension are very close to the melting point of the bulk surfactant).

To summarize the results of the PEO/PPO/Pluronic system, we conclude that this is *not* a model system for studying the effect of surfactant on capillary instabilities. A complex thermal history is needed to avoid non-retraction and auto-extension phenomena. Furthermore, this heating/cooling procedure causes air bubbles in the SDT sample tube, further complicating the experiment.

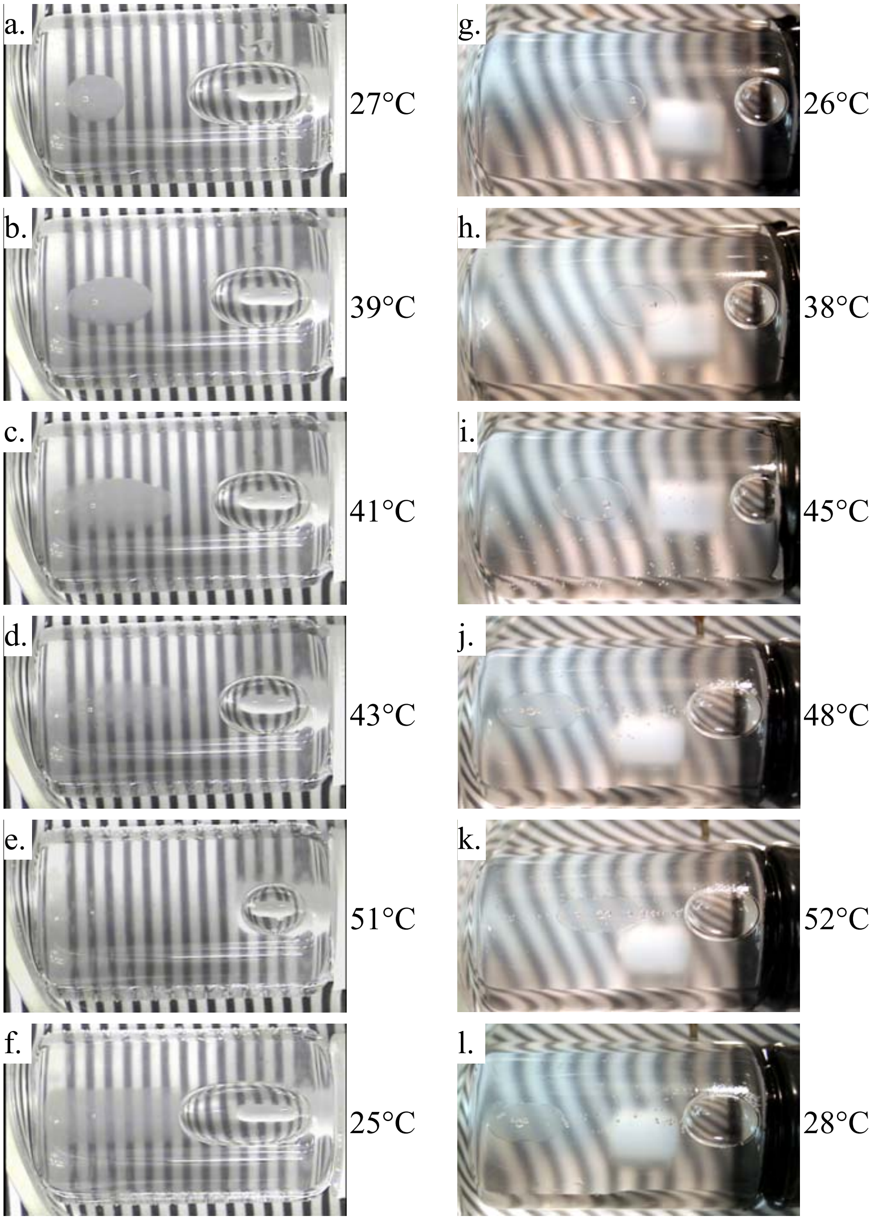

Figure 3.8: a-f.) Protocol A, and g-l.) Protocol B for a PEO-400 / PPO-3500 / Pluracol WSB125 system.

A second model system consisting of a low molecular weight polystyrene matrix phase and a PDMS drop phase was considered. However, this system also suffered from unforseen experimental difficulties. Specifically, the polystyrene drop, once extended, would not break up by capillary instabilities or even retract to a sphere. This could possibly be due to the fact that the low molecular weight polystyrene has a glass transition temperature very near to room temperature. Presumably, the lowest molecular weight polystyrene chains dissolved into the PDMS drop and the average molecular weight of the remaining polystyrene chains around the drop increased. The higher molecular weight polystyrene remaining at the interface has its glass transition temperature above room temperature and hence it formed a forming a glassy layer, stopping retraction. It should be stressed that this is only a hypothesis and we have no experimental evidence to support it.

To summarize, the effects of surfactant on capillary instabilities were investigated. However, model systems showed unusual behavior. The unusual behavior we saw is interesting in its own right because it shows surfactant effects that have not been seen before; however, since a goal of this work was to study surfactant effects on capillary instabilities, we have not pursued the original research further.

4.0 BLEND DYNAMICS UNDER SHEAR FLOW

While much basic information about two-phase flow with and without surfactant can be obtained by studying a single drop, a multi-drop system can give a great deal of direct information that is more pertinent and applicable to industrial blends. In this section, we study the effects of surfactant loading and droplet volume fraction on the blend morphology, dynamic oscillatory properties, and terminal complex viscosity in a multi-drop system. By choosing a suitable model system, we can use rheology to directly study the effects of compatibilizer on the rheological properties of blends. We also show that compatibilizers can be used to create unusual morphologies in polymer blends. If a compatibilizer has the ability to suppress coalescence, it can be used, along with specific mixing protocols, to create blends with droplet-in-droplet (double emulsion), and possibly high dispersed phase volume fraction morphologies.

4.1 EFFECT OF VOLUME FRACTION AND COMPATIBILIZER LOADING

4.1.1 Materials

As stated in Section 3.2.1, it is desirable to choose the components so that all of the desired aspects of surfactant phenomena can be highlighted without complications arising from bulk elasticity. For the same reasons discussed earlier, the polymers should be Newtonian and the viscosity ratio should be easily adjustable. The bulk materials should be completely immiscible without any flow-induced morphology changes such as phase separation, and the blends must be able to create the same range of microstructures that are seen in industrial blends. A previously studied system of PDMS and PIB with a PIB-PDMS diblock copolymer has been found to satisfy all of these requirements.[41,53]

The blends under investigation consisted of PDMS (Rhodorsil 47V60000 from Rhodia Chemicals) and PIB (PIB 32, Soltex Chemicals). A diblock copolymer of PIB (M_w = 6,150 g/mol, ρ = 904 kg/m^3) and PDMS (M_w = 8,000 g/mol, ρ = 972 kg/m^3) was used as a compatibilizer. This same diblock has been used in previous studies.[41,53] All experiments were conducted at 25°C where the viscosities of the bulk components are essentially equal. At 25°C the viscosities of PDMS and PIB are 56.2 and 57.3 Pa.s, respectively, resulting in a viscosity ratio, *p*, of about 1. Both components are liquid at 25°C and nearly Newtonian, with PDMS having a relaxation time on the order of 0.01 seconds and PIB even smaller.

4.1.2 Methodology

Each sample was prepared by adding the appropriate amounts of PDMS, PIB, and compatibilizer to a petri dish and hand mixing with a spatula for 10 minutes. The samples were then degassed under vacuum and placed in the rheometer. Samples will be designated by Bϕ_{PIB}-w_{comp} where ϕ_{PIB} is the volume fraction of PIB on a compatibilizer-free basis, and w_{comp} is the overall weight percent of compatibilizer. Blends ranging from 20 to 80 volume percent PIB and 0 to 0.5 weight percent compatibilizer were tested, with the majority of experiments conducted at compatibilizer weight fractions of 0 and 0.1%. It was verified previously that such small levels of compatibilizer do not affect the bulk rheology of the two phases significantly.

All blend experiments were conducted in a TA Instruments AR2000 stress controlled rheometer in a 40mm, 1° cone angle geometry using a Peltier cell to maintain the sample temperature. Samples were presheared at 480 Pa for 2000 strain units and the recovery was measured. A dynamic frequency sweep at 25% strain was performed and the sample was then sheared at 240 Pa followed by recovery and frequency sweep steps. This sequence was conducted for 480, 240, 120, 60, and 30 Pa steady shear stresses. An illustration of a typical experimental procedure is shown in Figure 4.1. Even for the highest drop volume fraction blends, there was essentially no change in the morphology over the timescale of a frequency sweep.

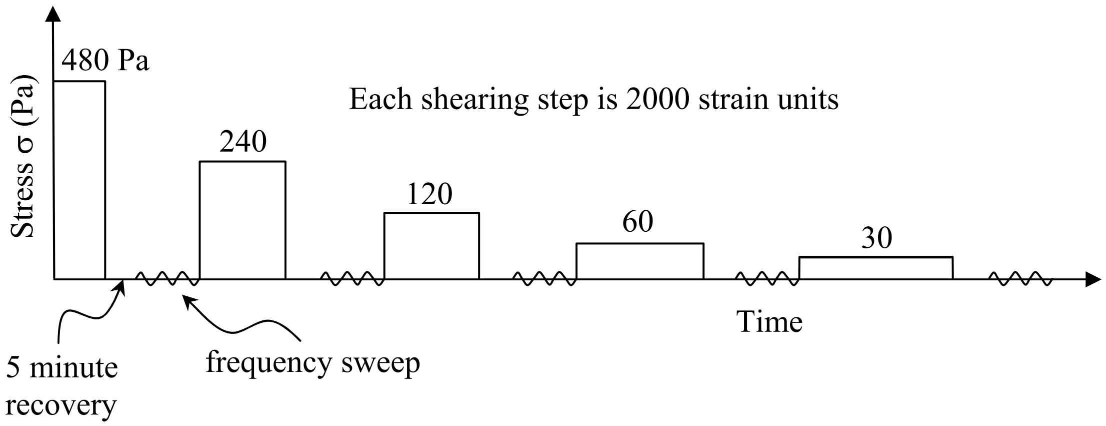

Figure 4.1: Experimental shear history. All steady-shear steps persist for 2000 strain units.

4.1.3 Results

We began this work with two observations from previous research.[54,55] The first was that compatibilized blends containing equal weight fractions of PIB and PDMS had remarkably high viscosities. A small increase in viscosity was documented in earlier experiments on 10% blends;[41] however, in 50% blends, as little as 0.5% compatibilizer increased the viscosity by a factor of three.[55] The second observation was that the PIB-PDMS diblock compatibilizer used in these blends is peculiar in that it suppresses coalescence only when PIB is the continuous phase. The immediate suspicion then was that these two observations are related: the compatibilizer was somehow changing the morphology and hence causing the increase in viscosity. In the following sections, we will first document the rheological behavior of blends with nearly equal amounts of PIB and PDMS, and then attempt to interpret the behavior in terms of microstructural changes and other surfactant-related phenomena.

4.1.3.1 Morphology and phase continuity

In this and the following sections, we are principally concerned with blends that contain either 40% or 60% PIB. Since the volume fractions of the immiscible phases are so close to each other, it cannot be presumed that the morphology remains droplet-matrix, or that the minority phase remains the dispersed phase. Therefore at least a qualitative examination of the morphology is essential.

Unfortunately, since both PIB and PDMS are liquid at room temperature and have very low glass transition temperatures, this system is ill-suited for electron microscopy, or any method that requires the sample to be “solidified”. Also, because the blends are not dilute, they scatter strongly and hence optical microscopy during shearing is quite difficult. We have conducted optical microscopy under quiescent conditions of samples placed between glass slides separated by a thin spacer. Images of both B40 and B60 compatibilized blends as-mixed, as well as blends withdrawn from the rheometer after shearing, always show droplet-matrix morphologies. Yet, from such images, it is not obvious which phase forms the drops. Since the issue of phase continuity is extremely important when interpreting the rheology, we tested this in more detail.

The standard method to test phase continuity in oil/water emulsions is to inject a small sample of the emulsion into a container of water. If the emulsion has water as the continuous phase, the oil droplets disperse rapidly, if oil is the drop phase, the emulsion sample does not disperse rapidly. Due to the high viscosity of the polymer blends studied here, this test cannot be applied easily since it is difficult to inject a PIB/PDMS blend into, say pure PIB due to the high viscous stresses involved. Fortunately, a selective solvent of low viscosity is available: silicone oil (low-MW PDMS) is miscible only with the PDMS in the blend. Therefore, the following procedure was developed. A small drop of the blend was placed on the tip of a bent wire and then gently immersed in silicone oil of viscosity one Pa.s. In all blends with PIB as the majority phase, the drop of blend remained on the needle, with only a slight change in shape due to interfacial tension and buoyancy (Figure 4.2a). In contrast, in blends with PDMS as the majority phase, the drop of the blend rose upwards in a plume due to buoyancy (Figure 4.2b), leaving behind a “trail”. In some cases when drops of the blend were large (e.g. in the uncompatibilized blend) single drops were evident in the rising plume. The above observations prove beyond doubt that if $\phi_{PIB} \leq 40\%$, PIB becomes the drop phase, whereas if if $\phi_{PIB} \geq 60\%$, PDMS becomes the drop phase.

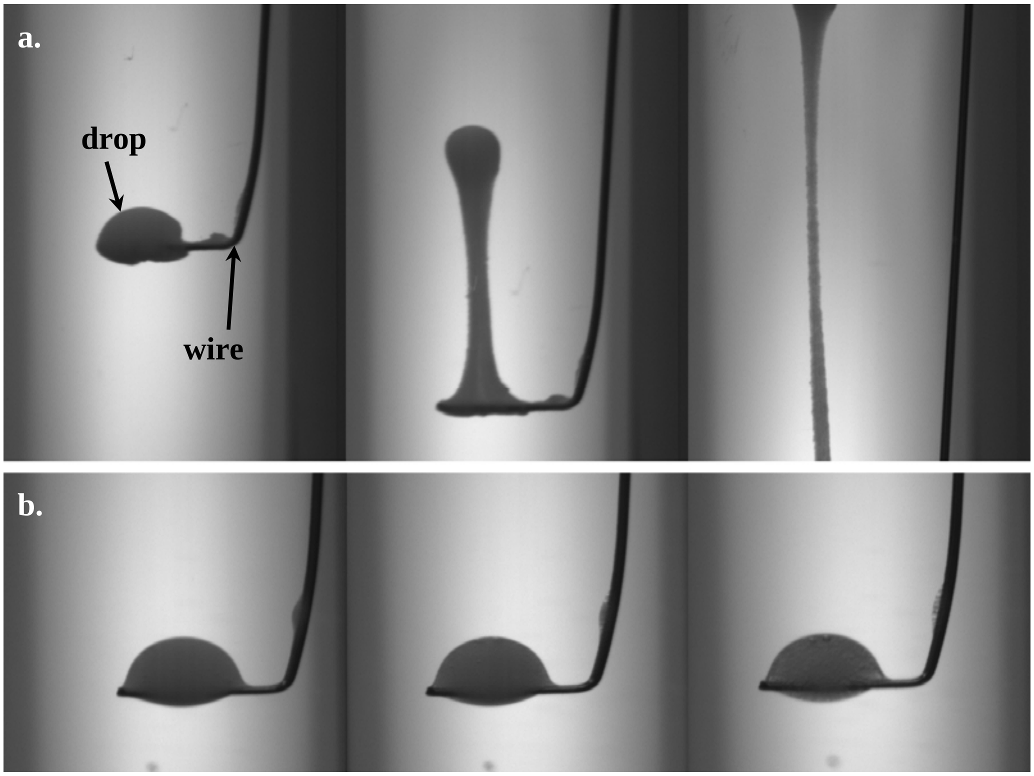

Figure 4.2: Tests of phase continuity by immersing blends in silicone oil: a.) B40-0.1, and b.) B60-0.1.

We have also conducted a similar experiment (bringing a blend in contact with pure PDMS or pure PIB) under an optical microscope. These experiments also confirm the above conclusion of phase continuity.

Similar to past publications in this area or research, the chief concern here is the rheological effects of adding compatibilizer and not the effect of compatibilizer on the drop sizes. We only mention that addition of compatibilizer reduces the drop size, and that B60 blends with compatibilizer have much smaller drops than B40 blends with compatibilizer. This is almost certainly attributable to the ability of the compatibilizer to suppress coalescence (discussed below).

To summarize, the morphology of the blends appears quite ordinary: 1). the droplet-matrix morphology is always obtained, at least under quiescent conditions, and unusual morphologies e.g. cocontinuity or fiber-like morphologies do not occur 2). blends do *not* show phase inversion, i.e. all blends with up to 40% PIB have PIB drops, and all blends with more than 60% PIB have PDMS drops.

Finally, we note that we have not tested the phase continuity of B50 blends. Since our system is equiviscous, we expect the phase inversion point to be around $\phi_{PIB} = 0.5$,[33] and hence such blends may have not have a droplet-matrix morphology under flow. For example, Jansseune *et al.*[56] observed a fibrillar morphology at high shear rates in PIB / PDMS blends near the phase inversion point.

4.1.3.2 Dynamic oscillatory behavior

Figures 4.3a and b show the elastic moduli, G', and the magnitudes of the complex viscosity, $|\eta^*|$, for the B40 and B60 blends respectively. For clarity, only the curves for G' versus ω and $|\eta^*|$ versus ω at the end of the highest stress (480 Pa) and lowest stress level (30 Pa) steady shear steps are shown. The curves at intermediate stresses lie between these limits in all cases. For clarity, each G' curve has been shifted upwards by a factor of 10 with respect to the previous one; curves for B40-0 and B60-0 have not been shifted. For clarity, each complex viscosity curve has been shifted upwards by 50 Pa.s with respect to the previous one; curves for B40-0 and B60-0 have not been shifted.

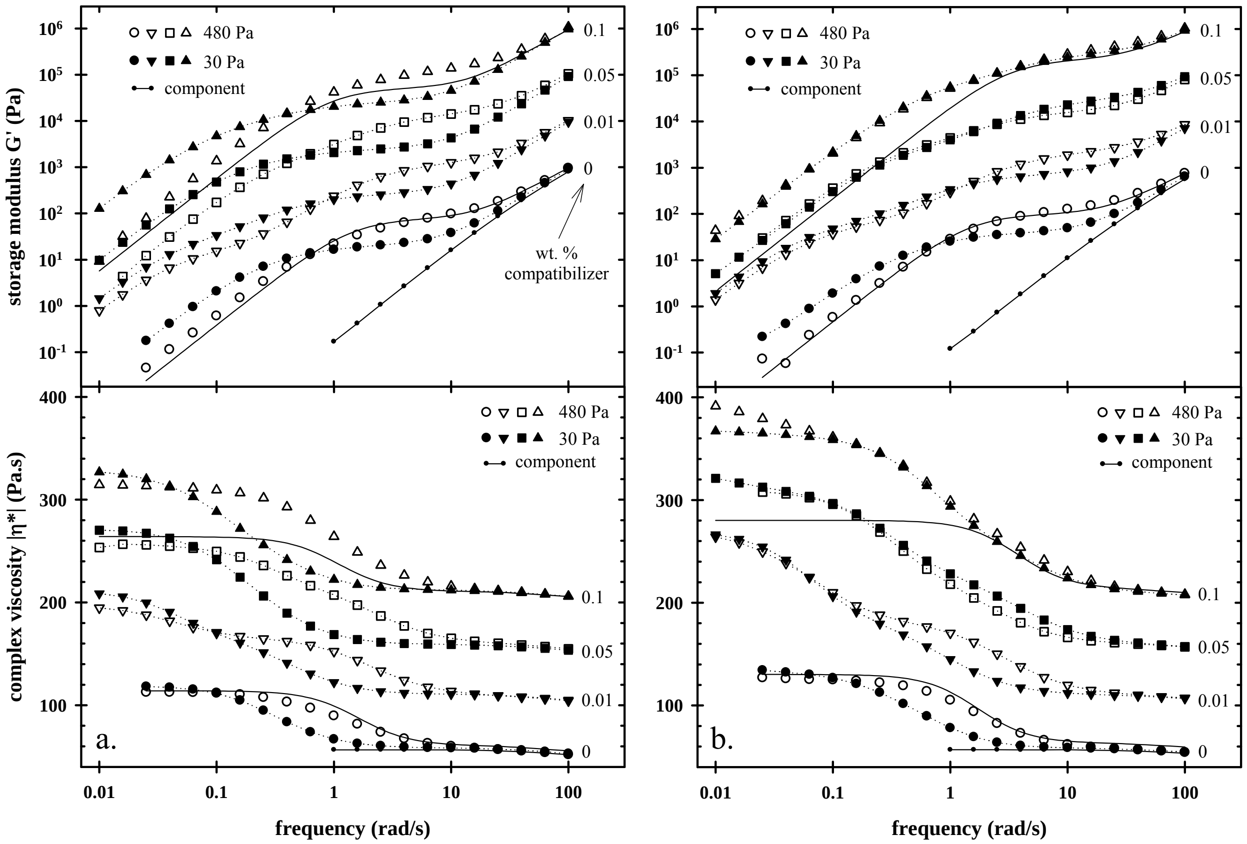

Figure 4.3: Dynamic oscillatory properties of a.) B40 blends, and b.) B60 blends. Open and filled symbols refer to experiments after shearing at 480 Pa and 30 Pa, respectively. Solid lines are best fits of the Palierne model[57] without interfacial viscoelasticity to the data at 480 Pa.

We will discuss the behavior of B40 blends first. Consider first the lowest set of results in Figure 4.3a, which correspond to the uncompatibilized B40-0 blend. Comparing this blend with the volume-average of the components (dashed lines), the most notable feature is the relaxation process, manifested as shoulders in G' and |η*|. Since this relaxation is absent in the components, it may be regarded as an interfacial relaxation process. This relaxation is well-known and arises from the deformation and relaxation of the droplets during the oscillatory experiment:[58] at frequencies substantially above the shoulder the drops deform along with the applied oscillatory flow, whereas at substantially lower frequencies, the drops remain nearly-spherical due to interfacial tension. Dimensional analysis suggests that the relaxation time corresponding to this interfacial relaxation process scales as $\frac{\eta_m R}{\alpha} f\left(\phi_d, p\right)$, where η_m is the viscosity of the matrix, R is the mean radius of the drops, α is the interfacial tension, ϕ_d is the volume fraction of drops, and p is the ratio of the viscosity of the drops to that of the matrix. Detailed predictions of the function $f\left(\phi_d, p\right)$ are available,[57,59] and the Palierne model in particular has been widely used in the literature.[60,61] An example of a fit of the Palierne model to the data for the B40-0 blend sheared at 480 Pa is shown in Figure 4.3a (solid lines). Evidently, good fits can be obtained using R/α as the only fitting parameter. In the case of uncompatibilized blends, all quantities except R are fixed. Upon reducing the stress from 480 Pa to 30 Pa, drops grow by coalescence, and this is apparent as a shift of the relaxation process to lower frequencies since the frequency at which the relaxation process occurs is inversely proportional to the drop size (see Figure 4.3a).

Upon addition of a small amount, 0.01wt.%, of compatibilizer (the middle set of curves in Figure 4.3a), the most obvious effect is the appearance of a second, much slower interfacial relaxation process, manifested by a second shoulder in $G'$and a corresponding shoulder in $|\eta^*|$ at low frequency. This slower relaxation has been seen previously[36,37,62] and has been attributed to flow-induced gradients in block copolymer concentration, and hence flow-induced interfacial tension gradients, on the interface. It is the relaxation of these gradients which is believed to cause the slow relaxation process: at frequencies well above the slow relaxation, the oscillatory shear is able to induce gradients in interfacial block copolymer concentration, whereas at much lower frequencies, the block copolymer remains at nearly uniformly distributed on the interface.

What is the mechanism by which the block copolymer remains at a uniform concentration over the drop surface at low frequencies? The first two possibilities, surface diffusion of compatibilizer, or interfacial diffusion of compatibilizer, seem unlikely since a previous calculation suggests that the diblock used here has a very low diffusivity.[53] The third possibility seems more likely: a Marangoni stress caused by the interfacial tension gradients acts tangentially along the interface to establish a uniform block copolymer concentration. In summary, two interfacial relaxation processes are evident in the presence of block copolymer, the faster one associated mainly with shape relaxation of the drops and the slower one associated mainly with relaxation of interfacial tension gradients.

This effect of interfacial tension gradients causing two relaxation processes can be modeled by endowing the interface with interfacial viscoelastic properties. In the simplest case, one may define an interfacial dilation modulus:[63]

$$\beta = A\frac{\partial \alpha}{\partial A} \tag{4.1}$$

where A is the area of the interface. The relaxation times of the two relaxation processes can then be shown to be of the form $\frac{\eta R}{\alpha} f\left(\phi_d, p, \frac{\beta}{\alpha}\right)$.[63,64] Corresponding expressions for the relaxation times are also available if other interfacial properties such as an interfacial shear modulus or an interfacial viscosity are considered.[64,65] Using such expressions, one may then obtain the interfacial viscoelastic properties from the observed relaxation times.[36,37,62,64] Since both relaxation times are predicted to be proportional to drop size, one may expect that with decreasing stress, coalescence would cause a shift in both the relaxation processes to low frequencies. Experimentally however, comparing the results at 480 Pa versus 30 Pa, only the faster process is seen to shift to lower frequency with reducing stress. The slower process appears independent of stress. A similar insensitivity of the slow relaxation to drop size was noted previously.[37,62]

Upon further increase in the amount of compatibilizer to 0.05%, the slow relaxation moves to higher frequencies. At 0.1% compatibilizer (the topmost curves in Figure 4.3a), the two shoulders merge together and are no longer evident separately. This convergence of the two relaxation processes with increasing compatibilizer loading was also observed by Van Hemelrijck.[37] A similar single shoulder in the G' versus ω curves was also noted in an earlier paper on B11 blends which only explored relatively high compatibilizer loadings.[53] While this single shoulder makes the dynamic oscillatory properties of this B40-0.1 blend appear to be qualitatively similar to those of the B40-0 blend, it must not be taken as an indication that there is no interfacial viscoelasticity or that interfacial tension gradients are not important. This is clearly apparent when one attempts to fit the Palierne model without interfacial viscoelasticity, i.e. with α/R as the only fitting parameter, to the data for the B40-0.1 blend: it is clear that without interfacial viscoelasticity, the strength of the relaxation process is greatly underestimated. Thus, this apparently-single relaxation process is best viewed as two processes with closely-spaced relaxation times. Theoretically as well, it has been shown that if the interfacial modulus is comparable to the interfacial tension, the two relaxation times approach each other until only a single shoulder is visible in G' and $|\eta^*|$.[64]

Finally, it must be emphasized that the apparently-single relaxation in B40-0.1 shifts to lower frequencies upon reducing stress. This suggests that flow-induced coalescence can still occur in B40-0.1. We will see significantly different behavior in the B60-0.1 blend below.

The above observations on B40 blends are all qualitatively similar to those discussed previously for B11 blends with compatibilizer. Evidently, moving from dilute B11 blends to concentrated B40 blends causes no qualitative change in the dynamic viscoelastic properties.

We now turn to B60 blends. The lowest set of curves in Figure 4.3b show that the uncompatibilized B60-0 blend behaves very similarly to the B40-0 blend: a single relaxation process is evident, and it moves to lower frequencies upon reducing stress indicating flow-induced coalescence. Once again, the Palierne model without interfacial viscoelasticity predicts the moduli well with α/R as the only fitting parameter. The effect of addition of 0.01% compatibilizer on the B60 blend is also quite similar to that discussed above for B40-0.01: a second, slower relaxation process appears which is insensitive to stress.

Upon increasing the compatibilizer level to 0.1%, two relaxation processes are still visible, however they have nearly merged, as expected from the B40-0.1 blend above. Once again, the Palierne model without interfacial viscoelasticity greatly underpredicts the strength of the relaxation process. However, a significant difference emerges: the dynamic oscillatory properties become almost insensitive to stress. Since the dynamic moduli are directly related to the size of the drops, this suggests that the drop size does not increase upon reducing stress, i.e. the 0.1% block copolymer suppresses coalescence in the B60 blend.

To summarize the qualitative discussion of the dynamic oscillatory properties in this section: both uncompatibilized blends, B40-0 and B60-0, show a single interfacial relaxation process corresponding to the shape-relaxation of drops. This relaxation slows down with reducing stress, suggesting flow-induced coalescence. In both B40 as well as B60 blends, upon adding 0.01% compatibilizer, two interfacial relaxation processes are evident. The faster of these two processes slows down with decreasing stress, whereas the slower process seems insensitive to stress. At 0.1% compatibilizer the two relaxation processes merge, but differences between B40 and B60 blends are evident: In the B40-0.1, the relaxation slows down with reducing stress suggesting that the compatibilizer does not suppress coalescence. In contrast, in B60-0.1 the dynamic moduli appear insensitive to stress indicating that compatibilizer is able to stop coalescence. This conclusion, that the compatibilizer can prevent coalescence when PIB is the continuous phase, but not when PDMS is the continuous phase, has been verified by direct visualization (see Section 4.1.3.6).

Next we conduct a quantitative analysis of the oscillatory moduli. Only two aspects of the oscillatory measurements will be discussed: the magnitude of the terminal complex viscosity $\left|\eta_0^*\right|$, and the relaxation time of the interfacial relaxation.

In most blends, $\left|\eta_0^*\right|$ was essentially independent of the stress prior to the oscillatory measurement (most of the differences in the $\left|\eta_0^*\right|$ after 480 Pa shearing versus after 30 Pa shearing in Figures 4.3a and b are random experimental error and typically well within 10% of the average). The only exception is B60-0.1 in which $\left|\eta_0^*\right|$ after the first two stresses (480 Pa shown in Figure 4.3b, and 240 Pa, not shown) was consistently higher than the $\left|\eta_0^*\right|$ after the lower stresses. In all cases including B60-0.1, we have simply averaged the $\left|\eta_0^*\right|$ values at all stresses. These average values are plotted as a function of compatibilizer loading in Figure 4.4 (referring to the right axis). The $\left|\eta_0^*\right|$ values can also be rendered dimensionless by a volume average of both components:

$$\left|\eta_{0r}^{*}\right| = \frac{\left|\eta_{0}^{*}\right|}{\phi_d \eta_d + \phi_m \eta_m} \tag{4.2}$$

where $\left|\eta_{0r}^{*}\right|$ is the relative terminal complex viscosity of the blend, $\left|\eta_{0}^{*}\right|$ is the terminal complex blend viscosity, and η_d, and η_m are the viscosities of the droplet phase and matrix phase, respectively. The denominator in Equation 4.2 is the simplest means of estimating the bulk contribution to the viscosity of a two-phase blend. This estimate can be very poor if the viscosities of the two phases are highly mismatched, but in the present case, since $\eta_d \approx \eta_m$, the approximation works very well. In fact, going from $\phi_{PIB} = 0$ to 1, the denominator of Equation 4.2 varies by less than 2%. The values of $\left|\eta_{0r}^{*}\right|$ thus calculated can be read off Figure 4.4, referring to the left axis.

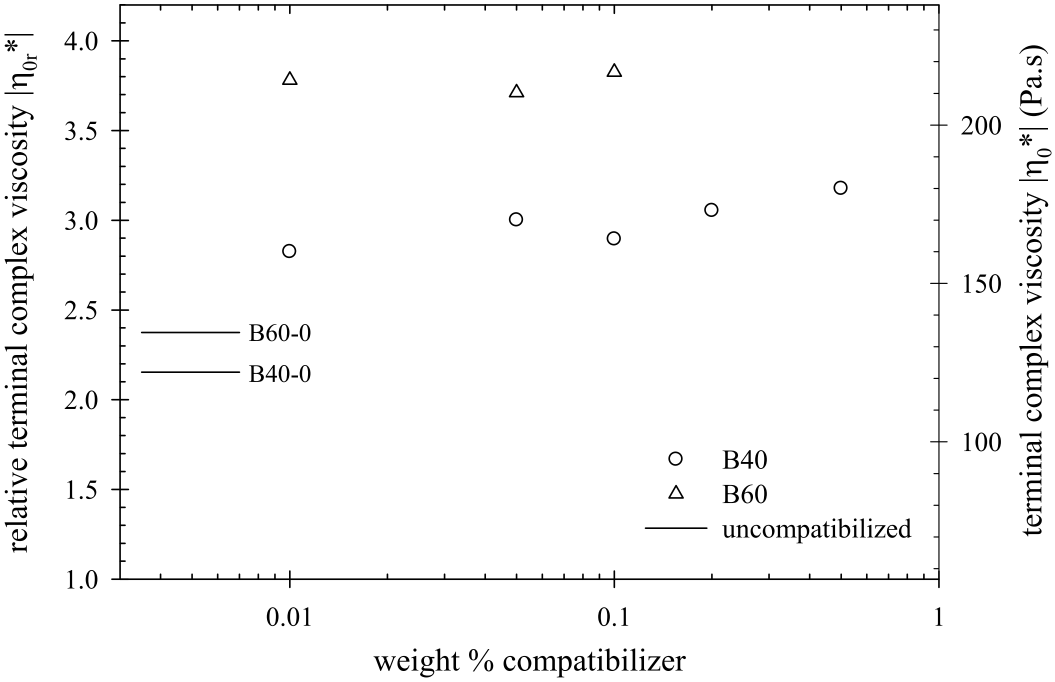

Figure 4.4: Dependence of terminal dynamic viscosity on compatibilizer loading for B40 and B60 blends.

The most surprising observation is the large effect of the compatibilizer on the terminal complex viscosity, especially in the B60 blends. A modest increase in the terminal complex viscosity with compatibilizer was reported previously for the B11 blends,[41] but the effect of compatibilizer seems to be much larger in the concentrated blends here: e.g. in the B60 blend, as little as 0.01% compatibilizer raises the terminal complex viscosity by more than 60%. Further addition of compatibilizer has relatively little effect on the terminal complex viscosity. As mentioned above, the effects of compatibilizer may be modeled by endowing the interface with an interfacial dilation modulus. In the case of dilute emulsions, such models[64,65] predict that if the interfacial modulus is frequency-independent, the zero-shear viscosity approaches that of a suspension of rigid spheres, regardless of the *magnitude* of the modulus. This may explain why the terminal complex viscosity is the same at all compatibilizer loadings: the interfacial modulus may increase with increasing compatibilizer loadings, but the terminal complex viscosity remains unaffected. This will be discussed further in Section 4.1.3.5.

Finally, it is of interest to examine the relaxation time of the blends quantitatively. For blends with 0.01% compatibilizer, this is difficult because due to the very slow relaxation process, the terminal region is barely reached in the experimentally-accessible frequency window. Therefore the analysis for relaxation times is restricted only to blends with 0% and 0.1% compatibilizer. This analysis follows the procedure detailed previously.[41,66] Briefly, the interfacial contribution to the storage modulus is defined as

$$G'_{\text{interface}} = G'_{\text{measured}} - G'_{\text{component}} = G'_{\text{measured}} - G'_{\text{Palierne}}(\alpha = 0) \tag{4.3}$$

where $G'_{\text{component}}$ is the bulk contribution to the modulus, obtained from the Palierne model by setting interfacial tension equal to zero. $G'_{\text{interface}}$ can then be fitted very well by a sum of very few Maxwell modes:[67]

$$\log[G'(\omega)] = \log\left[\sum_{k=1}^{n} \frac{\omega^2 \exp(\nu_k + 2\tau_k)}{1 + \omega^2 \exp(2\tau_k)}\right] \tag{4.4}$$

where $\exp(\nu_k)$ and $\exp(\tau_k)$ are the high-frequency modulus and the relaxation time of the k$^{\text{th}}$ Maxwell mode, respectively. In the present case, B40-0, B60-0, and B40-0.1 can be fitted very well by a single Maxwell mode (n = 1), whereas B60-0.1 requires two modes (n = 2). As previously, internal consistency was tested by verifying that the complex viscosity corresponding to the sum of Maxwell modes, defined as

$$\eta^*_{\text{interface}} = \eta^*_{\text{blend}} - \eta^*_{\text{Palierne}}(\alpha = 0) \tag{4.5}$$

was in good agreement with the interfacial contribution to the complex viscosity measured experimentally. More details of this procedure have been presented previously.[41,66]

Figure 4.5 plots the relaxation time of the interfacial relaxation process as a function of stress, σ, in the various blends. As discussed qualitatively above, in B40-0 and B60-0, the interfacial relaxation time increases as stress reduces. Figure 4.5 shows that the relaxation time has an approximately $\sigma^{-0.6}$ dependence on stress. In uncompatibilized blends, the drop size is proportional to the relaxation time, and hence we conclude that $R \propto \sigma^{-0.6}$ in both these blends. A similar dependence has been predicted by Vinckier *et al.*[68] for a coalescence-limited morphology, albeit in a rate-controlled experiment.

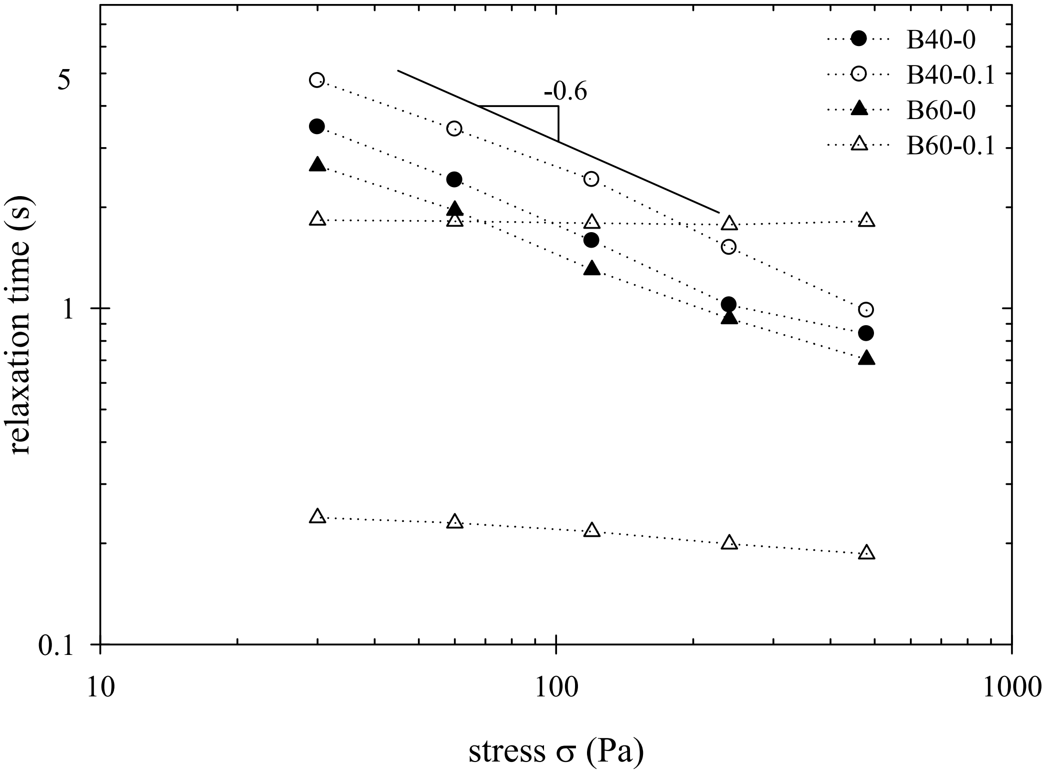

Figure 4.5: Relaxation times of the interfacial relaxation process in blends. B40-0, B40-0.1 and B60-0 could all be fitted with a single relaxation time. B60-0.1 required two relaxation times; both are shown above.

Addition of 0.1% compatibilizer to B40 raises the interfacial relaxation time by about 50% at all stresses. Such an increase of interfacial relaxation time with compatibilizer has been noted for B11 blends previously.[41,53] The stress dependence of the relaxation time of B40-0.1 still remains approximately $\sigma^{-0.6}$. This increase in relaxation time with reducing stress indicates an increase in drop size with reducing stress, although there may not be an exact proportionality between drop size and relaxation time in compatibilized blends. For the B60-0.1 blend, a single Maxwell mode is insufficient to capture the interfacial relaxation, and hence the relaxation times of both modes are shown. As discussed qualitatively above, since the dynamic moduli were insensitive to stress, the relaxation times are also insensitive to stress as well. This correlation gives a quantitative measure of coalescence suppression in these blends.

4.1.3.3 Steady shear viscosity

Both compatibilized as well as uncompatibilized blends were found to be shear-thinning. Since experiments were conducted at successively decreasing stresses, upon starting the shearing at a fixed stress level, the viscosity increased gradually to its steady state value at that stress. Typically, 100-400 strain units of shearing were required to reach the steady shear viscosity; compatibilized blends generally reached steady values at shorter shear strains than uncompatibilized ones. These steady shear values of the viscosity are plotted in Figure 4.6 (referring to the right axis). Similar to Equation 4.2, the steady shear values can also be rendered dimensionless:

$$\eta_r = \frac{\eta_{blend}}{\phi_d \eta_d + \phi_m \eta_m} \tag{4.6}$$

These values of η_r can be read off the left axis of Figure 4.6. Finally, the values of the terminal complex viscosity from Figure 4.4 are also added to Figure 4.6 as horizontal lines for comparison.

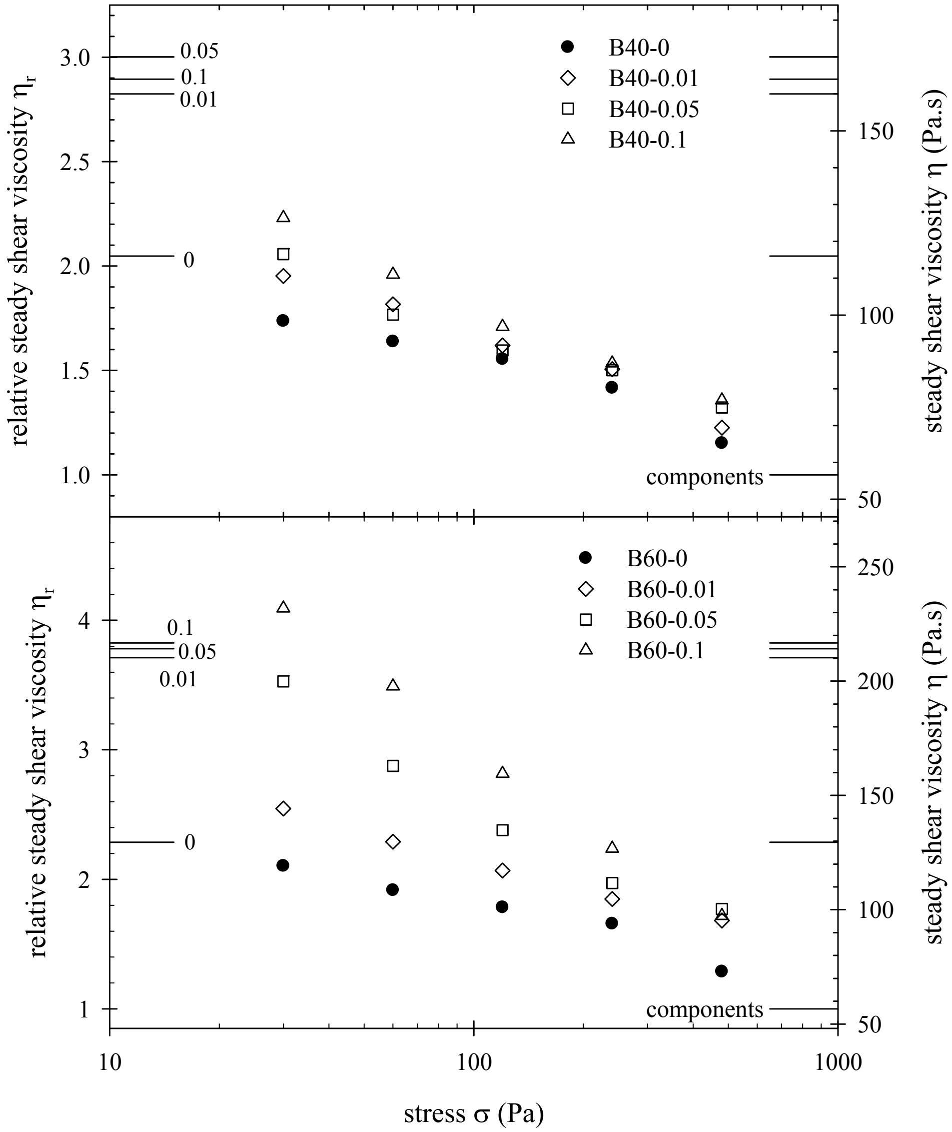

Figure 4.6: Steady shear relative viscosity as a function of shear stress for ϕ_{PIB} = 0.40 and 0.60. Relative terminal complex viscosities from dynamic oscillatory data are plotted as solid lines.

As in the previous section, the B40 blends are discussed first. Consider first the B40-0 blend which shows a steady shear viscosity that increases with decreasing shear stress. Shear-thinning in uncompatibilized droplet-matrix blends has been documented previously,[61] and is attributable to the deformation and velocity-alignment of the drops subjected to shear flow. Theory predicts that the magnitude of shear thinning of blends without compatibilizer is governed by the capillary number:[69,70]

$$Ca = \frac{\text{viscous stress}}{\text{interfacial stress}} = \frac{\sigma R}{\alpha} \tag{4.7}$$

This is essentially the capillary number written in Equation 2.5, except the viscous stress has been written as σ. This is done because the above definition is more appropriate in stress-controlled rheological experiments. The previous section showed that for the uncompatibilized B40-0 and B60-0 blends, $R \propto \sigma^{-0.6}$ is approximately correct. Therefore Equation 4.7 suggests the approximate dependence of $Ca \propto \sigma^{0.4}$, i.e. Ca decreases as stress decreases. Therefore with reducing stress, the drops deform less, resulting in an increased blend viscosity.[69,70] The η_r versus stress curve seems to approach $\left|\eta^*_{0r}\right|$ at low stresses, yet, a plateau viscosity, which would be indicative of the zero-shear value, is not apparent up to the lowest stress value of 30 Pa.

With addition of compatibilizer, all the steady shear viscosities increase. As explained previously,[41] this increase in viscosity may be attributed to flow-induced gradients in compatibilizer concentration: the corresponding Marangoni stresses and gradients in capillary pressure resist flow and hence increase the viscosity of the blend. In the B40 blends with compatibilizer (as well as B20 and B30 blends with compatibilizer, not shown), the increase in viscosity with compatibilizer was greatest at low stresses. There seems to be a significant discrepancy between the viscosity measured at the lowest stress level and $\left|\eta_0^*\right|$. Certainly, η must approach $\left|\eta_0^*\right|$ at sufficiently low stress, yet, from Figure 4.6, it appears that 30 Pa is far into the shear-thinning region for the B40 blends. A similar, although smaller, discrepancy is apparent in upon comparing the steady shear and terminal complex viscosities of the B30 compatibilized blends (not shown).

Next we consider the B60 blends. The B60-0 blend behaves quite similar to the B40-0 blend, although the actual values of the viscosity are somewhat higher for the B60-0. Upon addition of a small amount (0.01%) of compatibilizer, the behavior is similar to that of the B40-0.01 noted above: η increases at all stress levels, but there is still a large discrepancy between η at 30 Pa, and $\left|\eta_0^*\right|$, indicating that shear-thinning starts at much lower stresses. Upon increasing the compatibilizer loading, two quantitative differences appear: firstly, the viscosity increases to much higher values than in B40-0.1, secondly, the η vs. stress curve does seem to approach $\left|\eta_0^*\right|$. In fact, at 30 Pa, the steady shear viscosity seems to be larger than the terminal dynamic viscosity. This does not appear to be an error: three independent measurements on B60-0.1, as well as measurements on B70-0.1 and B80-0.1 blends show the same unusual feature. We can propose no mechanism for this unusual behavior.

Finally, it is interesting to note that in B60 blends, the terminal complex viscosity is independent of compatibilizer content (previous section and Figure 4.4), whereas steady shear viscosity increases with compatibilizer (Figure 4.6). This will be discussed further in Section 4.1.3.5.

4.1.3.4 Recovery after cessation of shear

During steady shear, the drops of an uncompatibilized blend deform and orient along the flow direction. After cessation of shear, these deformed drops retract back into spherical shapes and induce creep recovery of the blends. Recovery is attributable to the shape-recovery of initially-deformed drops,[46,71] and also to the relaxation of interfacial tension gradients along the drop surfaces for compatibilized blends.[43,47] In previous experiments on uncompatibilized blends, the creep recovery upon cessation of steady shear was found to be well-described by single-exponential kinetics with only two parameters: the ultimate recovery γ_∞, and the time required for recovery.[66,72] Thus, by fitting the recovery curves to a single-exponential, the recovery time could be obtained as the only fitting parameter (ultimate recovery is not a fitting parameter since it can be obtained directly from the recovery vs. time data). Experiments on B11 blends show that the recovery of compatibilized blends is more complicated and cannot be described by a single exponential process.[63] For example, the recoveries after shearing at 480 and 30 Pa of three blends, B40-0, B40-0.1, and B60-0.1, are shown in Figure 4.7, along with a single exponential. The B60-0 recovery is qualitatively similar to the B40-0 blend, and is not shown. Clearly, only the uncompatibilized blend could be described by a single exponential. Therefore, our results here agree with the previous observations: B40-0 and B60-0 can be well-represented by single-exponential kinetics, but the compatibilized blends cannot. Therefore we will discuss the creep recovery in terms of the ultimate recovery γ_∞ and the time for half-recovery, $\lambda_{1/2}$.

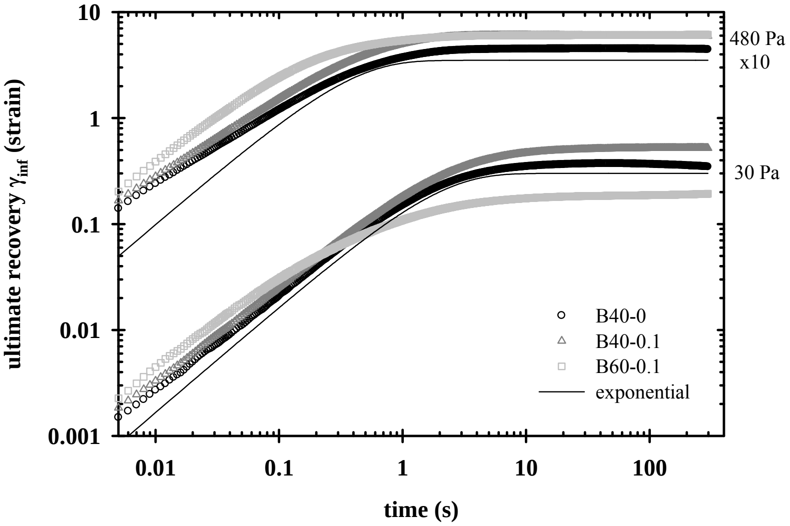

Figure 4.7: Recovery after cessation of shear for B40-0, B40-0.1, and B60-0.1 blends after shearing at 480 Pa (upper set of curves) and 30 Pa (lower set of curves).

Figures 4.8a and b show γ_∞ and $\lambda_{1/2}$ for the B40 and B60 blends. Consider first B40-0 and B60-0 uncompatibilized blends. Since drops coalesce with decreasing stress, one expects the $\lambda_{1/2}$ to increase as well, as is indeed evident in Figure 4.8b. Indeed, the approximate stress dependence of $\lambda_{1/2} \propto \sigma^{-0.6}$ is quantitatively in agreement with the relaxation time (and hence drop size) dependence on stress noted from Figure 4.5. The linear viscoelastic theory of the recovery of droplet-matrix blends also predicts that γ_∞ is proportional to Ca prior to cessation of shear[66,72]. Based on the discussion in the previous section, we expect $\gamma_\infty \propto Ca \propto \sigma^{0.4}$. However, experimentally, a weaker stress dependence is observed, perhaps because the actual Ca values are too large for the linear theory to hold quantitatively. These observations agree well with our previous research on uncompatibilized blends that shows that the linear viscoelastic theory predicts the recovery times almost exactly, but does not predict the ultimate recovery well.[66]

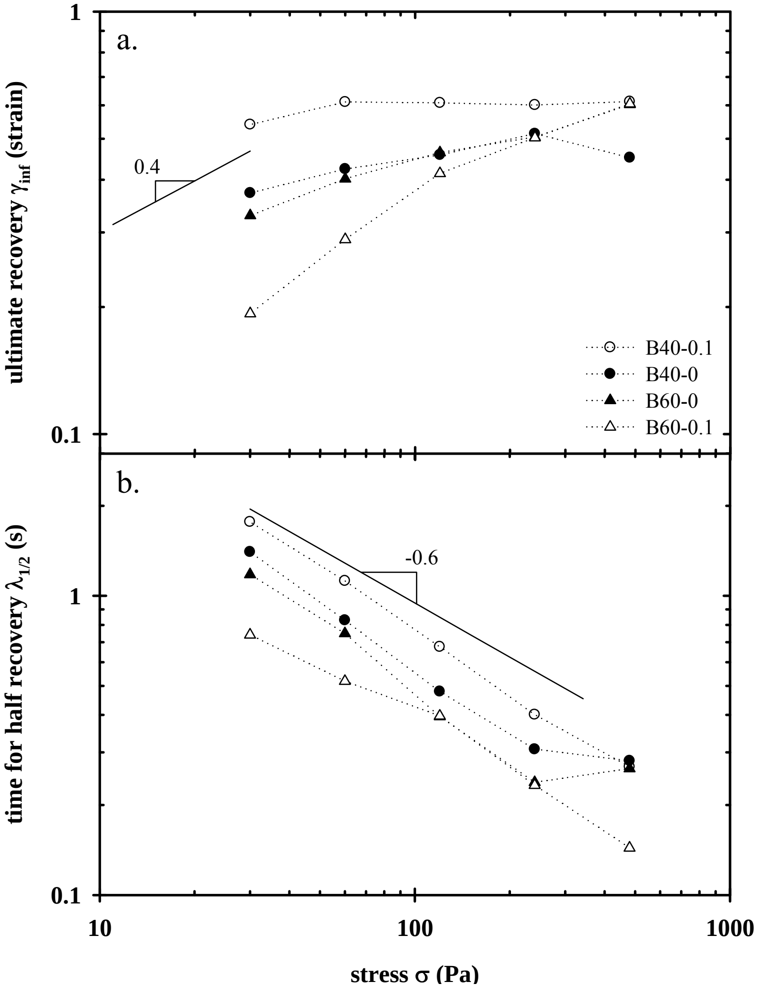

Figure 4.8: a). Ultimate recovery, and b). dimensionless half-recovery time for B40 and B60 blends.

Addition of compatibilizer to the B40 blend increases γ_∞ and $\lambda_{1/2}$ at all stress levels, consistent with previous results on compatibilized B11 blends.[63] Briefly, the mechanism proposed previously was as follows: for a compatibilized droplet-matrix blend under steady shear, the applied flow convects the compatibilizer to the tips of the drops, giving the tips a lower interfacial tension. This non-uniformity in interfacial tension affects the retraction of the drops upon cessation of shear, and hence the recovery. The interplay between various effects (Marangoni stresses, gradients in capillary pressure, change in the average interfacial tension during retraction) is complex,[43,47] but the net effect in this case appears to be an increase in γ_∞ upon addition of compatibilizer to both B11 as well as B40 blends. The only qualitatively new result as compared to Wang and Velankar[63] is the stress dependence of the γ_∞ which has not been studied previously: evidently, the stress dependence of these compatibilized blends is similar to that of uncompatibilized blends, with γ_∞ being weakly dependent on stress and $\lambda_{1/2}$ being approximately proportional to $\sigma^{-0.6}$.

In B60 blends on the other hand, addition of 0.1% compatibilizer has a qualitatively different effect than in the B40-0.1 blend. At the highest stress level, γ_∞ of B60-0.1 is higher than of B60-0. However, with decreasing stress, γ_∞ and $\lambda_{1/2}$ for B60-0.1 reduce sharply and becomes much lower as compared to B60-0. Qualitatively, this is attributable to coalescence suppression: with decreasing stress, the drops of B60-0.1 do not coalesce and hence at the lower stress levels, these smaller drops are less deformed (lower γ_∞) and recover faster (smaller $\lambda_{1/2}$). Moreover, as will be discussed in Section 4.1.3.5, in the B60-0.1 blends, the interface appears to be immobilized by the block copolymer, which is likely to further reduce drop deformation. For both of these reasons, the B60-0.1 blend is expected to have less deformed drops during steady shear, resulting in a lower γ_∞ than the B60-0 blend at low stresses.

4.1.3.5 Interfacial immobilization

The experiments of Section 4.1.3.1 show that at all compatibilizer levels studied here, B40 and B60 blends have a droplet-matrix morphology with the minority phase being the dispersed phase. Thus a morphological change is *not* the cause of this large increase in viscosity, and hence the quantitative difference between the effect of compatibilizer in dilute versus concentrated blends must be attributed to hydrodynamic interaction between drops. It is therefore of interest to examine in detail how the effect of compatibilizer varies with volume fraction of the drops.

We first consider the terminal complex viscosity of uncompatibilized blends. The relative terminal complex viscosities of uncompatibilized blends ranging from 20% PIB to 80% PIB are shown as filled circles in Figure 4.9. Taylor's analysis[73] provides the most basic equation for the viscosity of a surfactant-free emulsion in the low capillary number (or low-frequency) limit when the drops remain undeformed. However that analysis is restricted to dilute emulsions, and is not appropriate here. For concentrated blends, hydrodynamic interactions must be considered. Choi and Schowalter[70] have extended Taylor's analysis to include hydrodynamic interactions to obtain:

$$\eta_{0\mathrm{r}} = \frac{\eta_0}{\eta_m} = 1 + \phi_d \frac{5p+2}{2(p+1)} + \phi_d^2 \frac{5(5p+2)^2}{8(p+1)^2} \tag{4.8}$$

Ignoring the ϕ_d^2 term in Equation 4.8 recovers the Taylor equation.[73] Note that the η_m in the denominator of Equation 4.8 is within 2% of the denominator in Equation 4.2, and hence

Equation 4.8 can be compared straightforwardly to the $\left|\eta_{0r}^{*}\right|$ measured experimentally. This comparison is done in Figure 4.9a, and it is evident that Equation 4.8 overestimates the viscosity of uncompatibilized blends, as has also been noted previously.[74] Much better agreement with the measured $\left|\eta_{0r}^{*}\right|$ is achieved by the equation:

$$\eta_{0r}^{2/5}\left(\frac{2\eta_{0r}+5p}{2+5p}\right)^{3/5}=\frac{1}{1-\phi} \tag{4.9}$$

which was derived by Phan-Thien and Pham[75] using an effective medium approach.

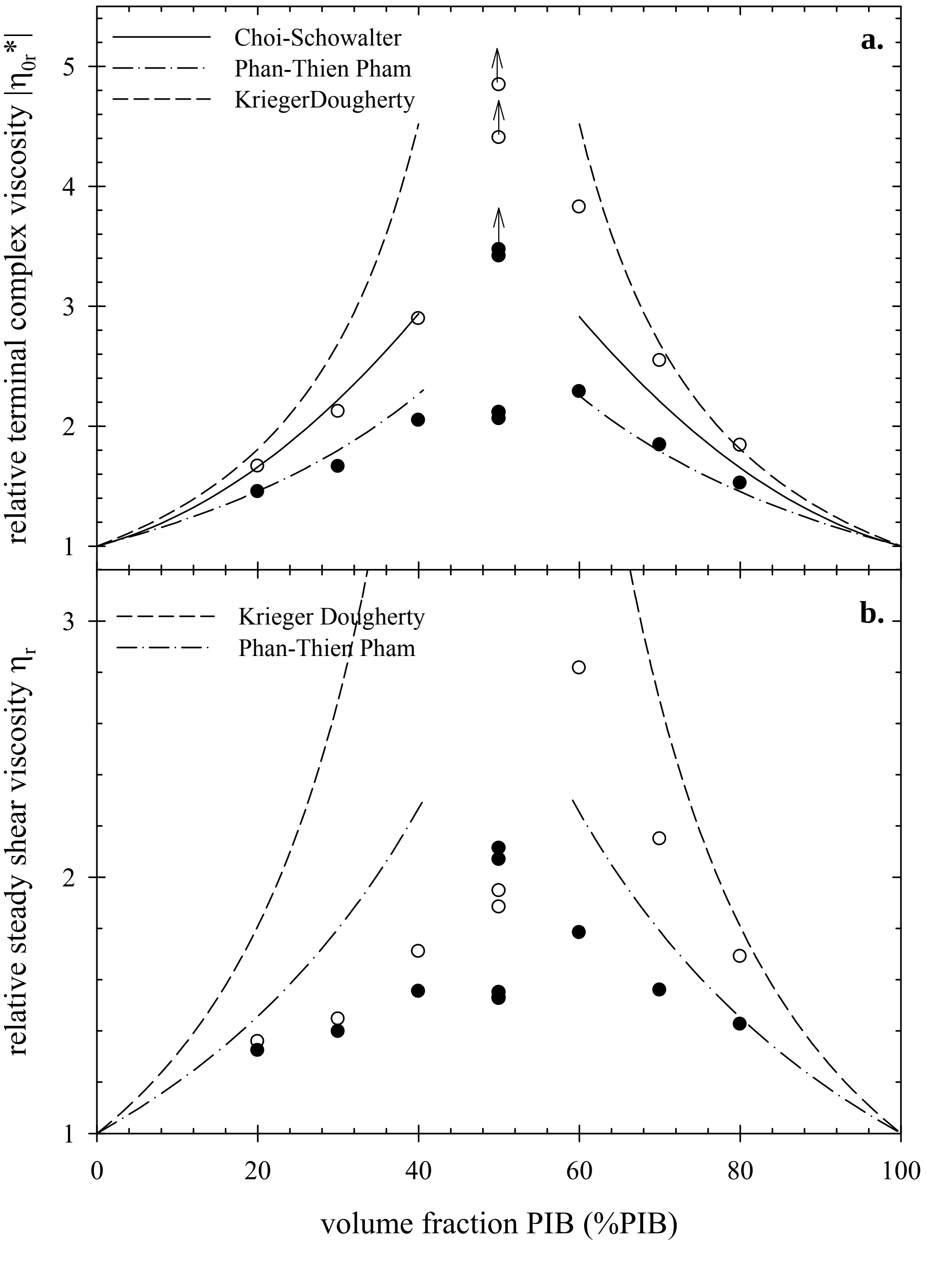

Figure 4.9: a.) Relative terminal complex viscosity. b.) Steady shear viscosity at 120 Pa. In both figures, closed symbols are the uncompatibilized blends, and open symbols are blends with 0.1% compatibilizer.

Next we turn to compatibilized blends. The relative terminal dynamic viscosities of all blends with 0.1% compatibilizer are plotted as open circles in Figure 4.9a. Since the terminal dynamic viscosity is nearly independent of compatibilizer content (Figure 4.4), the open circles are very close to the relative terminal dynamic viscosities at other compatibilizer levels, even as low as 0.01%. These data on the compatibilized blends now better quantify the observation that the effect of compatibilizer on the viscosity increases with increasing drop concentration. The remainder of this section is devoted to interpreting this observation.

A simple mechanism to explain the higher viscosity of compatibilized blends is to postulate that the compatibilizer immobilizes the interface. In the most extreme case of complete immobilization (interface behaves like a solid surface), it is appropriate to compare the viscosity of the blend to that of a suspension of rigid particles. Such a comparison may be made using the Krieger-Dougherty (KD) equation:[76]

$$\eta_r = \left(1 - \frac{\phi}{\phi_m}\right)^{-2.5\phi_m} \tag{4.10}$$

where ϕ_m is the volume fraction of particles at which the viscosity diverges. In the high shear rate limit (which is appropriate here since the drops are not Brownian), a value of $\phi_{max} = 0.68$ has been suggested.[76] Figure 4.9a shows that the KD equation agrees reasonably well with the relative terminal dynamic viscosity of blends with PIB as the continuous phase: the viscosity of B80-0.1 is predicted almost exactly, whereas the viscosities of B70-0.1 and B60-0.1 are slightly overpredicted. This conclusion holds even if slightly different values of ϕ_m are used. Thus we conclude that in the terminal region, 0.1% compatibilizer nearly immobilizes the PDMS drops in PIB, causing them to behave nearly like rigid particles. For PDMS-continuous blends on the other hand, $\left|\eta_{0r}^*\right|$ lies well below the Krieger-Dougherty prediction (once again, using slightly different values for ϕ_m does not change this), suggesting that the PIB drops in PDMS are only partially immobilized in the terminal region. In summary, our experiments suggest that 0.1% compatibilizer (or indeed even 0.01%, since from Figure 4.4 the terminal dynamic viscosity remains the same) is sufficient to nearly immobilize the drop interfaces in PIB-continuous blends, and partly immobilize them in PDMS-continuous blends.

What is the mechanism underlying this complete or partial immobilization of the interface? A possible mechanism is Marangoni stresses as discussed in Section 4.1.3.2: the oscillatory strain imposed on the sample can induce gradients in compatibilizer concentration on the interface. The resulting Marangoni stresses reduce the interfacial mobility. The degree of interfacial immobilization depends on the ratio of the Marangoni stresses to the viscous stresses, the Marangoni number:[77]

$$Ma = \frac{\Delta\alpha}{\sigma R} = \frac{\Delta\alpha}{\alpha}\frac{1}{Ca} \tag{4.11}$$

where σ is the characteristic viscous stress experienced by the drop, R is the drop size, and $\Delta\alpha$ is the characteristic change in interfacial tension induced by the viscous stress. In the terminal region of a dynamic oscillatory experiment, stress can be regarded as proportional to frequency and, hence, we can rewrite

$$Ma = \frac{\Delta\alpha}{\left|\eta_0^*\right|\omega\gamma_0 R} \tag{4.12}$$

where γ_0 is the amplitude of the oscillatory strain.

The characteristic timescale of an oscillatory flow is ω^{-1}. If the compatibilizer adsorbed on the interface equilibrates with that dissolved in the bulk rapidly, i.e., over a time scale much smaller than ω^{-1}, then the interfacial concentration of compatibilizer always remains close to its equilibrium value. In this case, the interfacial tension remains nearly uniform over the surface of the drop during oscillatory flow. Thus, $\Delta\alpha$ and Ma remain small and there is little immobilization of the interface. In the other extreme, if the compatibilizer is completely insoluble in the bulk, flow-induced changes in compatibilizer concentration on the interface do not equilibrate with the bulk. In this case, a significant $\Delta\alpha$ can be induced by the applied flow, Ma can be large, and significant immobilization can occur.

The greatest extent of interfacial immobilization occurs when $Ma \to \infty$. Equation 4.11 suggests that the conditions for this are that 1). $Ca \to 0$, i.e. $\sigma \to 0$, or equivalently $\omega \to 0$, since in an oscillatory experiment, σ can be considered proportional to frequency in the terminal regime, and 2). $\Delta\alpha$ still remain finite even as $\sigma \to 0$. These conditions correspond to the limit of an incompressible interface: one for which infinitesimal changes in compatibilizer concentration induce finite changes in interfacial tension.[77,78] Physically, an incompressible interface corresponds to a drop covered by an insoluble compatibilizer in the limit of zero applied stress or zero oscillatory frequency. In this limit (for dilute emulsions), theory,[40,79] numerical simulations,[77,80] and experiments[42] all show that the terminal dynamic viscosity approaches Einstein's equation for a dilute suspension of rigid particles.[81] This may explain the suspension-like viscosity of B80-0.1.

Yet, all compatibilized blends other than B80-0.1 have viscosities lower than that predicted by KD equation; some, such as B70-0.1 are only slightly lower, whereas others, such as B30-0.1 and B40-0.1 are substantially lower. Within the context of interfacial immobilization, two different mechanisms may be proposed to explain this.

The first addresses the much larger deviations from KD equation of the concentrated blends (B60-0.1 and B40-0.1) as compared to the dilute ones (B80-0.1 and B20-0.1). The key idea is that while a single drop with an incompressible interface may behave like a rigid particle, a pair of drops may not. This is because an incompressible interface can still permit "solenoidal" interfacial velocity fields i.e. fields that have zero divergence.[78,82] Thus, drops with an incompressible interface are still not completely immobile like rigid spheres, and in particular, have a weaker hydrodynamic interaction than rigid spheres. Accordingly, even if the interface is incompressible, the viscosity of such an emulsion should be lower than of a rigid particle suspension. This may be the reason why the viscosities of blends with larger volume fraction of drops deviate increasingly from the KD equation. Future simulations or theories that calculate the viscosity of concentrated emulsions with incompressible interfaces may be able to test this quantitatively.

The second possibility is that in some blends *Ma* is not infinite, but some finite value. This corresponds to a compressible interfacial layer of compatibilizer for which $\Delta\alpha$ does not remain finite, but instead decreases proportionately to the stress (or frequency in the terminal region). Simulations and theory[77] have shown that as *Ma* decreases from infinity to zero, the viscosity of a dilute emulsion decreases from Einstein's equation for a dilute suspension to Taylor's equation for a dilute emulsion. Thus, if different blends have different *Ma* values, they would also have different viscosities, all lower than that of a rigid sphere suspension. This explanation is however not mechanistic; we are unable to comment on the fundamental reason why *Ma* would change from one blend to another.

Next we turn to steady shear viscosity. Figure 4.9b shows the steady shear viscosity for all the blends of Figure 4.9a. Only the results at 120 Pa are shown but the discussion applies to all stress levels. As mentioned in Section 4.1.3.3, in our uncompatibilized blends, the capillary number increases with increasing shear rate. Hence, under steady shear conditions, the drops are more deformed and oriented along the flow direction causing shear thinning of the blend.[69,70] Accordingly, the η_r values for the uncompatibilized blends in Figure 4.9b lie well below the Phan-Thien and Pham prediction.

For compatibilized blends under steady shear, the situation is more complex. As explained previously,[41,77,80] there are now two effects to be considered: drop deformation which tends to reduce the blend viscosity, and interfacial tension gradients, which tend to increase the viscosity. In the limit of low shear rate (i.e. low *Ca*), the drops remain nearly spherical and hence the drop-deformation effect vanishes. Yet, interfacial tension gradients can still exist and partly or fully immobilize the interface, and hence the compatibilizer always increases the viscosity in the zero shear limit. As stress increases, two changes occur, 1). Marangoni stresses cannot keep the drop interfaces immobile (*Ma* decreases as per Equation 4.11) and hence finite gradients in compatibilizer concentration exist on the drop interfaces, and 2). *Ca* increases and the drops become increasingly deformed and oriented along the flow direction. Both these effects contribute to shear thinning. The net effect is that compatibilized blends are more shear-thinning than uncompatibilized ones.[77,80]

This physical picture drawn from theory and simulations[77,80] is qualitatively borne out in Figures 4.6 and 4.9b. It is obvious from Figures 4.6 and 4.9b that none of the blends have steady shear viscosities close to the rigid sphere limit. Even in blends such as B60-0.1 or B70-0.1, while the compatibilizer can maintain nearly-immobile interfaces at low frequencies, it cannot do so when a stress of 120 Pa is applied. Nevertheless, interfacial tension gradients continue to contribute to the steady shear viscosity. In PIB-continuous blends, this contribution is relatively large. Note for example the significantly larger viscosity of compatibilized B60 blends as compared to B60-0 (Figure 4.6). On the other hand, interfacial tension gradients contribute much less to the viscosity in PDMS-continuous blends, note for example that the viscosity of compatibilized B40 blends is only slightly larger than of B40-0 (Figure 4.6). Unfortunately, a quantitative comparison of Figure 4.6 with the simulations is not possible as specific properties of our compatibilizer needed for comparison to the simulations are unknown.

We have conducted the above discussion entirely in terms of Marangoni stresses (or correspondingly, an interfacial dilational modulus) as a mechanism of interfacial immobilization. It is important to realize that while this is probably the simplest explanation for the effect of compatibilizer on the viscosity, other explanations are possible. In particular, it is also possible that the compatibilizer immobilizes the interface by a different mechanism, e.g. by endowing the interface with a shear modulus or a yield stress.

Finally, Figures 4.9a and b show the viscosity of B50 blends. The different points refer to different, independently-prepared blends. It is immediately apparent that the viscosities are widely variable, even in the uncompatibilized B50-0 blend. Also, in some runs (points with upward arrows in Figure 4.9a), the dynamic viscosities showed no sign of leveling off to a terminal value, at least up to 0.01 rad/s, whereas in other runs a clear terminal plateau was evident. Evidently, the rheology, and presumably the morphology, of blends with equal amounts of PIB and PDMS are highly sensitive to the mixing history, leading to the irreproducibility.

4.1.3.6 Coalescence suppression

Now we return to the issue of coalescence suppression. In B40 and B60 blends, due to the proximity of the expected phase inversion point, there may be anomalous effects. It would be better to verify that coalescence suppression is actually occurring by conducting experiments on morphologies that are unambiguously droplet-matrix. Therefore, we will first present some limited data on B20 and B80 blends, compare these results to the B40 and B60 blends, and try to explain the coalescence suppression phenomena in terms of concepts introduced in section 4.1.3.5.

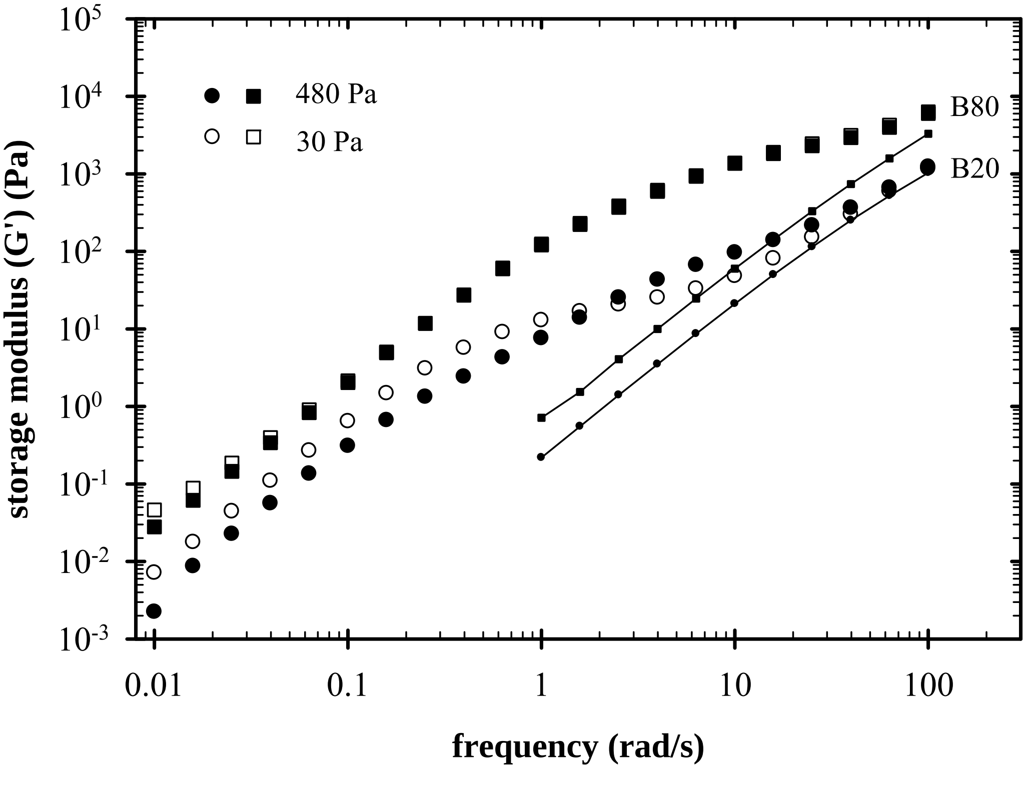

Figure 4.10: Dynamic oscillatory properties of B20-0.1 and B80-0.1 blends. G' values for B80-0.1 have been shifted upward by a factor of 10. Open and filled symbols correspond to experiments after shearing at 480 Pa and 30 Pa respectively. Solid lines are component contributions.

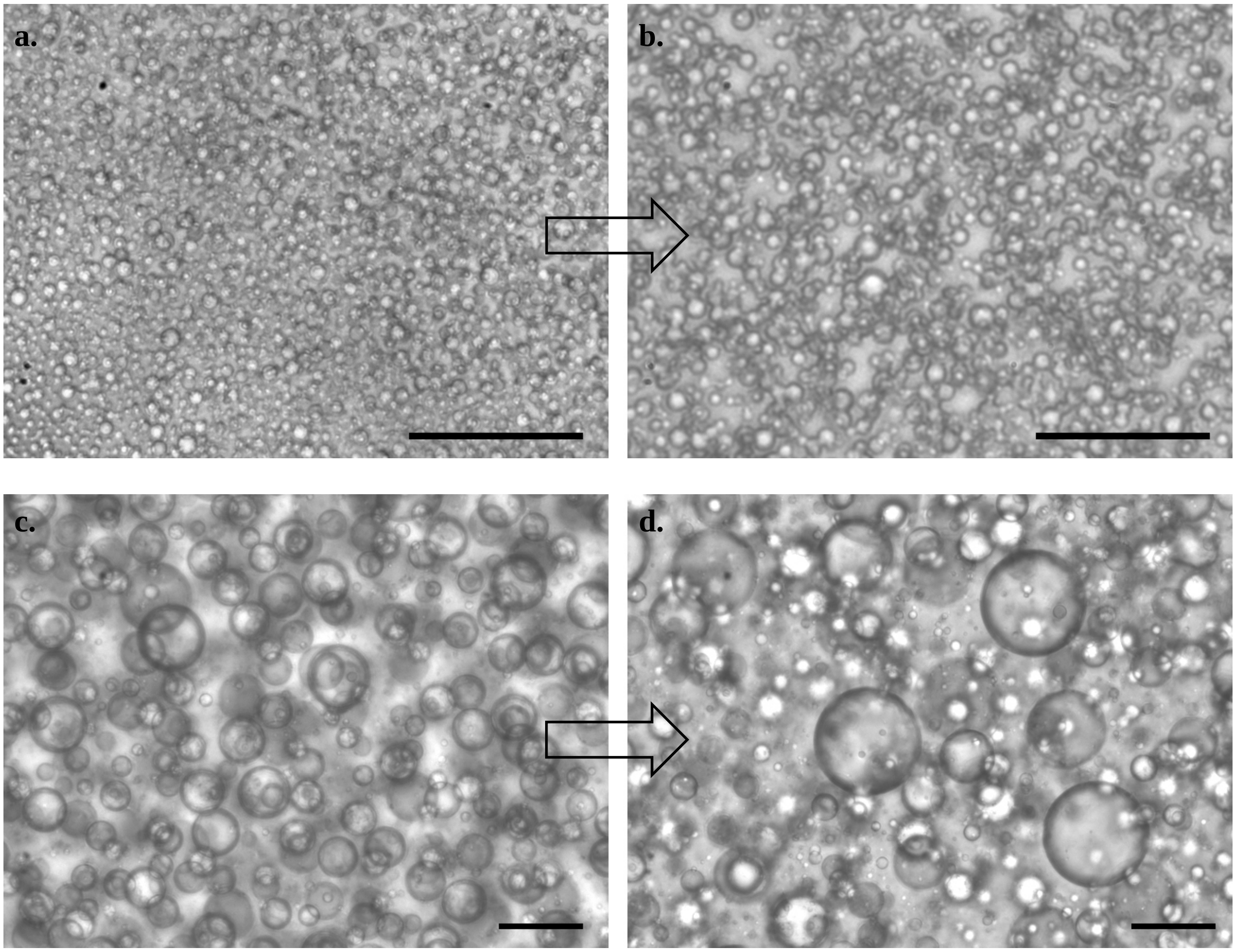

Figure 4.11: B20-0.1 blend a.) as mixed, and b.) after twelve hours of static coalescence; and B80-0.1 blend c.) as mixed, and d.) after four days of static coalescence. The scale bars represent 20 μm.

Figure 4.10 shows the dynamic oscillatory behavior of B20-0.1 and B80-0.1 blends. Again, for clarity, only the curves for G' vs. ω at the end of the highest stress (480 Pa) and lowest stress level (30 Pa) are shown, and the curves at intermediate stresses lie between these limits. Similar to the B60-0.1 blend in Figure 4.3b, the shoulder of the B80-0.1 blend does not change with stress, indicating that coalescence has been suppressed. Also, the shoulder of the B20-0.1 blend moves to lower frequencies with decreasing stress, indicating that coalescence has occurred and the average drop size has grown, similar to the B40-0.1 blend in Figure 4.3a. This confirms the hypothesis stated in Section 4.1.3.1 that coalescence is suppressed for PIB-continuous compatibilized blends, but not for PDMS-continuous compatibilized blends.

To confirm further, direct microscopic evidence of coalescence suppression is needed. Images of the B20-0.1 and B80-0.1 blends as mixed can be seen in Figure 4.11a and c, and images of the blends after allowing time for static coalescence to occur can be seen in Figure 4.11b and d. In Figure 4.11b, the appearance of large drops indicates that some amount of coalescence has occurred in the B20-0.1 blend. However, the average drop size appears to increase only slightly for the B80-0.1 blend in Figure 4.11c and d after *four days* under quiescent conditions. Thus, in accordance with our rheological studies, we conclude that the diblock copolymer can stop coalescence of PDMS drops in PIB, but not of PIB drops in PDMS for our B20-0.1 and B80-0.1 blends, analogous to the B40 and B60 compatibilized blends.

A final direct test of coalescence suppression is to leave the sample in a petridish under quiescent conditions. All uncompatibilized blends, and compatibilized blends with PDMS as the majority phase showed large-scale phase separation visible even to the naked eye after a week. However, compatibilized samples with PIB as the continuous phase maintained their uniformly white appearance for at least two months. For example, a B40-0.1 blend and B60-0.1 blend are shown as mixed in Figure 4.12a, and after two weeks under quiescent conditions at room temperature in Figure 4.12b. Large scale phase separation can be clearly seen in the B40-0.1 blend, whereas the B60-0.1 appears the same. Micrographs of each blend can be seen in Figure 4.12c-f. Clearly, the drop size grew dramatically in the B40-0.1 blend, and only slightly in the B60-0.1 blend. In summary, the conclusion drawn from the rheological experiments is validated:

the diblock copolymer can stop coalescence of PDMS drops in PIB, but not of PIB drops in PDMS. We will now attempt to discuss the mechanism causing coalescence suppression.

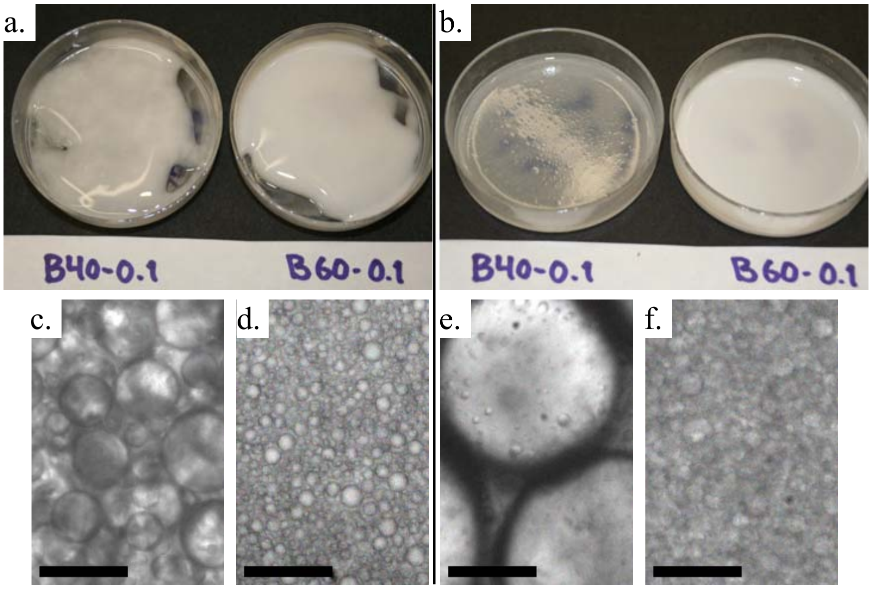

Figure 4.12: Photographs of petridishes containing B40-0.1 and B60-0.1before (a) and after (b) two weeks under quiescent conditions. c-f.: Corresponding optical microscope images. Scale bars represent 20 μm.

For over a decade it has been accepted that block copolymers can suppress coalescence in droplet-matrix blends.[3,83] In fact it is now believed that suppression of coalescence is the main reason why block copolymers promote blending of immiscible homopolymers. Yet, the asymmetric coalescence suppression in our blends is somewhat puzzling, considering that the block copolymer is not particularly asymmetric ($M_{w,PIB}$ = 6,150 g/mol and $M_{w,PDMS}$ = 8,000 g/mol). While asymmetric coalescence has not been well-documented in polymeric systems (however see Van Hemelrijck *et al.*,[62] discussed below), it is very well-known in oil/water/surfactant systems. There are even well-established rules on which surfactants prevent coalescence of oil drops in water and vice versa. For example, a common rule of thumb, Bancroft's rule, states that a stable water-in-oil emulsion results from an emulsion containing a surfactant that has higher solubility in oil than in water, and vice versa.

Two mechanisms have been proposed to explain suppression of coalescence in polymeric systems.[84] The first is that as two drops approach each other due to the externally-applied flow, the block copolymer must be squeezed out of the region between the two drops. This causes a gradient in the block copolymer concentration, and hence a Marangoni stress, which inhibits the drainage of the film between the colliding drops, and may also modify the trajectories of drops before they collide.[30,85,86] The strength of this effect can be gauged by the Marangoni number, Ma, a ratio of the Marangoni stress to the viscous stress[62,77] (Equation 4.11). If *Ma* is sufficiently large, the interface of the drops may become nearly-immobilized causing a severe decrease in the likelihood of coalescence. The Marangoni stress mechanism to explain coalescence suppression is based on continuum fluid mechanics and ignores the macromolecular nature of the compatibilizer. In fact it even applies to oil/water or other small molecule systems with surfactant; the only requirement is that the surfactant must be able to reduce the interfacial tension between the immiscible phases.

From a continuum perspective however, the B40-0.1 and B60-0.1 blends appear to be very similar. The same interfacial tension is expected regardless of which phase forms drops (the asymmetric effects in interfacial tension seen by Zeigler and Wolf[51] should only occur in blends with very low drop volume fractions). Furthermore, our PIB and PDMS have the same viscosity, and hence the hydrodynamics of drop collision and film drainage should be similar in B40 and B60 blends. Hence, at first glance it appears that the Marangoni stress mechanism cannot explain our asymmetric coalescence suppression. Yet, if there is a large difference in solubility and/or diffusivity of the block copolymer in the two bulk phases, the Marangoni stress mechanism can still predict asymmetric coalescence. In fact, Bancroft's rule for oil/water systems, which correlates coalescence suppression to the relative solubility of the surfactant between the two phases may be rationalized by the Marangoni stress mechanism.[87]

The second mechanism is one of steric hindrance.[3] As drops approach each other, the block of the block copolymer outside the drop must compress, and the force required for this compression corresponds to a repulsive potential between the drops that keeps the drops apart and prevents coalescence. This mechanism applies specifically to polymeric systems and requires that the bcp have a sufficiently high molecular weight.[88] In cases when the one block is short and the other is long, asymmetric coalescence suppression is expected. Indeed, Van Hemelrijck *et al.*[62] noted that a poly(isoprene)-PDMS diblock with a long poly(isoprene) block and a short PDMS block could suppress coalescence only when poly(isoprene) was the continuous phase. As mentioned above, in the present case, the block copolymer used in this work is not especially asymmetric. However, from a molecular perspective, the PIB and PDMS homopolymers used here are not at all similar. They have a large difference in molecular weight: M_w = 1300 g/mol for PIB versus M_w exceeding 100,000 g/mol for PDMS. Thus, we speculate that the PIB block is highly swollen by the low MW PIB homopolymer, and hence is an effective steric barrier to coalescence when PIB is the continuous phase. In contrast, we speculate that the PDMS block is not at all swollen, and hence in a collapsed conformation which cannot hinder coalescence when PDMS is the continuous phase. It must be emphasized that this explanation is only tentative and we do not have direct evidence supporting it.

4.1.3.7 Differences between PIB-continuous and PDMS-continuous blends

We will now summarize the differences between B40 and B60 compatibilized blends. This discussion extends to all compatibilized blends studied with PIB continuous phase (B80, B70, B60) and those with PDMS continuous phase (B20, B30, B40). The differences we saw were: 1.) compatibilizer suppresses coalescence in PIB-continuous blends, 2.) the terminal dynamic viscosities of compatibilized PIB-continuous blends are close to or slightly lower than those of rigid particle suspensions, whereas terminal dynamic viscosities of compatibilized PDMS-continuous blends are substantially lower, 3.) PDMS-continuous blends undergo shear-thinning at far lower stresses than PIB-continuous blends, 4.) the compatibilizer increases the steady-shear viscosity much more in PIB-continuous blends. All of these differences may be explained by postulating that the compatibilizer immobilizes the interface much more when PIB is the continuous phase. While it is not clear why the degree of immobilization depends on which phase is continuous, it may make modeling easier. For example, all the four differences above may be modeled by endowing the interface with interfacial viscoelastic properties that depend on which phase is continuous. We reiterate that this is not a mechanistic approach and the fundamental reason why the PIB-continuous blends are immobilized to a greater extent remains unknown.

Finally we note that the *uncompatibilized* blends themselves do not show fully-symmetric behavior, e.g. both $\left|\eta_{0r}^{*}\right|$ as well as η_r are not symmetric about the 50/50 composition. While the differences between uncompatibilized PIB-continuous blends and uncompatibilized PDMS-continuous blends are not as large as those in the presence of compatibilizer, we are unable to propose a mechanism to explain them.

5.0 MORPHOLOGICAL CONTROL BY VARYING SEQUENCE OF BLENDING

Careful optical microscopy of our compatibilized B40 blends revealed that the PIB drops contained some smaller PDMS drops. Presumably, these small PDMS drops were trapped inside the PIB drops during blending and could not coalesce with the surrounding PDMS phase because of the compatibilizer. This is consistent with section 4.1.3.6 in which we noted that PDMS drops in PIB do not coalesce in a compatibilized blend.

For over a decade, it has been known that some compatibilizers (polymeric surfactants) can suppress coalescence in blends of immiscible homopolymers.[2,29,32,34,37,88] Likewise, it is well-known that oil/water emulsions can be stabilized by surfactants. In fact, the surfactant is one of the chief factors determining which phase becomes continuous: with some types of surfactants, the emulsion prefers to have a oil-in-water morphology (or "type"), whereas with other surfactants, a water-in-oil morphology is preferred.[89,90] In oil/water systems, mechanistically, the surfactant plays two major roles: 1.) it lowers the interfacial tension thus promoting breakup of drops when the emulsion is prepared, and 2.) it helps prevent subsequent coalescence of drops, thus stabilizing the emulsion. Surfactant-induced coalescence suppression is a means of kinetic trapping, i.e. metastable emulsion morphologies may persist for long periods because drops cannot coalesce and allow the emulsion to evolve into a more preferred morphology. Therefore surfactants offer a powerful method of controlling the morphology and phase continuity in oil/water systems. In particular, by carefully controlling the emulsion-preparation protocol, it is possible to realize kinetically-trapped emulsion morphologies, such as drops inside of drops or “double emulsion” morphologies, that are different from the preferred morphology.

Because compatibilizers can suppress coalescence of drops in immiscible polymer blends, the possibility is raised of applying ideas of structure control from oil/water emulsions to immiscible polymer blends. In particular, we hypothesize that a compatibilizer and some specific blending protocols can be used to control the structure and phase continuity in polymer blends.

5.1 PIB/PDMS BLENDS

5.1.1 Materials and methodology

As mentioned previously, we wish to test whether preparation protocols can be used to control the morphology of blends of immiscible polymers. Experiments are conducted on model blends of polyisobutylene (PIB) and polydimethylsiloxane (PDMS), compatibilized by a PIB-PDMS diblock copolymer. Two preparation protocols drawn from the literature on oil/water emulsions are applied to the polymer blends.

In the “double blending” protocol, a droplet-matrix blend is blended with additional drop-phase fluid. As in oil/water emulsions, this yields a drop-within-drop “double emulsion” morphology. The role of the compatibilizer in suppressing coalescence is crucial to realizing stable double emulsion morphologies. We hypothesize that stable double emulsion morphologies can be prepared when coalescence is suppressed in our polymeric system.

In the “multistep concentration” protocol, the drop phase is added gradually (rather than all at once) to the matrix phase. While this protocol can realize a high-dispersed phase emulsion in oil/water systems, in the present case, a high-dispersed phase blend was not achieved; phase inversion occurred when the drop volume fraction exceeded 0.5.

Again, PDMS and PIB are used as the blend components(η_{PDMS} = 56.2 Pa.s and η_{PIB} = 57.3 Pa.s at 25°C), with the same PIB-PDMS diblock copolymer ($M_{w,PIB}$ = 6,150 g/mol and $M_{w,PDMS}$ = 8,000 g/mol,) as the compatibilizer.

Samples were examined with an Olympus CKX-41 inverted microscope in brightfield transmission mode without temperature control, and images were recorded with a Basler A302 area scan camera.

Rheological experiments were performed in a TA Instruments AR2000 stress-controlled rheometer using a 40mm diameter, 1° cone and plate geometry and a Peltier cell to maintain the sample temperature at 25°C.

5.1.2 Double blending protocol

In this section, we will discuss the rheological and morphological consequences of both the “double step” and “multistep concentration” blending protocols performed on the PIB/PDMS system.

Figure 5.1 schematically shows the standard “single-blending” procedure for blending together two immiscible fluids A and B, along with a small amount of any surface-active species. This same procedure was used in all of our previous research. We applied this procedure to the B20-0.1 blend: the two homopolymers and the compatibilizer were weighed into a petridish and blended with a spatula. As mentioned above, the minority phase always becomes the dispersed phase in this blend system; indeed optical microscopy revealed the PIB-in-PDMS droplet-matrix morphology of Figure 5.1. (Note that Figure 5.1 by itself does not indicate whether the drops are PIB or PDMS, however, the continuous phase has been verified to be PDMS using the procedure described previously in Section 4.1.3.1).

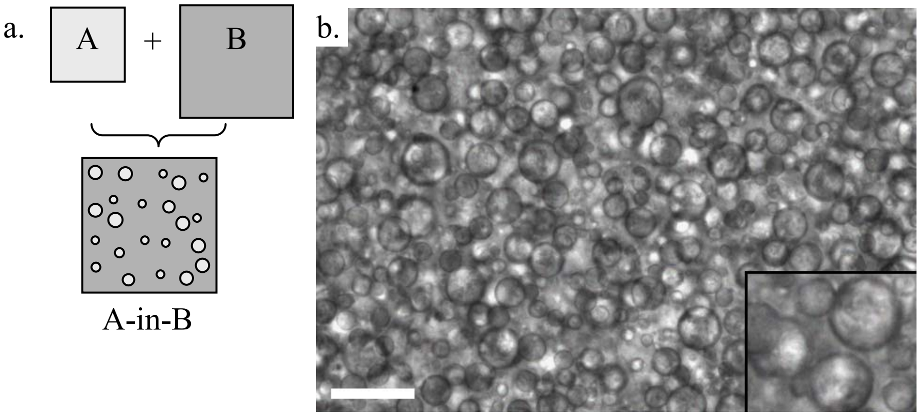

Figure 5.1: a.) Schematic of the standard single-blending procedure. b.) A B20-0.1 blend with a simple PIB-in-PDMS morphology realized by single-blending. Scale bar represents 20 μm for the main image and 10 μm for the inset.

Figure 5.2a illustrates an alternate "double-blending" protocol for blending together the same components. In the first step, the phase A is blended with only a small portion of phase B. Since B is a minority, a B-in-A morphology is expected. This blend is then itself blended with the remaining B to realize a B-in-A-in-B "double emulsion" morphology. We applied this double-blending procedure to the PIB/PDMS system. In the first step, a B60-0.1 blend with a PDMS-in-PIB morphology (Figure 5.2b) was prepared by single-step blending. It was then blended in a 1:2 ratio with B0-0.1 (i.e. PDMS with 0.1% compatibilizer) so as to realize a blend whose *overall* composition was identical to the B20-0.1 of Figure 5.1b. The resulting morphology (Figure 5.2c) was however dramatically different from Figure 5.1b: the PIB drops had a significant number of PDMS sub-drops. Realizing such a PDMS-in-PIB-in-PDMS double emulsion morphology requires that the inner PDMS drops do not “leak” out during blending, and hence the second blending step involved only gentle blending.

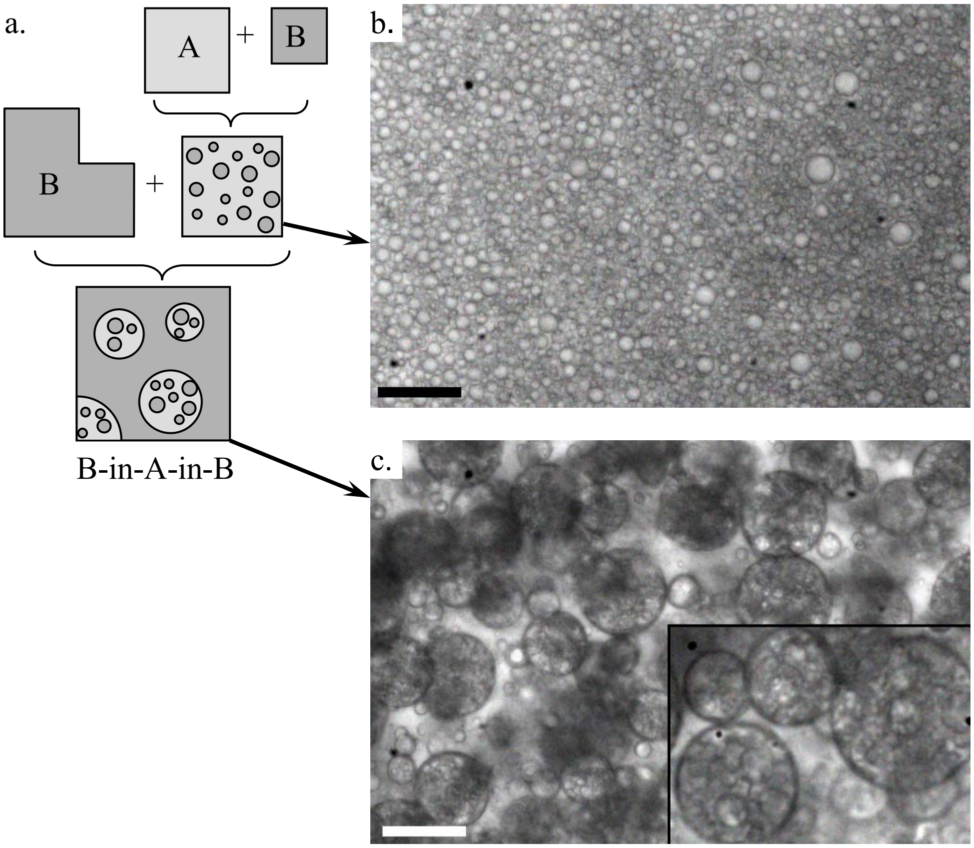

Figure 5.2: a**.**) Schematic of the double-blending procedure. b.) A B60-0.1 blend with a PDMS-in-PIB morphology. c.) A B20-0.1 blend prepared by gently blending b. with B0-0.1 (i.e. PDMS with 0.1% compatibilizer). Scale bars represent 20 μm for the main images, and 10 μm in the inset to c.

The double blending procedure to realize double emulsion morphologies is well-known in the literature on oil/water emulsions, and such double emulsions have been considered for controlled release of pharmaceuticals or food compounds.[91-93] However, to our knowledge, this is the first example of applying such a procedure to a blend of polymer melts. (Impact-modified polystyrene or other rubber-toughened glassy plastics can show such a "double emulsion" morphology, often called a "salami" morphology.[94-96] However, such a PS-in-rubber-in-PS morphology is achieved not by a melt blending procedure, but by phase inversion occurring during polymerization. In such cases, a large fraction of graft copolymer is essential to observe a salami structure. A double emulsion morphology was also obtained due to thermodynamic interactions between the block copolymer and the homopolymers.[97] In this case samples were solvent-cast, and contained a far larger quantity (15%) of block copolymer.)

Coalescence suppression is crucial to realizing a double emulsion morphology. We applied the double blending procedure to two systems in which coalescence of the sub-drops is not suppressed. The first is a compatibilizer-free version of Figure 5.2, i.e. a B60-0 sample was prepared and then blended with additional PDMS so as to realize a final composition of B20-0 (Figure 5.3a). The second is an inverted version of Figure 5.2: A B40-0.1 blend with a PIB-in-PDMS morphology was first prepared and was then blended with a B100-0.1 (i.e. PIB with 0.1% compatibilizer) to prepare a B80-0.1 sample (Figure 5.3b). In both cases, the sub-drops readily coalesced with each other. Many of these large sub-drops also coalesced with the external matrix, but some survived the blending process. Therefore some of the external drops in Figures 5.3a and b, especially in Figure 5.3b, show a single large sub-drop. In summary, sub-drop coalescence must be suppressed to realize a stable double emulsion morphology.

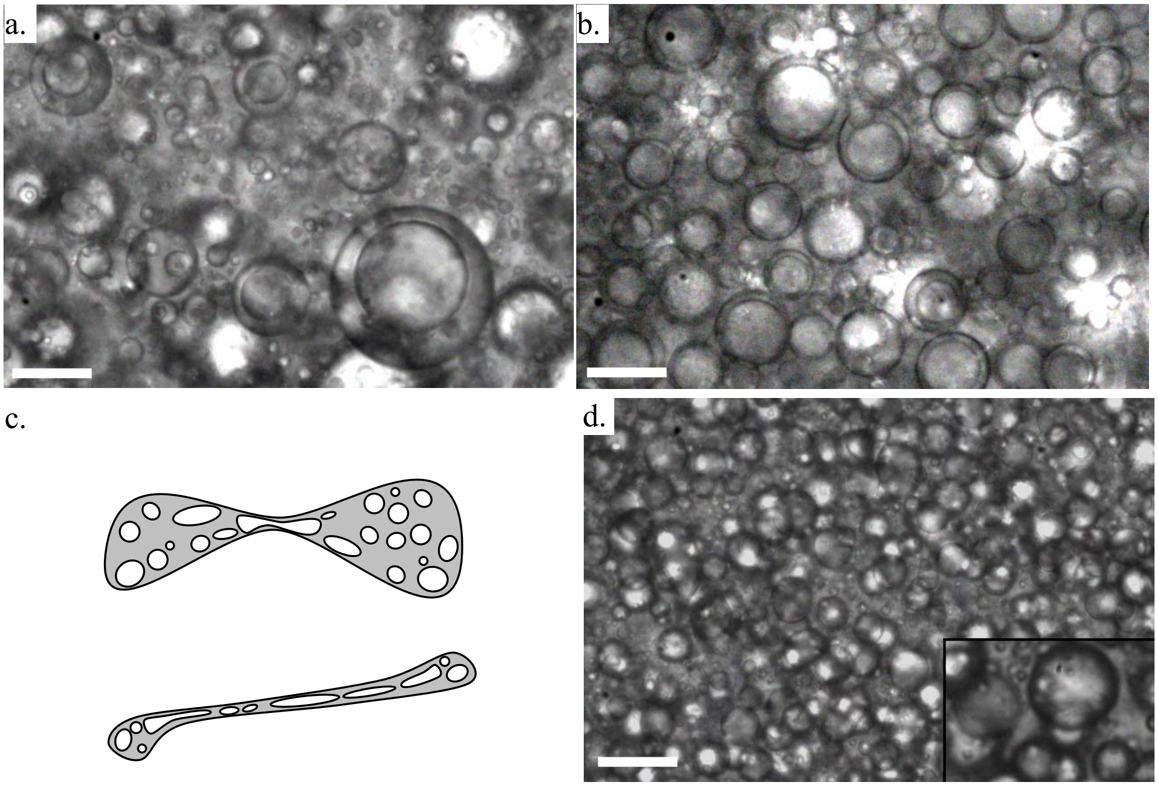

Figure 5.3: a.) B20-0 prepared by gently blending B60-0 with PDMS. b.) B80-0.1 prepared by gently blending B40-0.1 and B100-0.1. c.) Schematic of double emulsion drops deforming when subjected to vigorous blending. Some sub-drops are likely to leak out during deformation and breakup. d.) The blend of Fig. 5.2c. subjected to vigorous blending. Scale bars represent 20 μm for the main images and 10 μm for the inset to d.

However, coalescence suppression by itself is not sufficient realize a double emulsion morphology. It is also essential that the second blending step be done gently. If the second blending is vigorous, the large stresses induce breakup of double emulsion drops (shown schematically in Figure 5.3c), and can lead to substantial leakage of sub-drops. This can be illustrated by subjecting the B20-0.1 double emulsion of Figure 5.2c to vigorous blending; in this case, virtually all drops leaked out into the continuous phase during blending and a simple droplet/matrix morphology resulted (Figure 5.3d). The fact that vigorous blending induces substantial leakage is also well-known in the oil/water emulsion literature; indeed, standard procedures call for using a high-shear homogenizer when preparing the first emulsion, but only gentle stirring when dispersing this emulsion into additional drop-phase fluid.[93]

To confirm that the PDMS sub drops were indeed leaking into the matrix phase, we performed a slight variation on the double blending procedure, where a small amount of fluorescently-tagged PDMS was added to the PDMS in the first mixing step (Figure 5.4b). The blend was mixed gently in the second mixing step, and imaged with a confocal microscope. Many sub-drops can be seen in Figure 5.4c, with little, if any, fluorescence present in the matrix PDMS. Therefore, we conclude that the gentle mixing caused a minimal amount of leakage. This blend was then subjected to vigorous blending for five minutes (Figure 5.4d). During the vigorous mixing, virtually all sub-drops have coalesced with the matrix phase. This is evident not only from the lack of sub-drops, but the presence of fluorescence in the matrix phase and lack of fluorescence in the PIB drop phase. We therefore conclude that vigorous mixing causes substantial sub-drop leakage in our PIB/PDMS double emulsion blends. Even though the compatibilizer is able to suppress the coalescence of PDMS drops with each other and with the matrix phase under quiescent and gentle blending conditions, it is not able to do so under high-stress mixing conditions. We hypothesize that the compatibilizer is not able to suppress coalescence under high-stress conditions because under these conditions, drops are extended a great deal, and when the interfacial area of a sub-drop increases its interfacial compatibilizer concentration decreases below a point where it is able to suppress coalescence (see Figure 5.3c).

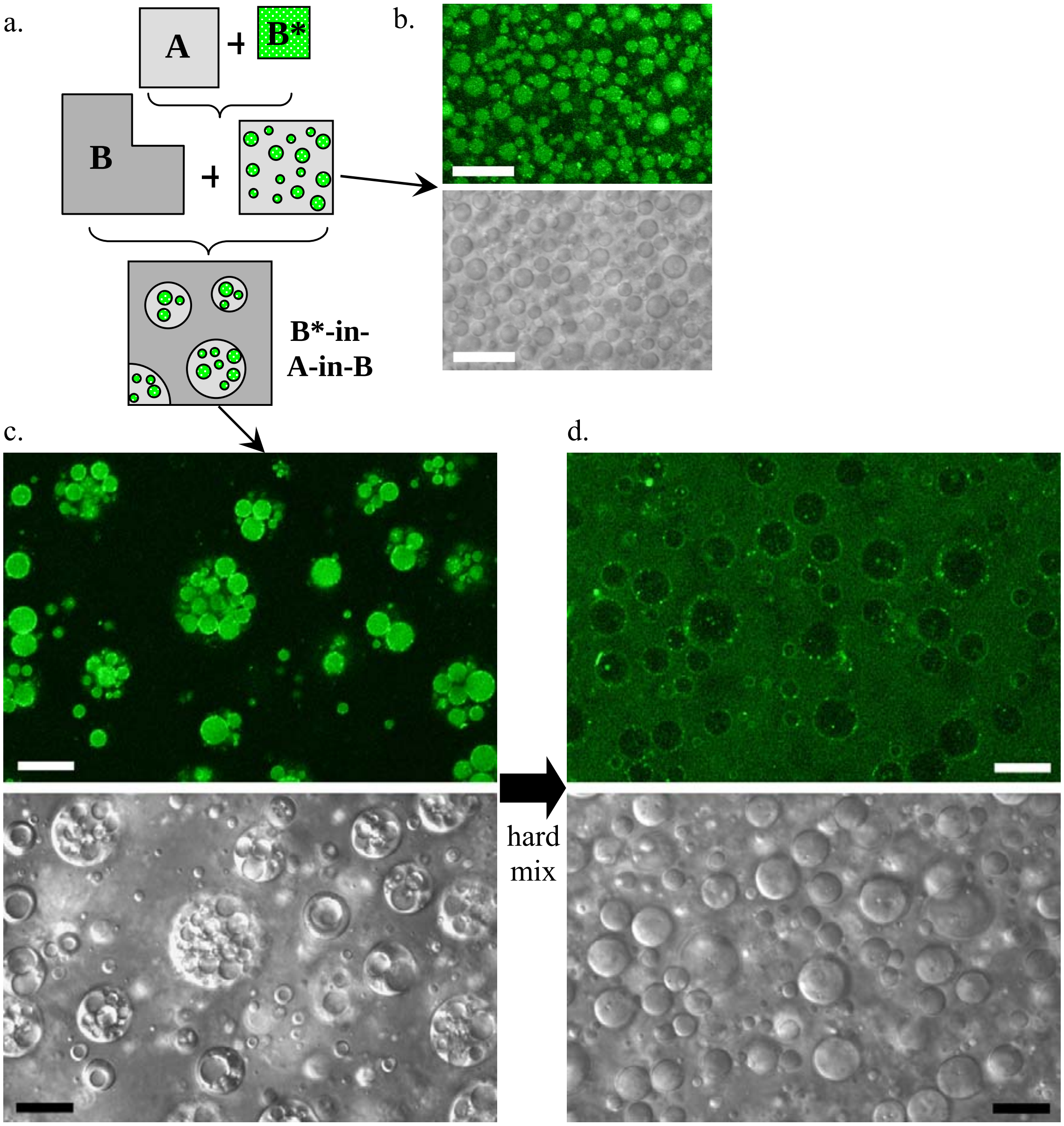

Figure 5.4: a.) "Double blending" protocol with fluoro-PDMS in the first step. b.) Precursor B60-0.1 blend. c.) Double emulsion blend with fluoro-PDMS sub drops. d.) Blend from part c. subjected to vigorous mixing. Scale bars represent 20 μm.

Finally, we note that it is difficult to quantitatively judge the extent of leakage from optical microscopy. Images such as Figure 5.3a, b, and d, and Figure 5.4d show hardly any sub-drops, and hence massive amounts of leakage can be readily inferred. However, images such as Figure 5.2c are more difficult to evaluate: it is not clear whether the drops of blend of Figure 5.2c have an internal sub-drop volume fraction of 0.4 (same as Figure 5.2b), or whether some leakage occurred and the internal sub-drop volume fraction is less than 0.4. One of the goals of this section is to investigate whether rheology can be used more quantitatively to estimate the leakage.

5.1.2.1 Rheological properties of double-blended samples

The rheology of oil/water double emulsions with an appreciable dispersed phase volume fraction is complex. For example, Pal[98] states that, if the double emulsion morphology is simplified to a core-shell morphology (equivalent to all sub-drops coalescing with each other), the relative viscosity of the double emulsion is a function of five variables: the ratio of the core drop to outer shell radii, the ratio of the core to the matrix viscosity, the ratio of the core to the shell viscosity, the volume fraction of the core-shell droplets, and the maximum packing volume fraction of undeformed core-shell droplets.[98] Since our double emulsion system is of the type PDMS-in-PIB-in-PDMS, and our PIB and PDMS are equiviscous, the core, shell, and matrix fluids all have equivalent viscosities. Therefore, the relative viscosity of our PIB/PDMS double emulsion blends should be a function of primarily the volume fraction of the internal droplets, and hence an "effective" dispersed phase volume fraction ϕ_{eff}.

The rheological properties of B20-0.1 samples prepared by the double-blending procedure depend on the intensity of blending; the more gentle the blending, the larger is the fraction of sub-drops that survive the blending process. Therefore we will illustrate the range of rheological behavior possible by showing results for two specific B20-0.1 samples, one blended gently (same sample as Figure 5.2c, henceforth denoted B20-0.1g) and the other blended extremely vigorously (same sample as Figure 5.3d, henceforth denoted B20-0.1v). These two samples will be compared against the reference case of the single-blended B20-0.1 sample.

Figure 5.5 compares the storage modulus G' and the magnitude of the complex viscosity $|\eta^*|$ of these three samples; we emphasize that all three have the same overall composition, but only differ in their preparation method. These measurements were conducted on "as-loaded" samples with no additional shearing. All blends show qualitatively similar behavior: at high frequencies, the properties approach the volume-weighted average of the components, whereas at low frequencies, the blends show an additional relaxation process which is manifested as a pronounced shoulder in G' and an increase in the terminal complex viscosity. In the case of uncompatibilized blends, this "interfacial relaxation process" is attributable to the deformation and relaxation of drop shapes due to the applied oscillatory flow.[57,58,99] In compatibilized blends, the interfacial relaxation is attributable to both drop shape relaxation, as well as relaxation of gradients in interfacial tension on the drop interfaces (see Section 4.1.3.2).[37,100]

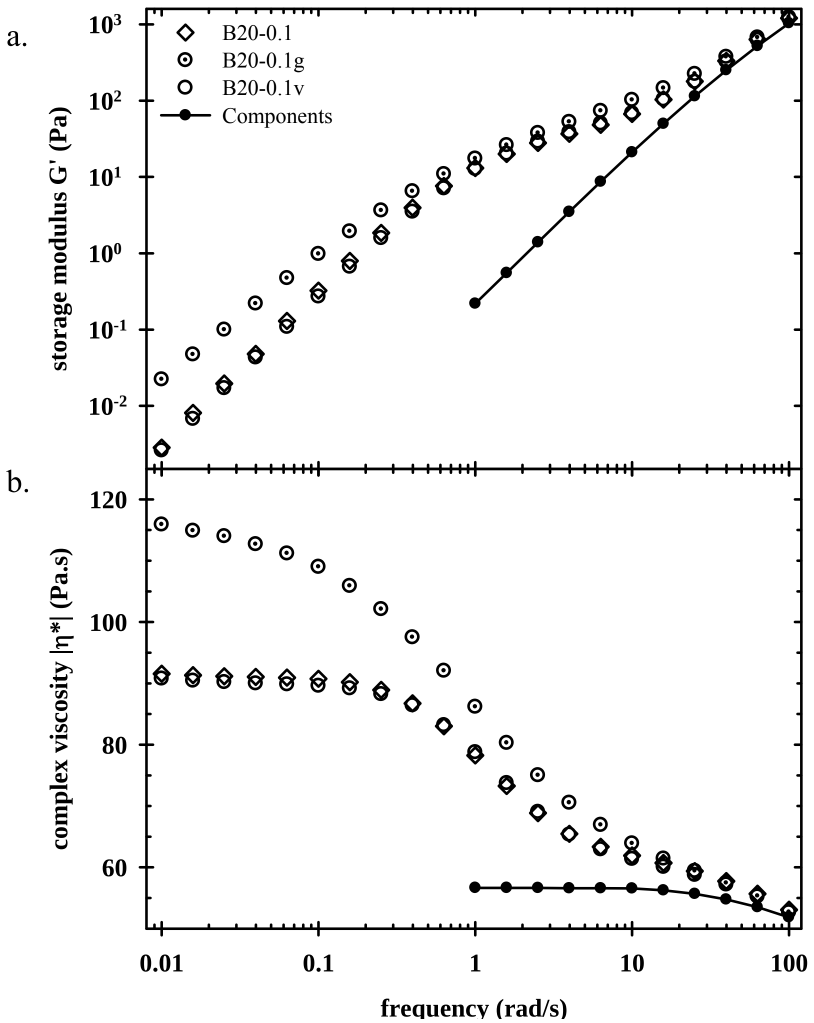

Figure 5.5: Dynamic oscillatory properties of various blends "as-loaded" in the rheometer. The "components" curve is a volume-weighted average of the PIB and PDMS homopolymers.

Figure 5.5 makes two noteworthy observations. First, the terminal complex viscosity of the double-blended B20-0.1g is substantially larger than that of the single-blended B20-0.1. Second, the rheological properties of the B20-0.1v blend are comparable to the single-mixed B20-0.1, as is indeed expected from the almost complete leakage of the sub-drops noted by microscopy (Figure 5.3d). We also note that the G' of the B20-0.1g blend is substantially higher than of the other two blends, especially at low frequencies. This is likely attributable to the very large drop size caused by gentle blending, rather than to the double emulsion morphology *per se*.

In Section 4.1, we used the shear protocol of Figure 4.1 to examine the effect of stress on various rheological properties. Here we will apply the same shear protocol to the three B20-0.1 samples prepared by various methods, and compare their rheological properties. The shear protocol consists of steady shearing at a specific stress for 2000 strain units, followed by strain recovery after cessation of shear, followed by an oscillatory frequency sweep at 25% strain under quiescent conditions. These three steps are repeated at successively lower stresses. Optical microscopy of blends recovered from the rheometer at the end of this test sequence shows that the double emulsion morphology persists under shear, i.e. sub-drop leakage is not obviously evident. A further comment on this is made when discussing Figure 5.8a below.

The steady-shear viscosities of the blends, η, obtained at each stress are shown in Figure 5.6a (read off the right axis). The relative viscosity, η_r, is obtained by normalizing the viscosity with the volume-weighted average of the components (Equation 4.6). The values of the relative viscosity are shown in Figure 5.6a on the left axis. All three blends are seen to be shear-thinning. The reasons for the shear-thinning have been discussed previously: with increasing stress, the drops deform and orient along the flow direction, and the contribution of interfacial tension gradients to the shear stress also decreases.[41] The chief observation of Figure 5.6a is that the viscosity of B20-0.1g double emulsion morphology is significantly higher than of the other two blends at all stresses.

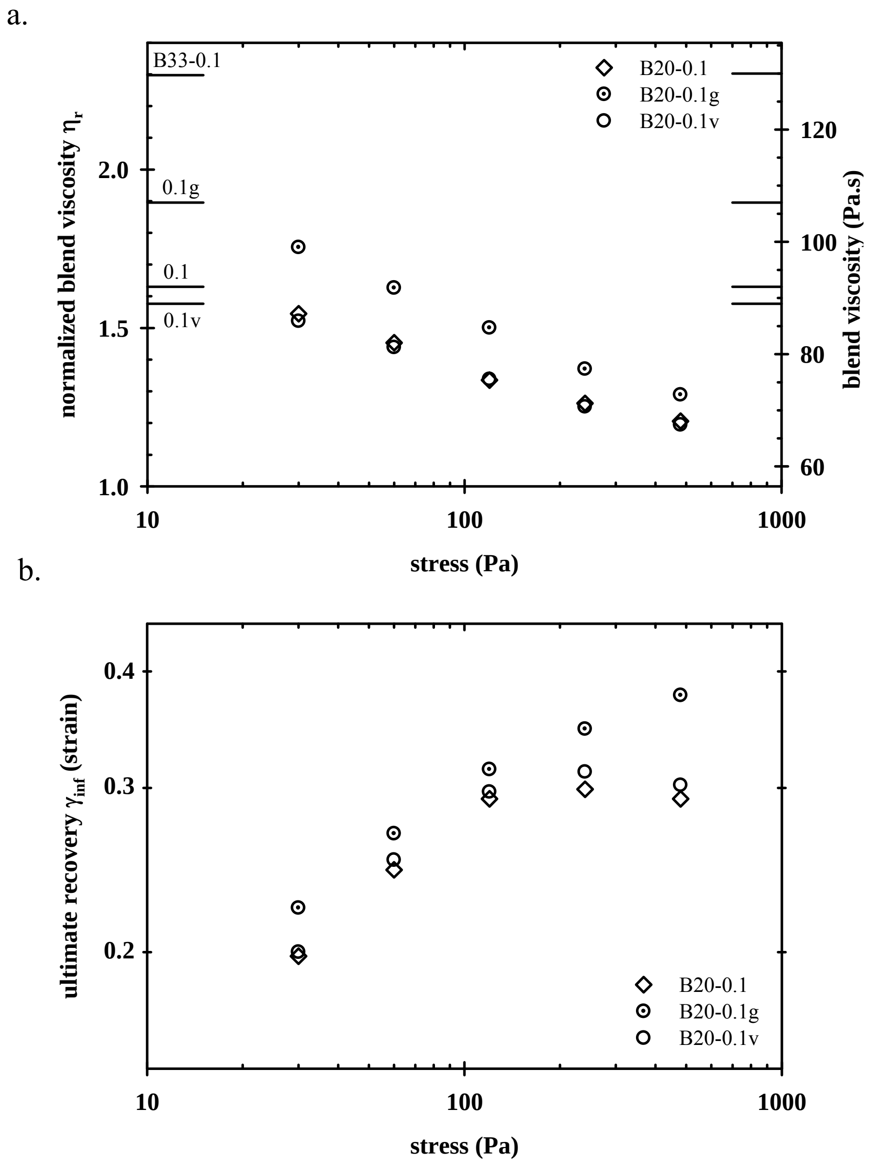

Figure 5.6: a.) Viscosity (symbols) and terminal complex viscosity (horizontal lines), and b.) Ultimate recovery for select double emulsion blends. Note that the y-axis in b. is logarithmic.

As described in Section 4.1.3.4, blends show strain recovery upon cessation of steady shear. As stated previously, recovery is attributable to the shape-recovery of initially-deformed drops[46,71] and also to the relaxation of interfacial tension gradients along the drop surfaces for compatibilized blends.[43,47] As previously, the kinetics of recovery cannot be captured by a single time constant (see Section 4.1.3.4),[66,71] and therefore it is convenient to characterize the recovery in terms of only one quantity, the ultimate recovery, γ_∞. The ultimate recovery for the three blends is shown in Figure 5.6b. The ultimate recovery decreases with decreasing stress as noted previously for blends with a higher volume fraction of drops (Section 4.1.3.4). The chief observation is that the B20-0.1g blend has slightly higher recovery than the other two blends.

The detailed procedure for extracting the terminal relaxation time has been described previously.[41] As in Section 4.1.3.2, the viscoelastic contribution of the bulk is subtracted from the measured G' data, and the results are fitted to a sum of a small number of Maxwell modes (see Equations 4.3 and 4.4). For the single-blended B20-0.1 blend and the B20-0.1v blend, only a single Maxwell mode was adequate to capture the interfacial relaxation process accurately. For the B20-0.1g sample, two modes were necessary, presumably due to the broad (nearly bimodal) drop size distribution inherent in double emulsion morphologies. Sample fits to the oscillatory data are shown in Figure 5.7. Once again, internal consistency was tested by verifying that the complex viscosity (see Equation 4.5) corresponding to the sum of Maxwell modes was in good agreement with the interfacial contribution to the complex viscosity measured experimentally. The absolute value of the complex viscosity, $|\eta^*_{\text{interface}}|$ is plotted in Figure 5.7 along with the absolute value of the complex viscosity corresponding to the multi-mode Maxwell model

$$\left|\eta^*(\omega)\right| = \frac{\left|G^*(\omega)\right|}{\omega} = \frac{\sqrt{G'(\omega)^2 + G''(\omega)^2}}{\omega} \tag{5.1}$$

where *G*'(ω) is given by Equation 4.4 and *G*"(ω) is given by

$$G''(\omega) = \sum_{k=1}^{n} \frac{\omega \exp(\nu_k + 2\tau_k)}{1 + \omega^2 \exp(2\tau_k)} \tag{5.2}$$

The terminal relaxation times thus obtained are plotted in Figure 5.8b. The chief observation is that the double emulsion blend B20-0.1g has a much higher terminal relaxation time than the other two blends.

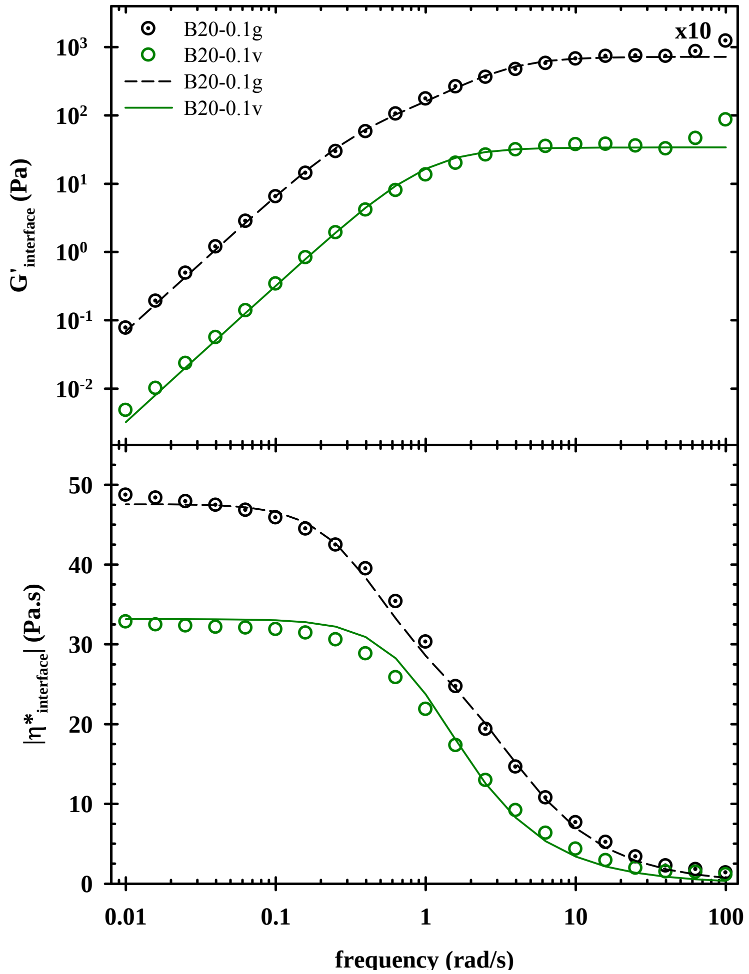

Figure 5.7: Sample fits of $G'_{\text{interface}}$ and $|\eta^*_{\text{interface}}|$ to a multi-mode Maxwell model. Data is from 120 Pa step.

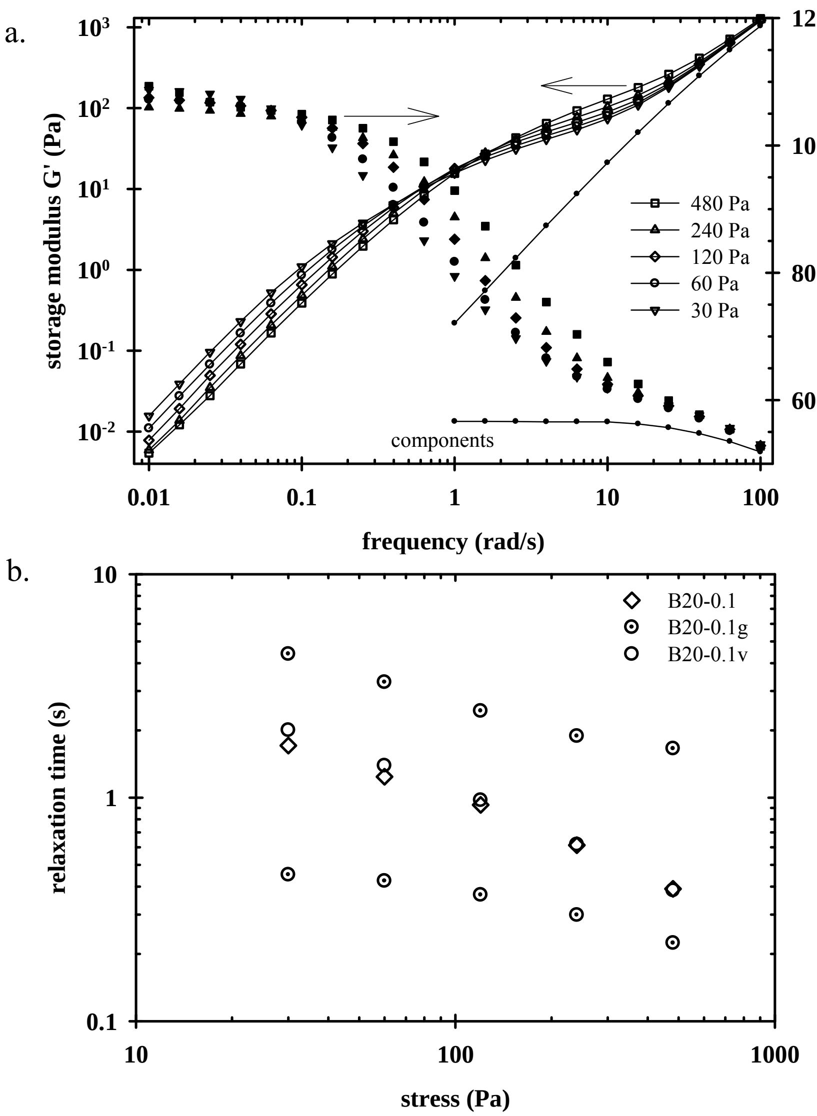

Figure 5.8: a.) Storage modulus and magnitude of the complex viscosity for B20-0.1g after shearing at each stress level. b.) Relaxation times obtained from the oscillatory data. B20-0.1g required two relaxation times; both are shown above.

From an examination of Figures 5.6 and 5.8, the following comments can be made. First, all the rheological properties of the double-blended B20-0.1v blend are close to those of the single-blended sample, thus quantitatively proving the nearly complete absence of sub-drops in the vigorously-blended sample. Thus, in the limit of vigorous blending, the rheological properties of the double-blended samples are identical to those of the single-blended sample.

The gently-blended B20-0.1g sample may be regarded as the other limit. The rheological properties of B20-0.1g are qualitatively similar to the simple droplet-matrix blends, however, quantitatively B20-0.1g has a higher terminal complex viscosity, higher steady shear viscosity, higher relaxation time, and slightly higher ultimate recovery. These quantitative differences may, at the simplest, be interpreted by regarding the B20-0.1g double emulsion morphology as a simple droplet-matrix morphology, but with an effective drop volume fraction $\phi_{eff} > \phi_{PIB}= 0.2$, and an effective drop viscosity ratio exceeding one. This immediately suggests using the rheology to estimate the effective volume fraction, and therefore the extent of leakage. Of the properties displayed in Figures 5.6 and 5.8, the steady shear viscosity, strain recovery, and relaxation time all depend on the applied stress and on the drop size. In contrast, since the terminal complex viscosity is expected to be independent of drop size and stress, it may be best-suited for estimating the ϕ_{eff}, and hence the extent of leakage. Unfortunately, leakage of sub-drops affects the terminal complex viscosity of the blend in several different ways: 1.) most directly, leakage decreases the volume fraction of the drops, thus reducing the blend viscosity. 2.) Leakage also reduces the effective drop viscosity ratio of the drops (as the sub-drop volume fraction decreases). This also indirectly reduces the viscosity of the double emulsion.[70] 3.) Leakage may also redistribute the compatibilizer, raising the amount of compatibilizer adsorbed on the interface of the drops. This may raise the terminal complex viscosity. For all these reasons, it is not possible to use the magnitude of the terminal complex viscosity to quantitatively estimate extent of leakage. Qualitatively however, $|\eta_0^*|$ is still an excellent indicator of the stability of the double emulsion morphology against leakage of sub-drops. For example, comparing B20-0.1g from Figure 5.5b (as-loaded sample) versus Figure 5.8a (sheared sample), $|\eta_0^*|$ is seen to reduce after the first shearing step of 480 Pa, but then remain nearly constant. This is indicative of some leakage in the very first shearing step (perhaps as the initially-large drops breakup when sheared for the first time), but no further leakage on extended shearing at lower stresses.

Finally, it is interesting to compare the measured $|\eta_0^*|$ against that expected in the limiting case in which none of the sub-drops leak out. The B20-0.1g blend was prepared by blending B60-0.1 and B0-0.1 in a 1:2 ratio. In the absence of any sub-drop leakage, the volume fraction of the PMDS sub-drops is 0.4 x 0.333 = 0.133. Accordingly, the effective volume fraction of the drops, $\phi_{eff} = 0.2 + 0.133 = 0.333$, i.e. the viscosity of such a zero-leakage double emulsion should be comparable to that of a B33-0.1 blend. In fact, the viscosity may be even higher since the double-emulsion drops, which are comprised of the B60-0.1 blend, now have an effective drop viscosity ratio of about four (see Figure 4.6). Figure 5.6b however shows that the zero-shear viscosity of the B20-0.1g double emulsion is substantially lower than of a B33-0.1 blend, indicating that even the gently-mixed B20-0.1g blend had significant leakage. Thus, although the optical image of Figure 5.2c shows the presence of numerous sub-drops, the rheological results suggest that gentle blending did not completely prevent leakage.

The central hypothesis of this section is that the precise sequence in which various components are blended affects the two-phase morphology. This is well-established in the oil/water emulsion literature and we have shown that it is possible, at least in principle, in polymer blends. We have tested only one blending protocols thus far, but many others may be devised to modify the morphology. Even variations of the double blending protocol considered here can significantly modify the morphology. For example, a simple variation of the double-blending protocol is to add all the compatibilizer in the first step and none in the second step (instead of distributing the compatibilizer in both blending steps as done in Figure 5.2). We implemented this variation i.e. blended B60-0.3 with pure PDMS to realize a B20-0.1 blend (see Figure 5.9b). It is clear that the initial B60-0.3 blend in Figure 5.9b is composed of much finer PDMS drops, thus the final double emulsion morphology had sub-drops that were much smaller than in Figure 5.9a. It is easy to conceive of other variations that would also affect the morphology, e.g. blend the initial A-in-B emulsion into additional A in a gradual fashion (instead of all-at-once as done here). Changing the overall concentration of compatibilizer would offer even more possibilities for morphological control.

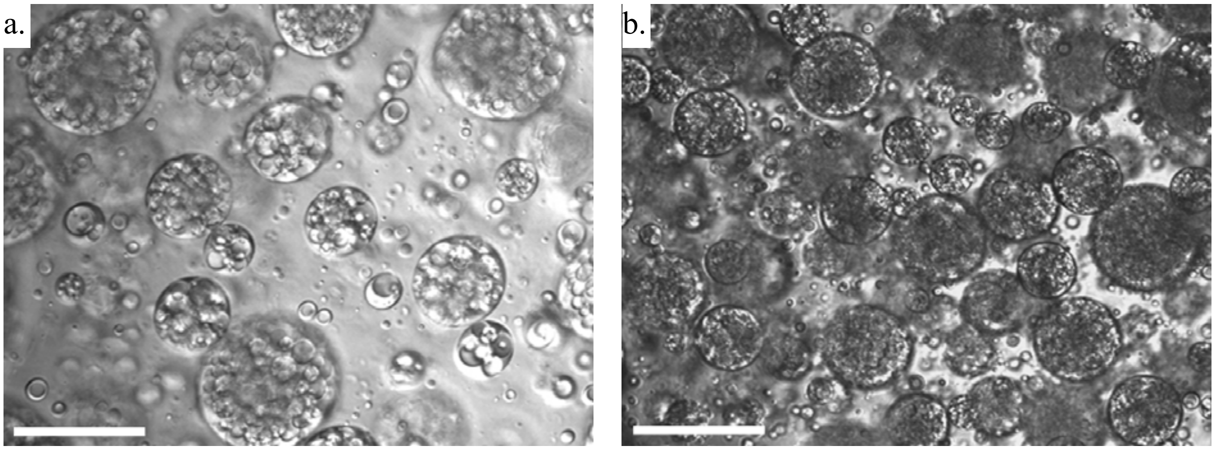

Figure 5.9: B20-0.1g double emulsion blends created by blending a.) a B60-0.1 blend with B0-0.1, and b.) a B60-0.3 blend with B0-0 (pure PDMS). Scale bars represent 20 μm.

Furthermore, the rheology of the blend in Figure 5.9a differed slightly from the blend in Figure 5.9b. For example, the steady shear and terminal complex viscosities for the blend with the finer internal dispersion are an average of 8% higher than the blend with larger sub-drops. The ultimate recoveries of both blends are comparable; however, the times for half-recovery for the blend in Figure 5.9a are an average of 8% higher. We hypothesize that the internal blend in Figure 5.9a contains more compatibilizer and thus has a smaller droplet size (B60-0.3 compared to B60-0.1), and that this is contributing to a higher internal blend viscosity and therefore a higher effective viscosity ratio. Indeed, it has been shown that both steady-shear and terminal complex viscosity increase with increasing p in dilute compatibilized blends.[41] It has also been shown that increasing p causes longer relaxation times, but little effect on the ultimate recovery in dilute compatibilized blends.[43] However, these observations are for dilute, simple droplet-matrix blends, and our double emulsion system shows undoubtedly more complex behavior. Nevertheless, these observations warrant further investigation.

5.1.3 Multistep concentration protocol

We will now turn to the "multistep concentration" protocol. Multistep concentration is the basis of recipies[101] for home-made mayonnaise that require that oil be added *drop-wise* into an aqueous phase containing egg yolk so as to result in an oil-in-water emulsion of high oil fraction (typically over 65%) and hence a "creamy" consistency. Also similar to the previous double-blending case, it is crucial that the emulsifier prevent coalescence of oil drops, a role played by an egg yolk protein, lecithin.[102] If coalescence occurs, the emulsion will undergo phase inversion into a water-in-oil mayonnaise with a "runny" consistency.

We implemented the multistep concentration procedure in PIB/PDMS blends to examine whether a high-dispersed phase morphology could be realized in our polymeric system. The experimental protocol (Figure 5.10a) was chosen such that a B20-0.1 sample would be prepared by gradual addition of pure PDMS to a compatibilizer/PIB mixture. Accordingly, the starting point was a B100-0.5 blend, i.e. 0.5wt% mixture of the compatibilizer in the PIB. In the first blending step, 0.228 g of PDMS was blended vigorously with 0.779 g of B100-0.5, resulting in 1.01 g of a PDMS-in-PIB blend with ϕ_{PIB}= 0.78. As per the nomenclature of this paper, this sample is designated B78-0.41. In the second step, an additional 0.16 g of PDMS was added and blended vigorously. This process was continued with roughly 0.2 +/- 0.04 g of PDMS being added in each step. An accurate determination of phase continuity is critical in this experiment and hence the following protocol was devised for testing the phase continuity after each blending step: a small drop of the blend was placed on a glass slide and a drop of pure PIB was placed adjacent to it. As the two drops spread on the slide, they contacted each other. Phase continuity could be unambiguously determined from this experiment: with a PDMS-in-PIB morphology, no interface was evident once the two drops contacted each other. The sequence of images collected after each blending step is shown in Figures 5.10b-g. It is clear that a high-dispersed phase morphology was not realized at all; after the fifth blending step (i.e. transition from Figure 5.10e to Figure 5.10f), when ϕ_{PDMS} increased to 0.56, the blend phase-inverted into a PDMS-in-PIB-in-PDMS double emulsion morphology. Upon further addition of PDMS, when ϕ_{PIB}= 0.4, virtually all sub-drops leaked out due to the vigorous blending and the rheological properties of this sample (not shown) were virtually identical to those of the corresponding single-mixed PIB-in-PDMS B40 blend (Figure 4.3a). In contrast, if a high dispersed phase blend was realized, we know from Section 4.1.3.5 (Figure 4.9) that our PDMS in PIB compatibilized drops behave like rigid particles, and therefore the rheological properties would compare to that of a suspension of 60% particles. The Kreiger-Dougherty equation (Equation 4.10), predicts that the viscosity of such a suspension would have been considerably higher.

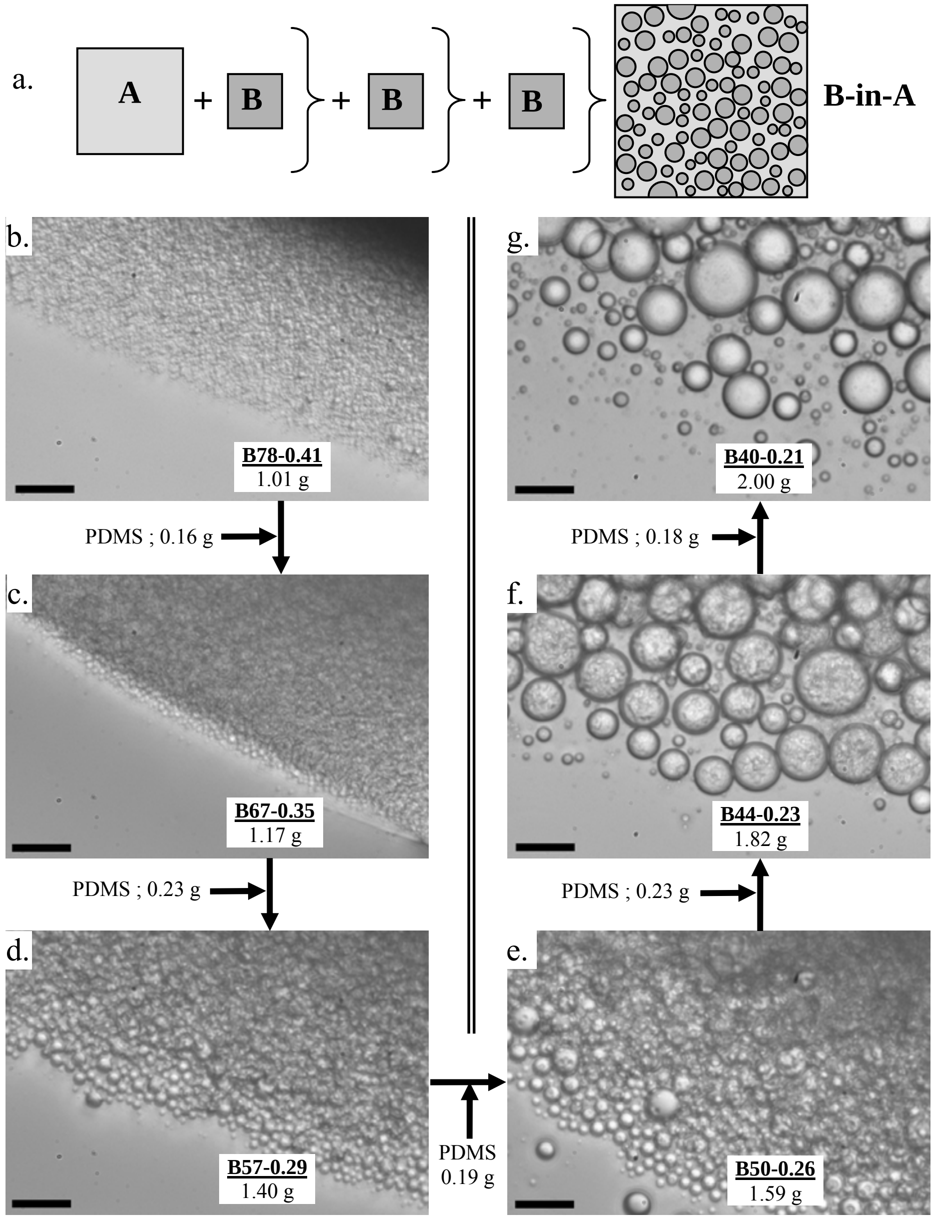

Figure 5.10: a.) Schematic of the “multistep concentration” protocol. b-g.) Sequence of samples realized during multistep concentration. Each blend results from blending pure PDMS with the previous blend. Scale bars represent 10 μm.

We have conducted the above experiment with some variations: placing the compatibilizer in the PDMS phase being added gradually (rather than in the matrix phase PIB present at the beginning), and adding the drop phase in finer increments in each blending steps. The results were identical: 1.) when the PIB volume fraction decreased below 50%, the PDMS-in-PIB morphology was lost, and 2.) full phase inversion with negligible sub-drops was evident at ϕ_{PIB}= 0.4. Bouchama et al.[103] have noted that in oil/water systems, exceedingly small changes in the overall composition – drop volume fraction changing by $O(10^{-3})$ in each blending step – may be necessary to extend the phase inversion to higher drop volume fractions. In our case, that would correspond to additions of mg-quantities of PDMS in each blending step, not possible experimentally.

The type of phase inversion relevant here – that induced by changing the relative volume fraction of the two phases – is generally called a "catastrophic" phase inversion in the oil/water emulsion literature. Ostwald's theory is generally recognized as the earliest model of phase inversion.[104,105] Ostwald suggested that phase inversion occurs when the volume fraction of the dispersed phase approaches close packing (0.74 for monodisperse drops; higher for polydisperse drops). Certainly, the volume fraction at phase inversion of 0.5 observed in Figure 5.10 is far from close packing. More sophisticated theories of phase inversion account for the thermodynamics of the emulsion using catastrophe theory[106] the competitive kinetics of drop breakup and coalescence.[107,108] Yet, these explanations are phenomenological and do not address the mechanism whereby inversion occurs. Specifically, if the coalescence of PDMS drops in PIB is suppressed, why did the additional PDMS added in step five not get dispersed as drops, but instead become the continuous phase?

While we are unable to answer this question in detail, it is important to note one general aspect of the multistep concentration procedure, viz. with every successive step, the fresh PDMS being added must be blended with a blend of an increasing (and therefore more mismatched) viscosity. For example, in step five, the PDMS was blended with B50-0.26 whose zero-shear viscosity was at least four-fold larger (See Figure 4.6). It is well-known that in two-phase systems with a large viscosity difference, the phase inversion composition is shifted towards the low viscosity component, i.e. the low-viscosity component becomes the continuous phase when it is still in a minority (see Figure 2.6).[33] Accordingly, the additional PDMS added in step 5 has a tendency to encapsulate the higher-viscosity blend, thus forming a double emulsion. Upon continued blending, the double emulsion sub-drops leak out as illustrated in Figure 5.3c. Such leakage is then responsible for the complete phase inversion into a simple PIB-in-PDMS morphology. Indeed, in the oil/water emulsion literature, phase inversion is sometimes accompanied by an intermediate double emulsion structure.[103,108-110]

To summarize, a compatibilizer can sometimes suppress coalescence of drops in a polymer blend. In such cases, it is possible to exploit coalescence suppression to control the blend morphology. We have compared two blending procedures drawn from the literature on oil/water emulsions.

In the double blending procedure, a droplet/matrix blend is first prepared and then dispersed into additional drop phase fluid. In oil/water emulsions, this can give rise to a drop-within-drop morphology, called a double emulsion. We show that a double emulsion morphology can be realized in polymer blends as well, provided the second blending step is conducted gently. Rheological properties of the double emulsion morphology qualitatively resemble those of a simple droplet-matrix morphology, but with a higher effective drop volume fraction and a higher effective drop viscosity ratio.

Finally, the multistep concentration procedure consists of adding the drop phase in a gradual fashion, rather than all at once, into the dispersed phase. In oil/water systems, such a procedure can yield a high-dispersed phase emulsion. In the polymer blend case, we were unsuccessful in realizing a high-dispersed phase morphology; phase inversion occurred when the drop volume fraction exceeded 0.5 for systems using both pre-made compatibilizers and reactive compatibilization. The multistep concentration procedure inevitably involves blending two fluids with a highly mismatched viscosity, and we speculate that this viscosity mismatch is responsible for the phase inversion.

5.2 PA/PS BLENDS

5.2.1 Materials and Methodology

We also attempted to create double emulsion and high dispersed phase volume fraction blends using commercially relevant polymers and polymer processing equipment. Materials used were nylon 6,6 (PA, polyamide) (Zytel 101, DuPont) ($\eta \approx 130$ Pa.s), polystyrene (PS) (Styron 666D, Dow) ($M_w = 200{,}000$ g/mol) ($\eta \approx 230$ Pa.s), and a polystyrene-*co*-maleic anhydride random copolymer (PS-MA) (Aldrich) ($M_w = 225{,}000$ g/mol, 7% MA groups) ($\eta \approx 720$ Pa.s) as a compatibilizer. Unlike the PIB/PDMS system, this system is compatibilized by the reaction between the maleic anhydride groups of the PS-MA and the primary amine end groups of the nylon. One advantage of this system is that the reaction occurs very quickly at the interface,[111,112] *whenever any new interface is formed*.

Both the “double blending” and “multistep concentration” protocols were performed on the PA/PS system, except that the PS phase was instead a 25% by weight master batch of PS-MA in PS (denoted “PS*”). All blends were prepared using a DSM microcompounder (DSM Xplore, Geleen, The Netherlands). The DSM microcompounder (see Figure 5.11) is a polymer blending apparatus than can achieve twin-screw-like mixing on samples as small as 5 grams. It can operate in either batch or continuous mode, making it ideal for both the mixing protocols described earlier.

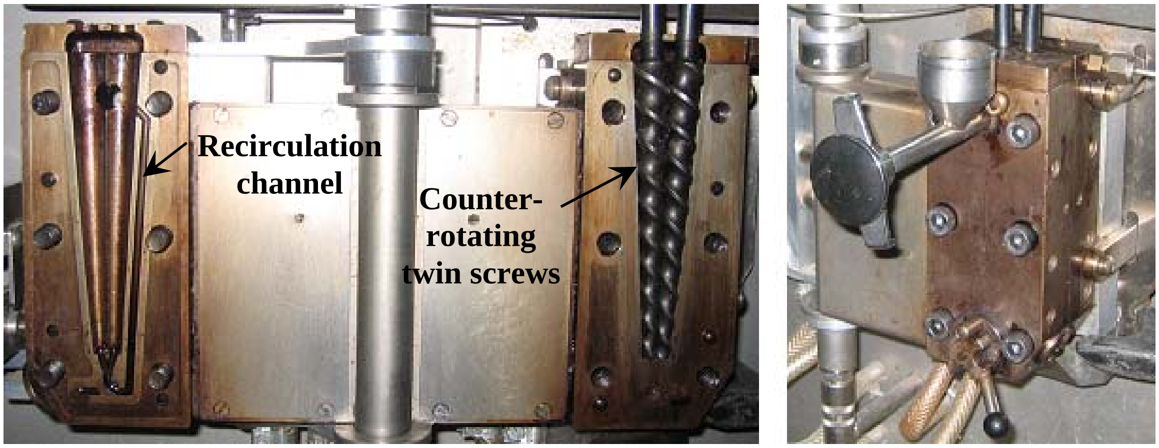

Figure 5.11: DSM microcompounder, left view shows microcompounder open. Note the recirculation channel at left.

For all compatibilized blends, the PS* masterbatch was prepared in the microcompounder by mixing the appropriate amounts of PS and PS-MA at 270 °C and 100 rpm screw rotation for five minutes. The PS* masterbatch was then extruded and pelletized. For the “double blending” protocol, the appropriate amounts (five grams total sample weight) of the PS* and nylon polymer pellets were dry mixed and loaded into the microcompounder. The preliminary blend of PS* in nylon was blended at 270 °C and 50 rpm for five minutes, then extruded. After pelletizing, the appropriate amount of the PS* in nylon preliminary blend was dry mixed with the appropriate amount of PS* pellets, loaded back into the microcompounder, and blended at 270 °C and 10 rpm for five minutes. For the "multistep concentration" protocol, the appropriate amounts of PS* and nylon were dry mixed, loaded into the microcompounder, and blended at 270 °C and 50 rpm for five minutes. While mixing, a small amount (< 1 gram) of the blend was extruded and roughly the same amount of PS* was added to the blend in the microcompounder. The blend was then mixed for five minutes at 270 °C and 50 rpm, after which another small amount of the blend was extruded and the appropriate amount of PS* added. This sequence was then repeated multiple times.

5.2.2 Results

We performed the two-step mixing protocol shown in Figure 5.2a using a 25% by weight master batch of PS-MA in PS, denoted PS*, to ensure an appropriate amount of compatibilizer in the blends.

The PA/PS* double emulsion blend and precursor blend can be seen in Figure 5.12. It appears as though a double emulsion morphology was created, but with fewer sub drops than expected (roughly compare to Figure 5.2c). As briefly discussed earlier (Section 5.1.2), sub drops can "leak" out of the outer drops and coalesce with the matrix, especially during high-stress mixing. We hypothesize that most PS* sub drops are coalescing with the matrix PS* during blending in the microcompounder. Unfortunately, it may not be practical or even possible to conduct blending gentle enough in a twin-screw-like extruder to prevent leakage of double emulsion drops, the stresses involved are just too high.

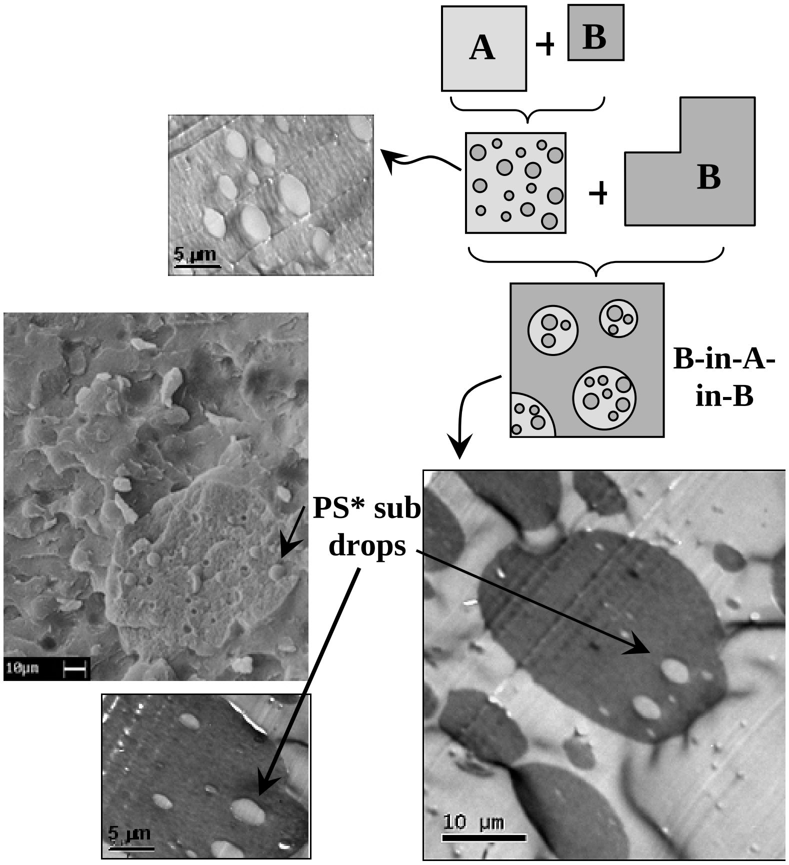

Figure 5.12: SEM and TEM micrographs of double emulsion and precursor blends of PA and PS*.

We also attempted to make a high dispersed phase volume fraction PA/PS* blend (Figure 5.10a following the procedure outlined in Section 5.1.3. Eight sequential steps were performed, taking a 30/70 by weight PS*/PA blend to a 92/8 by weight PS*/PA blend. This corresponds to extruding approximately 0.54 grams of the blend and adding the same amount of PS* at each step. To determine if phase inversion occurred, we conducted an experiment analogous to that shown in Figure 4.2. (According to Equation 2.6, and assuming a linear combination of PS and

PS-MA viscosities, the phase inversion point for this system would occur at $\phi_{PS} = 0.73$.) A sample of the blend from each step was placed in toluene for several days. Since the original blend was nylon-continuous, it should not dissolve in toluene, and any of the blends that are nylon continuous would likewise not dissolve in toluene. If a high dispersed phase volume fraction blend was created, none of the blend samples from any of the sequential mixing steps should dissolve in toluene.

SEM micrographs were also taken of samples from the first 5 steps of the mixing protocol. These samples were fractured under liquid nitrogen and the fracture surface was submerged in toluene for fifteen minutes to dissolve away the PS* phase. From Figure 5.13a it appears as though the blend phase inverted somewhere between 63 and 74% by weight PS*. Furthermore, from the SEM micrographs it can be seen that the 56 and 63% PS* blends have a co-continuous morphology. Unfortunately, it appears as though a *droplet-matrix* high dispersed phase blend was not created by this protocol in this system. Interestingly, the 56% blend appears to have many PS* sub-drops, which consequently leaked out into the matrix phase upon further blending. However, we have yet to compare the morphology for the 63% PS* blend with that of a single-blended sample with the same weight fractions.

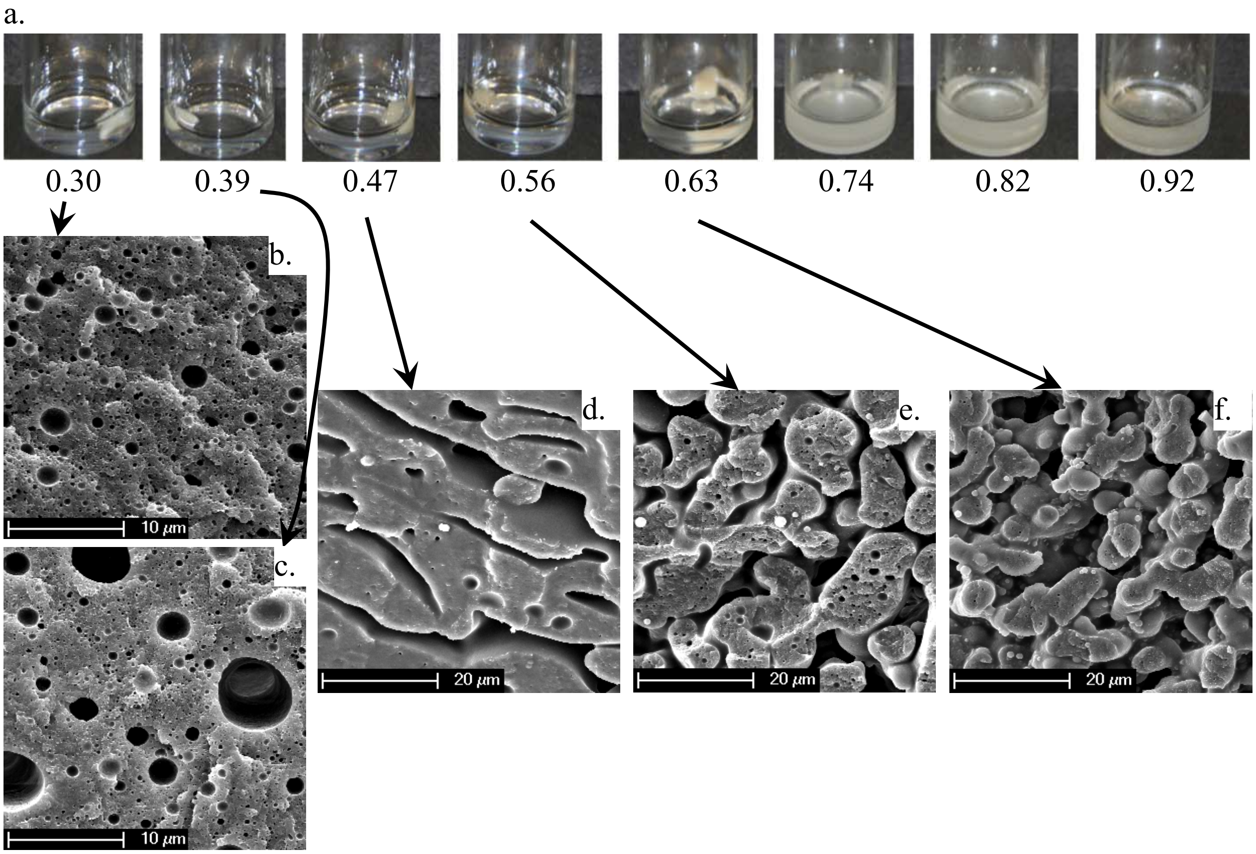

Figure 5.13: a.) Toluene dissolution experiment on PA/PS* blends from the high dispersed phase volume fraction mixing protocol. Weight fractions of PS* in PA for each blend are listed under the corresponding images. b.) – f.) SEM images of blends having w_{PS*} = 0.30, 0.39, 0.47, 0.56, and 0.63, respectively.

6.0 SUMMARY

The goal of this work was to investigate the effect of surface active species, termed compatibilizers in this context, on the dynamics of two-phase flow of polymer blends.

Experiments on the effect of compatibilizers on single drop dynamics in a PEO/PPO/Pluronic system showed complex and previously unknown behavior. We hypothesize that our sample preparation protocol (blend while hot, coalesce while cold) resulted in a compatibilizer interfacial concentration far above the equilibrium value. We believe that the compatibilizer was forming an aggregated structure on the interface and the compatibilizer structure “melted” upon heating causing the interfacial tension to rapidly decrease and the drop to autoextend. The ability of the compatibilizer to form an aggregated structure on the interface is most likely the cause of the nonretraction behavior as well. During retraction, interfacial area is decreasing and interfacial compatibilizer concentration increases to the point where an aggregated structure is formed. As a result, we hypothesize that the interface develops a yield stress and retraction stops once the interfacial forces driving retraction balance the interfacial yield stress. The fact that heating irreversibly eliminates the nonretraction behavior suggests that the behavior is idiosyncratic to our system. On the other hand, the autoextension behavior is likely to be generally present whenever compatibilizer can be trapped on the interface. As long as compatibilizer bulk solubility and/or diffusivity is low, it should be possible to kinetically trap an excess of compatibilizer on the interface and realize autoextension behavior by following specific blending and thermal histories.

We also conducted experiments on the effect of compatibilizer on many-drop systems (immiscible PIB/PDMS polymer blends) close to the phase inversion point. We showed that the compatibilizer does not affect the phase inversion composition and does not significantly change the morphology, at least at the low to moderate compatibilizer loadings studied here. The effect of compatibilizer on recovery after cessation of shear is complex. A complex interplay exists between various effects (Marangoni stresses, gradients in capillary pressure, change in the average interfacial tension during retraction),[43,47] but the net effect in this case appears to be an increase in γ_∞ upon addition of compatibilizer. The compatibilizer was able to immobilize the interface through Marangoni stresses, causing an increase in the steady-shear and terminal complex viscosities. Interestingly, the compatibilizer was able to immobilize the interface more for PDMS-in-PIB blends than for PIB-in-PDMS blends. We currently have no explanation for this phenomenon. However, the asymmetry in interfacial immobilization explains the asymmetric coalescence suppression: the compatibilizer was able to suppress coalescence for PDMS drops in PIB but not for PIB drops in PDMS.

Coalescence suppression creates opportunities for kinetic trapping, and we have shown that the morphology of compatibilized polymer blends can be varied by using specific blending protocols. For example, by blending a PDMS-in-PIB blend (where coalescence is suppressed) into more PDMS, a double emulsion morphology was created. The rheology of these double emulsion blends is complex, but it appears that most of the rheological behavior can be attributed to a higher effective dispersed phase volume fraction and a higher effective viscosity ratio. These double emulsion blends were stable under quiescent and steady-shear conditions up to at least 480 Pa; however, the compatibilizer was not able to prevent the sub-drops from coalescing with the matrix phase under high-stress conditions. A reactively-generated graft copolymer compatibilizer was also not able to prevent sub-drops from coalescing with the matrix phase under high-stress conditions in PA/PS blends. Another blending protocol, multistep concentration, was performed in an attempt to create blends with dispersed phase volume fractions higher than the phase inversion point. Unfortunately, neither a simple diblock (PIB/PDMS) nor a reactively-generated compatibilizer (PA/PS) were “robust” enough to prevent phase inversion from occurring. The multistep concentration procedure inevitably involves blending two fluids with a highly mismatched viscosity, and we speculate that this viscosity mismatch is responsible for the phase inversion. We hypothesize that that diblocks or graft copolymers are too simple to create high dispersed phase volume fraction blends, a mechanically “robust” interface is needed. Preliminary observations on a reactive PI/PDMS system show that the interface can become crosslinked due to the nature of the reactive species.[113] A crosslinkable interface could be robust enough to realize a high dispersed phase volume fraction blend.

7.0 FUTURE WORK

7.1 MULTISTEP CONCENTRATION PROTOCOL

At the end of the previous section, we proposed that an interface that is mechanically robust may allow more opportunities for structure control. One way of making a mechanically robust interface is to *locally* crosslink the interface. Preliminary experiments in our group by Ms. Candice DeLeo showed some interesting behavior that could facilitate the preparation of high dispersed phase blends: for a system of PI and PDMS with reactive compatibilization, a "skin" formation was seen on interface, and non-spherical drops and network-like structures were also seen.[113] It was concluded that the compatibilization reaction was cross-linking the interface and forming "skins" that have appreciable mechanical strength. If the strength of these skins is strong enough to facilitate the creation of non-spherical drops and network-like structures, we hypothesize that the skins will provide a good enough mechanical barrier against coalescence to achieve a high dispersed phase volume fraction blend.

We performed the multistep concentration protocol adding small amounts of two masterbatches, one of PDMS and PDMS with pendant amine groups (PDMS-NH_2), and one of poly(isoprene) (PI) and poly(isoprene-*graft*-maleic anhydride). The PDMS masterbatch (η = 96 Pa.s) will be denoted PDMS*, and the PI masterbatch (η = 131 Pa.s) will be denoted PI*. The terminal amine groups at the interface react with the maleic anhydride groups in the graft copolymer and form a compatibilizer at the interface. Not only is this reaction very fast,[112] the compatibilizer actually cross-links on the interface in this system due to the multifunctional nature of both PDMS-NH_2 and PI-MA.[55] A cross-linked interface may provide enough mechanical stability to completely suppress coalescence of droplets and thus make it more likely to achieve a high dispersed phase blend.

Figure 7.1 shows images from the mulistep concentration of a PI*/PDMS* blend. The nomenclature used is on a PI and PI-MA basis, e.g. B61-1.0 corresponds to a blend with 61% by volume PI/PI-MA masterbatch, 49% by volume PDMS/PDMS-NH_2 masterbatch, and 1.0% PI-MA by total sample weight. A small amount of PI* with varying PI-MA concentration was added in each step so that the maleic anhydride groups stoichometrically balanced the amine groups in the added PDMS*.

It appears as though the B50-0.085 blend, and all blends following, have an elongated, network-like droplet structure. Evidently, long fibrils of PDMS were formed during blending near the phase inversion point. Once these fibrils were formed, the compatibilization reaction cross-linked the interface, locking in the microstructure. This network structure is interesting in its own right, but it appears as though a high dispersed phase droplet-matrix blend have not been realized using the PI*/PDMS* reactive system.

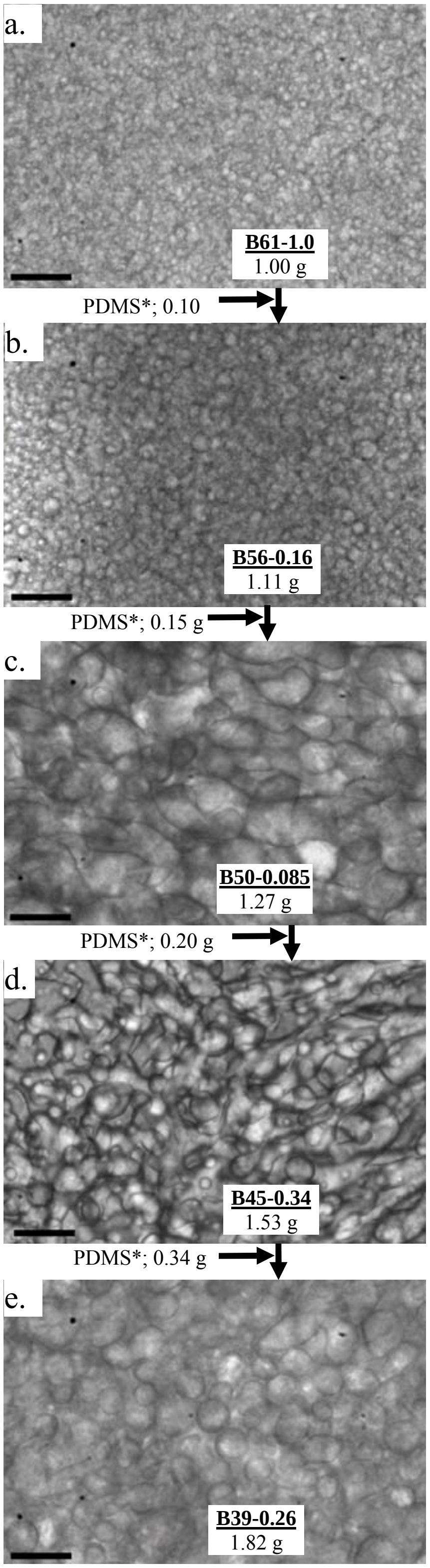

Figure 7.1: Samples realized during PI/PDMS multistep concentration. Each blend results from blending a PDMS* and a small amount of PI* with the previous blend. Scale bars represent 20 μm.

As a control experiment, a B39-0.20 blend was prepared in one mixing step. This blend is shown in Figure 7.2, along with the image from the final mixing step of the multistep concentration protocol. The single step B39 blend appears to have a droplet-matrix morphology with a few non-spherical drops, similar to the multistep blend. It was verified that the single mixed blend is PDMS-continuous by placing a drop of pure PDMS on a glass slide next to the blend as described in Section 5.1.3.

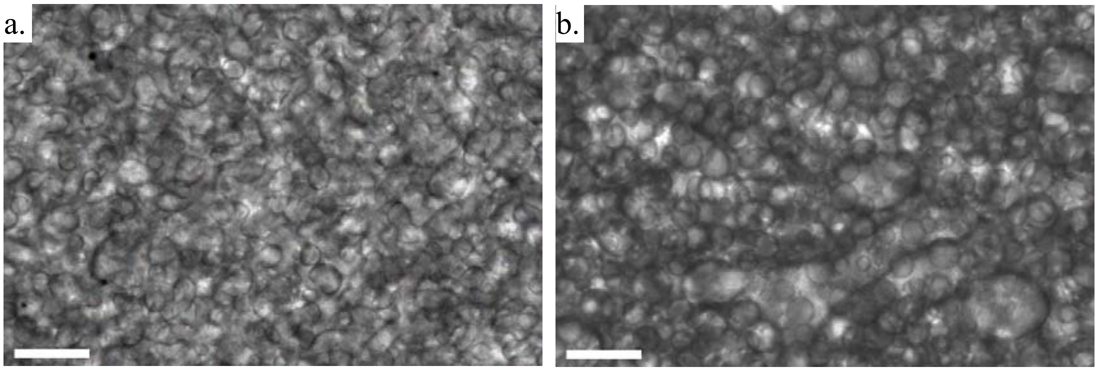

Figure 7.2: Images of a.) the B39-0.26 blend from the multistep concentration protocol shown in Figure 7.1, and b.) a B39-0.20 blend prepared in a single mixing step.

In summary, the experiments discussed in this section constitute only very preliminary work and, even though a high dispersed phase volume fraction blend was not realized, crosslinking *locally* at the interface offers a new strategy of compatibilization worthy of further investigation.

APPENDIX A

DYNAMIC METHODS FOR THE IMBEDDED FIBER RETRACTION METHOD

The two dynamic methods for determining interfacial tension by the IFRM, the Cohen and Carriere (CC),[10] and Tjahjadi, Ottino, and Stone (TOS)[11] methods, are detailed here.

Experimentally, regardless of the details of initial fiber shape, the fiber rapidly takes on an approximately spherocylindrical (cylinder with hemispherical endcaps) shape. Subsequent shape evolution is imaged periodically. The fiber retracts towards a spherical shape at a rate that is determined by the interfacial tension driving the retraction, and the viscous resistance to the retraction. The principle of the fiber retraction method is to obtain the interfacial tension by fitting a theoretical model of the retraction to the experimental retraction kinetics. While polymers are generally viscoelastic, due to the very low interfacial stress driving retraction, it is generally reasonable to assume that the fiber and the matrix behave as Netwonian fluids.

Even with the assumption of Netwonian behavior however, the retraction of a cylindrical fiber is quite complex: the shape can evolve from an initial cylinder into a “dumbbell” with bulbous ends, followed by an ellipsoid, and finally a sphere. Therefore models of retraction only deal with some convenient geometrical features of the fiber shape. These features are shown in Figure A.1. The first is the overall length of the fiber, denoted as $2L$. The second is the effective diameter, $2a$, of a spherocylinder with the same volume as the fiber. The last is the radius, R_0, of the sphere finally resulting at the end of retraction. Obviously

$$\text{volume of fiber} = \frac{4}{3}\pi R_0^3 = 2\left[\pi a^2 (L-a) + \frac{2}{3}\pi a^3\right] \tag{A.1}$$

The initial length and effective radius are denoted as L_0 and a_0 respectively. Experimentally one may either measure $L(t)$ and R_0 (if the fiber retracts all the way up to spherical shape) or $L(t)$ and a_0 (if the experiment is stopped before complete retraction). In either case, the fiber volume can be calculated, allowing $a(t)$ to be calculated from $L(t)$.

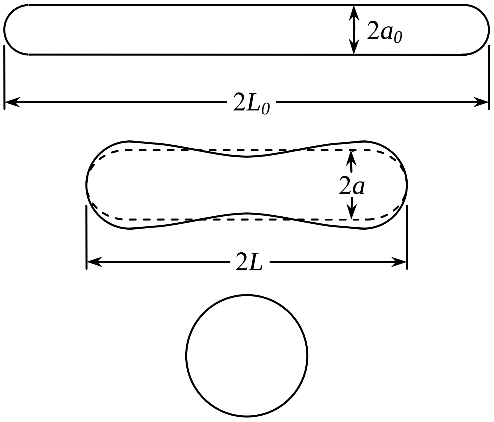

Figure A.1: Schematic of a retracting drop. Drop depicted in dotted lines is a spherocylinder with volume equal to the actual drop.

A.1 COHEN AND CARRIERE METHOD

Due to the considerable complexity of the retraction process[12] there is no rigorous analytical equation to describe the evolution of the geometric features with time. Hence Cohen and Carriere, who first proposed the fiber retraction method, devised an approximate model of the retraction kinetics. They assumed that the fiber remained spherocylindrical *at all times* and predicted[10]

$$f\left(\frac{a}{R_0}\right)-f\left(\frac{a_0}{R_0}\right)=\frac{t\alpha}{R_0\eta_e} \tag{A.2}$$

where

$$f(x)=1.5\ln\left(\frac{\sqrt{1+x+x^2}}{1-x}\right)+\frac{3^{1.5}}{2}\arctan\left(\frac{\sqrt{3}x}{2+x}\right)-\frac{x}{2}-\frac{x}{4} \tag{A.3}$$

In Equation A.2, α is the interfacial tension, t is the time, and η_e is an effective viscosity:[114]

$$\eta_e=\eta_m\frac{1+1.7p}{2.7} \tag{A.4}$$

The effective viscosity is intended to capture the dependence of the retraction kinetics on both the matrix as well as the fiber viscosity.

To apply the CC model, $L(t)$ is measured experimentally, the equivalent radius a is determined by solving Equation A.1, and $f\left(\frac{a}{R_0}\right) - f\left(\frac{a_0}{R_0}\right)$ is plotted versus time. Equation A.2 suggests that a straight line will be obtained with a slope $\frac{\alpha}{R_0 \eta_e}$.

A.2 TJAHJADI, OTTINO, AND STONE METHOD

Recognizing that the CC model is approximate, Tjahjadi *et al.*[11] subsequently took a more rigorous approach. Assuming that only the *initial* shape of the fiber is a spherocylinder, they integrated the Stokes equations exactly using the boundary integral method to calculate the subsequent shapes during retraction. For experimental convenience, the results of the evolution of L with time were presented as a fourth-order polynomial approximation:

$$\frac{L}{R_0} = \sum_{n=0}^{4} k_n \left(\frac{t\alpha}{\eta_m a_0} \right)^n \tag{A.5}$$

Dimensional analysis requires that the polynomial coefficients k_n depend on only two dimensionless parameters, the viscosity ratio p and the initial aspect ratio, L_0/a_0. Accordingly, values of k_n are tabulated at several values of p and L_0/a_0.[11]

To apply the TOS model, the coefficients k_n at the experimental p and L_0/a_0 are first determined by linear interpolation of the tabulated k_n. Then the experimental L/R_0 are plotted versus time and fitted to Equation A.5 using α as a fitting parameter.

BIBLIOGRAPHY

(1) Utracki, L. A. *Polymer alloys and blends : thermodynamics and rheology*; Hanser: New York, 1990.

(2) Sundararaj, U.; Macosko, C. W. *Macromolecules* **1995**, *28*, 2647-2657.

(3) Macosko, C. W.; Guegan, P.; Khandpur, A. K.; Nakayama, A.; Marechal, P.; Inoue, T. *Macromolecules* **1996**, *29*, 5590-5598.

(4) Tan, N. C. B.; Tai, S. K.; Briber, R. M. *Polymer* **1996**, *37*, 3509-3519.

(5) Princen, H. M.; Zia, I. Y. Z.; Mason, S. G. *Journal of Colloid and Interface Science* **1967**, *23*, 99-107.

(6) Joseph, D. D.; Arney, M. S.; Gillberg, G.; Hu, H.; Hultman, D.; Verdier, C.; Vinagre, T. M. *Journal of Rheology* **1992**, *36*, 621-662.

(7) Taylor, G. I. *Proceedings of the Royal Society of London A - Mathematical and Physical Sciences* **1934**, *146*, 501.

(8) Rallison, J. M. *Annual Review of Fluid Mechanics* **1984**, *16*, 45-66.

(9) Luciani, A.; Champagne, M. F.; Utracki, L. A. *Journal of Polymer Science Part B-Polymer Physics* **1997**, *35*, 1393-1403.

(10) Cohen, A.; Carriere, C. J. *Rheologica Acta* **1989**, *28*, 223-232.

(11) Tjahjadi, M.; Ottino, J. M.; Stone, H. A. *Aiche Journal* **1994**, *40*, 385-394.

(12) Stone, H. A.; Leal, L. G. *Journal of Fluid Mechanics* **1989**, *198*, 399-427.

(13) Rayleigh, L. *Proceedings of the Royal Society of London* **1879**, *29*, 71-97.

(14) Tomotika, S. *Proceedings of the Royal Society of London A* **1935**, *150*, 322-337.

(15) Elemans, P. H. M.; Janssen, J. M. H.; Meijer, H. E. H. *Journal of Rheology* **1990**, *34*, 1311.

(16) Edwards, D. A.; Brenner, H.; Wasan, D. T. *Interfacial Transport Processes and Rheology*; Butterworth-Heinemann, 1991.

(17) Hansen, S.; Peters, G. W. M.; Meijer, H. E. H. *Journal of Fluid Mechanics* **1999**, *382*, 331-349.

(18) Tucker, C. L.; Moldenaers, P. *Annual Review of Fluid Mechanics* **2002**, *34*, 177-210.

(19) Grace, H. P. *Chemical Engineering Communications* **1982**, *14*, 225-277.

(20) Stone, H. A.; Leal, L. G. *Journal of Fluid Mechanics* **1990**, *220*, 161-186.

(21) Milliken, W. J.; Stone, H. A.; Leal, L. G. *Physics of Fluids a-Fluid Dynamics* **1993**, *5*, 69-79.

(22) Pawar, Y.; Stebe, K. J. *Physics of Fluids* **1996**, *8*, 1738-1751.

(23) Milliken, W. J.; Leal, L. G. *Journal of Colloid and Interface Science* **1994**, *166*, 275-285.

(24) Stebe, K. J.; Lin, S. Y.; Maldarelli, C. *Physics of Fluids a-Fluid Dynamics* **1991**, *3*, 3-20.

(25) Hu, Y. T.; Lips, A. *Physical Review Letters* **2003**, *91*.

(26) Gonzalez-Mancera, A. In *Mechanical Engineering*; University of Maryland: College Park, 2007.

(27) Eggleton, C. D.; Tsai, T. M.; Stebe, K. J. *Physical Review Letters* **2001**, *87*.

(28) Smith, P. G.; Vandeven, T. G. M. *Colloids and Surfaces* **1985**, *15*, 191-210.

(29) Van Puyvelde, P.; Velankar, S.; Moldenaers, P. *Current Opinion in Colloid & Interface Science* **2001**, *6*, 457-463.

(30) Chesters, A. K.; Bazhlekov, I. B. *Journal of Colloid and Interface Science* **2000**, *230*, 229-243.

(31) Van Puyvelde, P.; Velankar, S.; Mewis, J.; Moldenaers, P. *Polymer Engineering and Science* **2002**, *42*, 1956-1964.

(32) Hudson, S. D.; Jamieson, A. M.; Burkhart, B. E. *Journal of Colloid and Interface Science* **2003**, *265*, 409-421.

(33) Paul, D. R.; Barlow, J. W. *Journal of Macromolecular Science - Reviews in Macromolecular Chemistry and Physics C* **1980**, *18*, 109-168.

(34) Milner, S. T.; Xi, H. W. *Journal of Rheology* **1996**, *40*, 663-687.

(35) Galloway, J. A.; Jeon, H. K.; Bell, J. R.; Macosko, C. W. *Polymer* **2005**, *46*, 183-191.

(36) Riemann, R. E.; Cantow, H. J.; Friedrich, C. *Macromolecules* **1997**, *30*, 5476-5484.

(37) Van Hemelrijck, E.; Van Puyvelde, P.; Velankar, S.; Macosko, C. W.; Moldenaers, P. *Journal of Rheology* **2004**, *48*, 143-158.

(38) Martin, J.; Velankar, S. *Journal of Rheology* **2007**, *51*, 669-692.

(39) Van Hemelrijck, E.; Van Puyvelde, P.; Moldenaers, P. *Langmuir* **2004**, *20*, 3498-3500.

(40) Jacobs, U.; Fahrlander, M.; Winterhalter, J.; Friedrich, C. *Journal of Rheology* **1999**, *43*, 1495-1509.

(41) Velankar, S.; Van Puyvelde, P.; Mewis, J.; Moldenaers, P. *Journal of Rheology* **2004**, *48*, 725-744.

(42) Van Hemelrijck, E.; Van Puyvelde, P.; Moldenaers, P. *Macromolecular Symposia* **2006**, *233*, 51-58.

(43) Wang, J.; Velankar, S. *Rheologica Acta* **2006**, *45*, 741-753.

(44) Carriere, C. J.; Cohen, A.; Arends, C. B. *Journal of Rheology* **1989**, *33*, 681-689.

(45) Xing, P. B., M.; Rodrigue, D. *Macromolecules* **2000**, *33*, 8020-8034.

(46) Gramespacher, H.; Meissner, J. *Journal of Rheology* **1992**, *36*, 1127-1141.

(47) Velankar, S.; Zhou, H.; Jeon, H. K.; Macosko, C. W. *Journal of Colloid and Interface Science* **2004**, *272*, 172-185.

(48) Puig, J. E.; Seeto, Y.; Pesheck, C. V.; Scriven, L. E. *Journal of Colloid and Interface Science* **1992**, *148*, 459-468.

(49) Demarquette, N. R.; De Souza, A. M. C.; Palmer, G.; Macaubas, P. H. P. *Polymer Engineering and Science* **2003**, *43*, 670-683.

(50) Palmer, G.; Demarquette, N. R. *Polymer* **2005**, *46*, 8169-8177.

(51) Ziegler, V. E.; Wolf, B. A. *Langmuir* **2004**, *20*, 8688-8692.

(52) Martin, J.; Velankar, S. *Macromolecules* **2005**, *38*, 10614-10618.

(53) Velankar, S.; Van Puyvelde, P.; Mewis, J.; Moldenaers, P. *Journal of Rheology* **2001**, *45*, 1007-1019.

(54) Wang, J. In *Chemical and Petroleum Engineering*; University of Pittsburgh: Pittsburgh, 2005.

(55) Velankar, S. *Unpublished*.

(56) Jansseune, T.; Moldenaers, P.; Mewis, J. *Journal of Rheology* **2003**, *47*, 829-845.

(57) Palierne, J. F. *Rheologica Acta* **1990**, *29*, 204-214.

(58) Graebling, D.; Muller, R.; Palierne, J. F. *Journal De Physique Iv* **1993**, *3*, 1525-1534.

(59) Oldroyd, J. G. *Proceedings of the Royal Society of London. Series A, Mathematical and Physical Sciences* **1950**, *200*, 523-541.

(60) Graebling, D.; Muller, R.; Palierne, J. F. *Macromolecules* **1993**, *26*, 320-329.

(61) Vinckier, I.; Mewis, J.; Moldenaers, P. *Journal of Rheology* **1996**, *40*, 613-632.

(62) Van Hemelrijck, E.; Van Puyvelde, P.; Macosko, C. W.; Moldenaers, P. *Journal of Rheology* **2005**, *49*, 783-798.

(63) Wang, J.; Velankar, S. *Rheologica Acta* **2006**, *45*, 741 - 753.

(64) Jacobs, U.; Fahrländer, M.; Winterhalter, J.; Friedrich, C. *Journal of Rheology* **1999**, *43*, 1497-1509.

(65) Oldroyd, J. G. *Proceedings of the Royal Society of London* **1955**, *A232*, 567-577.

(66) Wang, J.; Velankar, S. *Rheologica Acta* **2006**, *45*, 297-304.

(67) Secor, R. B. In *Rheology: Principles, Measurements, and Applications*; Macosko, C. W., Ed.; Wiley-VCH: New York, 1994; pp 127-133.

(68) Vinckier, I.; Moldenaers, P.; Terracciano, A. M.; Grizzuti, N. *AIChE Journal* **1998**, *44*, 951-958.

(69) Frankel, D. A.; Acrivos, A. *Journal of Fluid Mechanics* **1970**, *44*, 65-78.

(70) Choi, S. J.; Schowalter, W. R. *Physics of Fluids* **1975**, *18*, 420-427.

(71) Vinckier, I.; Moldenaers, P.; Mewis, J. *Rheologica Acta* **1999**, *38*, 65-72.

(72) Vinckier, I.; Moldenaers, P.; Mewis, J. *Rheologica Acta* **1999**, *38*, 65-72.

(73) Taylor, G. I. *Proceedings of the Royal Society of London* **1932**, *A138*, 41-48.

(74) Grizzuti, N.; Buonocore, G.; Iorio, G. *Journal of Rheology* **2000**, *44*, 149-164.

(75) Phan-Thien, N.; Pham, D. C. *Journal of Non-Newtonian Fluid Mechanics* **1997**, *72*, 305-318.

(76) Larson, R. G. *Structure and Rheology of Complex Fluids*; Oxford University Press: New York, 1999.

(77) Blawzdziewicz, J.; Vlahovska, P.; Loewenberg, M. *Physica A* **2000**, *276*, 50-85.

(78) Blawzdziewicz, J.; Wajnryb, E.; Loewenberg, M. *Journal of Fluid Mechanics* **1999**, *395*, 29-59.

(79) Oldroyd, J. G. *Proceedings of the Royal Society of London* **1953**, *A218*, 122-132.

(80) Li, X.; Pozrikidis, C. *Journal of Fluid Mechanics* **1997**, *341*, 165-194.

(81) Einstein, A. *Annalen der Physik (Leipzig)* **1906**, *19*, 289.

(82) Ramirez, J. A.; Davis, R. H.; Zinchenko, A. Z. *International Journal of Multiphase Flow* **2000**, *26*, 891-920.

(83) Beck Tan, N. C.; Tai, S. K.; Briber, R. M. *Polymer* **1996**, *37*, 3509-5519.

(84) Van Puyvelde, P.; Velankar, S.; Moldenaers, P. *Current Opinion in Colloid and Interface Science* **2001**, *6*, 457-463.

(85) Hu, Y. T.; Pine, D. J.; Leal, L. G. *Physics of Fluids* **2000**, *12*, 484-489.

(86) Milner, S. T.; Xi, H. *Journal of Rheology* **1996**, *40*, 663-687.

(87) Binks, B. P., Ed. *Modern Espects of Emulsion Science*; Royal Society of Chemistry, 1998.

(88) Lyu, S.; Jones, T. D.; Bates, F. S.; Macosko, C. W. *Macromolecules* **2002**, *35*, 7845-7855.

(89) Binks, B. P. *Modern Aspects of Emulsion Science*; Royal Society of Chemistry, 1998.

(90) Sjöblom, J. *Encyclopedic handbook of emulsion technology*; Marcel Dekker: New York, 2001.

(91) Buezello, K.; Muller, B. W. *Emulsions as drug delivery systems*; Marcel Dekker: New York, 2000.

(92) Salager, J. L. *Formulation concepts for the emulsion maker*; Marcel Dekker: New York, 2000.

(93) Garti, N.; Benichou, A. *Double emulsions for controlled release applications - Progress and Trends*; Marcel Dekker: New York, 2001.

(94) Wagner, E. R.; Robeson, L. M. *Rubber Chemistry and Technology* **1970**, *43*, 1129-1137.

(95) Sperling, L. H. *Recent advances in polymer blends, grafts, and blocks*; Plenum Press: New York, 1974.

(96) Schierholz, J. U.; Hellmann, G. P. *Polymer* **2003**, *44*, 2005-2013.

(97) Adedeji, A.; Jamieson, A. M.; Hudson, S. D. *Macromolecules* **1995**, *28*, 5255-5261.

(98) Pal, R. *Journal of Colloid and Interface Science* **2007**, *307*, 509-515.

(99) Oldroyd, J. G. *Proceedings of the Royal Society of London Series a-Mathematical and Physical Sciences* **1950**, *200*, 523-541.

(100) Oldroyd, J. G. *Proceedings of the Royal Society of London Series a-Mathematical and Physical Sciences* **1955**, *232*, 567-577.

(101) Rombauer Becker, M.; Becker, E.; Rombauer, I. S. *Joy of Cooking*; Scribner: New York, 1997.

(102) McGee, H. *On food and cooking: the science and lore of the kitchen*; Scribner: New York, 2004.

(103) Bouchama, F.; van Aken, G. A.; Autin, A. J. E.; Koper, G. *Colloids and Surfaces a-Physicochemical and Engineering Aspects* **2003**, *231*, 11-17.

(104) Ostwald, W. *Kolloid Zeitschrift* **1910**, *6*.

(105) Salager, J. L.; Marquez, L.; Pena, A. A.; Rondon, M.; Silva, F.; Tyrode, E. *Industrial & Engineering Chemistry Research* **2000**, *39*, 2665-2676.

(106) Salager, J. L. *Phase transformation and emulsion inversion on the basis of Catastrophe theory*; Marcel Dekker: New York, 1983.

(107) Davies, J. T. *Proceedings of the International Congress on Surface Activity* **1957**, *1*, 426-438.

(108) Nienow, A. W. *Advances in Colloid and Interface Science* **2004**, *108-09*, 95-103.

(109) Brooks, B. W.; Richmond, H. N. *Chemical Engineering Science* **1994**, *49*, 1065-1075.

(110) Pacek, A. W.; Nienow, A. W.; Moore, I. P. T. *Chemical Engineering Science* **1994**, *49*, 3485-3498.

(111) Orr, C. A.; Cernohous, J. J.; Guegan, P.; Hirao, A.; Jeon, H. K.; Macosko, C. W. *Polymer* **2001**, *42*, 8171-8178.

(112) Macosko, C. W.; Jeon, H. K.; Hoye, T. R. *Progress in Polymer Science* **2005**, *30*, 939-947.

(113) DeLeo, C.; Velankar, S. *In Preparation*.

(114) Cohen, A.; Carriere, C. J. *Rheologica Acta* **1989**, *28*, 223-232.